FEBRUARY 2024

M.Sc. in Materials Science and Engineering

MELİKE TÜRKOĞLU

REPUBLIC OF TÜRKİYE

GAZİANTEP UNIVERSITY

GRADUATE SCHOOL OF NATURAL & APPLIED SCIENCES

PRODUCTION AND CHARACTERIZATION OF PARALLEL ALIGNED ELECTROSPUN PAN/GO NANOFIBER BUNDLES

M.Sc. THESIS

IN

MATERIALS SCIENCE AND ENGINEERING

BY

MELİKE TÜRKOĞLU

FEBRUARY 2024

PRODUCTION AND CHARACTERIZATION OF PARALLEL ALIGNED ELECTROSPUN PAN/GO NANOFIBER BUNDLES

M.Sc. Thesis

in

Materials Science and Engineering

Gaziantep University

Supervisor

Assoc. Prof. Dr. Halil İbrahim İÇOĞLU

Co-Supervisor

Prof. Dr. Mehmet TOPALBEKİROĞLU

by

Melike TÜRKOĞLU

February 2024

I hereby declare that all information in this document has been obtained and presented in accordance with academic rules and ethical conduct. I also declare that, as required by these rules and conduct, I have fully cited and referenced all material and results that are not original to this work.

Melike TÜRKOĞLU

ABSTRACT

PRODUCTION AND CHARACTERIZATION OF PARALLEL ALIGNED ELECTROSPUN PAN/GO NANOFIBER BUNDLES

TÜRKOĞLU, Melike
M.Sc. in Materials Science and Engineering
Supervisor: Assoc. Prof. Dr. Halil İbrahim İÇOĞLU
Co-Supervisor: Prof. Dr. Mehmet TOPALBEKİROĞLU

February 2024

85 pages

The aim of this thesis is to investigate the morphologies, nanofiber alignment, mechanical, structural, and thermal properties of parallel aligned polyacrylonitrile/graphene oxide (PAN/GO) nanofibers. For this purpose, firstly, graphene oxide (GO) was synthesized from graphite by the modified Hummers method and analyzed by SEM, FTIR, XRD and Raman spectroscopy. Secondly, PAN nanofibers were produced using different parallel electrodes with plate thickness of 1 and 1.5 mm, plate width of 5, 8 and 10 mm, and gap distance of 20, 30, 40 mm. Thirdly, PAN/GO nanofibers were produced at different ratios to determine their morphology and alignment according to a selected parallel electrode parameter. Finally, PAN/GO nanofibers were produced in bundle form and their mechanical, structural, and thermal properties of were analyzed. The highest nanofiber alignment was produced at 1.5 plate thickness, 10 mm plate width, and 40 mm gap distance. The alignment of nanofibers increased as the addition of GO increased up to 4 wt.% ratio in PAN/GO nanofibers. Structural analyses of PAN/GO nanofibers by FTIR and XRD, thermal analysis by TGA and DSC, nanofiber productivity, tensile strength, % elongation and Young's modulus analyses were performed. As a result of structural, thermal, and mechanical analyses, 3 wt.% GO ratio was determined as the critical value.

Key Words: Electrospinning, Parallel Electrode, Alignment, Graphene Oxide

ÖZET

ELEKTRO ÇEKİM YÖNTEMİ İLE PARALEL HİZALANMIŞ NANOLİF ŞERİTLERİN ÜRETİMİ VE KARAKTERİZASYONU

TÜRKOĞLU, Melike
Yüksek Lisans Tezi, Malzeme Bilimi ve Mühendisliği
Danışman: Doç. Dr. Halil İbrahim İÇOĞLU
İkinci Danışman: Prof. Dr. Mehmet TOPALBEKİROĞLU

Şubat 2024

85 sayfa

Bu tezin amacı paralel yönlenmiş poliakrilonitril/grafen oksit (PAN/GO) nanoliflerin morfolojilerini, nanolif hizalanmasını, mekanik, yapısal ve termal özellerini incelemektir. Bu amaçla ilk olarak, grafen oksit (GO) modifiye Hummers yöntemiyle grafitten sentezlenmiştir. İkinci olarak, PAN nanolifleri 1 ve 1,5 mm kalınlık, 5, 8 ve 10 mm çubuk genişliği ve 20, 30, 40 mm boşluk mesafesine göre farklı paralel elektrotlar kullanılarak üretilmiştir. Üçüncü olarak, PAN/GO nanolifler farklı oranlarda seçilen bir paralel elektrot parametresine göre morfolojik ve hizalanmalarının belirlenmesi için üretilmiştir. Son olarak, PAN/GO nanolifler, şerit formunda üretilerek mekanik, yapısal ve termal özellikleri analiz edilmiştir. SEM, FTIR, XRD ve Raman spektroskopisi analiz sonuçlarına göre GO'nun literatür ile uyumlu başarılı bir şekilde sentezlendiği belirlenmiştir. En yüksek nanolif hizalanması 1,5 elektrot kalınlığı, 10 mm plaka genişliği ve 40 mm boşluk mesafesinde üretilmiştir. PAN/GO nanoliflerde, ağırlıkça % 4 katkı oranına kadar GO miktarı arttıkça nanoliflerin hizalanması artmıştır. PAN/GO nanoliflerin FTIR ve XRD ile yapısal analizleri, TGA ve DSC ile termal analizleri, nanolif üretkenlikleri, tex değerleri, kopma mukavemeti, % uzama ve Youngs modülü analizleri yapılmıştır. Yapısal, termal ve mekanik analizler sonucunda ağırlıkça % 3 GO katkı oranı kritik değer olarak belirlenmiştir.

Anahtar Kelimeler: Elektro Çekim, Paralel Elektrot, Yönlendirme, Grafen Oksit

Dedicated to all women who fought for their freedom…

ACKNOWLEDGEMENTS

First of all, I would like to thank my dear supervisor Assoc. Prof. Dr. Halil İbrahim İÇOĞLU, who guided me in my studies and supported me.

Endless thanks to Behzat Yıldırım, with whom I drank water from the same beaker in the laboratory for 3 years and who made me believe that there is no such thing as impossible. I learned a lot from you not only academically but also in real life. Your future students are very lucky :))

I would like thanks to Asst. Prof. Dr. Ali KILIÇ and Prof. Dr. Mehmet TOPALBEKİROĞLU for their support in the project we carried out.

It was very nice to work with you, my project friends Ahmet Mustafa KÖŞ and Salih KÖKTEN, thank you for your support.

I would like to thank Halil AKARDENİZ and Canan KILIÇ from textile engineering.

I would like to thanks my companion Emre EKER, who did not leave me alone during this process. I'm sorry for studying instead of drinking coffee with you :))

Of course, my family, who supported my decisions throughout my life and made their presence felt... I would like to thanks firstly my father Bünyamin TÜRKOĞLU and my mother Sema TÜRKOĞLU, and then my siblings Ömer & Tuana. I love you :))

This thesis was supported by TÜBİTAK-ARDEB (program 1001, project number 119M342), TÜBİTAK-BİDEB (2210/C Domestic Priority Doctoral Scholarship Program), Gaziantep University Scientific Research Projects (BAP, project). number MF.YLT.22.21).

TABLE OF CONTENTS

Page

ABSTRACT ..... **v**

ÖZET ..... **vii**

DEDICATION ..... **viii**

ACKNOWLEDGEMENTS ..... **viii**

TABLE OF CONTENTS ..... **ix**

LIST OF TABLES ..... **xi**

LIST OF FIGURES ..... **xii**

LIST OF ABBREVIATIONS ..... **xiv**

CHAPTER 1 INTRODUCTION **1**

1.1 Introduction 1

1.2 Objective of Thesis 2

1.3 Nanofibers and Nanotechnology 3

1.4 Nanofiber Production by Electrospinning 3

1.4.1 Electrospinning 3

1.4.2 Important Parameters in Electrospinning 5

1.5 Nanofiber Alignment in Electrospinning 9

1.6 Graphene Oxide 10

1.6.1 Graphene Oxide Synthesis 10

1.6.2 Application Areas of Graphene Oxide 13

CHAPTER 2 LITERATURE SURVEY **14**

2.1 Polyacrylonitrile/Graphene Oxide Studies 14

2.2 Parallel Electrode Studies 17

CHAPTER 3 MATERIALS AND METHODS **21**

3.1 Materials 21

3.1.1 Materials for Parallel Electrode Study 21

3.1.2 Materials for PAN/GO Study 21

3.2 Method 21
3.2.1 Electrospinning Design and Installation 21
3.2.2 Graphene Oxide Synthesis 22
3.2.3 Nanofiber Fabrication 23
3.3 Characterization 25
3.3.1 GO Characterization 25
3.3.2 Solution Characterization 25
3.3.3 Nanofiber Characterization 26
3.3.4 Statistical Analysis 27
CHAPTER 4 RESULT AND DISCUSSION 28
4.1 Graphene Oxide Study Results 28
4.1.1 SEM Analysis 28
4.1.2 FTIR Analysis 28
4.1.3 XRD Analysis 29
4.1.4 Raman Spectroscopy Analysis 30
4.2 Parallel Electrode Study Results 31
4.2.1 Solution Properties 31
4.2.2 Morphology Analysis 31
4.2.3 Nanofiber Alignment 35
4.3 PAN/GO Study Results 41
4.3.1 Solutions Properties 41
4.3.2 Morphology Analysis 43
4.3.3 Alignment Measurement 46
4.3.4 Structural Analysis 49
4.3.5 Thermal Analysis 52
4.3.6 Mechanical Analysis 55
CHAPTER 5 CONCLUSIONS AND RECOMMENDATIONS 58
REFERENCES 61
CURRICULUM VITAE 84

LIST OF TABLES

Page

Table 1.1 Parameters affecting the electrospinning process 5
Table 1.2 Graphite, graphene and graphene oxide comparison 10
Table 1.3 GO synthesis methods with different oxidants 11
Table 3.1 Production process table for PAN polymer..... 24
Table 3.2 Production process table for PAN/GO solutions..... 25
Table 4.1 XRD analysis results for the 002 plane of graphite and GO..... 29
Table 4.2 The average nanofiber diameters by plate width, gap distance and plate thickness..... 33
Table 4.3 Effect of plate width, gap distance and plate thickness on nanofiber diameter [nm]..... 33
Table 4.4 Deviation [°] from 0° according to electrode widths and gap distance for 1 mm electrode thickness 39
Table 4.5 Deviation [°] from 0° according to electrode widths and gap distance for 1.5 mm electrode thickness 41
Table 4.6 GO addition PAN/DMF electrospinning solution properties..... 42
Table 4.7 Effect of GO ratio on nanofiber diameter [nm]..... 46
Table 4.8 Deviation from 0° result according to different GO ratios 49
Table 4.9 TGA analysis results of PAN and PAN/GO nanofiber bundles..... 53
Table 4.10 DSC data of PAN and PAN/GO nanofiber bundles..... 54
Table 4.11 Productivity and count nanofiber bundle according to GO ratio 55
Table 4.12 Elongation, tensile strength and Young's modulus nanofiber bundle according to different ratio of GO..... 55

LIST OF FIGURES

Page

Figure 1.1 Basic electrospinning set-up 4

Figure 1.2 Some collector types used in electrospinning: a) stationary plate, b) rotating drum, c) rotating disk, d) parallel rings, e) conveyor belt, f) liquid bath, g) metal grid 8

Figure 1.3 Collector types utilized in electrospinning 9

Figure 3.1 Schematic representation of the electrospinning setup to align nanofibers 22

Figure 3.2 a) Aluminum electrodes cut with a laser, b-c) placement of the electrodes into the conveyor belt 22

Figure 3.3 Graphene oxide synthesis steps 23

Figure 3.4 The stages of preparing the PAN/GO solution 24

Figure 4.1 SEM images; a) GO [5 kX], b) GO [30 kX], c) GO [50 kX] 28

Figure 4.2 FTIR spectrum of graphite and GO 29

Figure 4.3 XRD spectrum of graphite and GO 30

Figure 4.4 Raman spectrum of graphite and GO 30

Figure 4.5 SEM images for electrodes with plate thickness of 1 mm [6 kX] 31

Figure 4.6 SEM images for electrodes with plate thickness of 1.5 mm [6 kX] 32

Figure 4.7 Effect of plate width (a), gap distance (b) and plate thickness (c) on nanofiber diameter 34

Figure 4.8 A two-dimensional surface-arrow plot illustrates the electric field strength and vectors within the x-y plane, contingent upon variations in both plate width and gap distance. 35

Figure 4.9 The electric potential exhibits distinct alterations with varying plate widths: a) 5 mm, b) 8 mm, c) 10 mm 36

Figure 4.10 SEM images of PAN nanofibers produced with 1 mm electrode thickness [15 kX] 37

Figure 4.11 Alignment of nanofibers depending on the gap distance for different widths of 1 mm thick electrodes (W): a) 5 mm, b) 8 mm, c) 10 mm 38

Figure 4.12 SEM images of PAN nanofibers produced with 1.5 mm electrode thickness [15 kX] 39
Figure 4.13 Alignment of nanofibers depending on the gap distance for different widths of 1.5 mm thick electrodes (W): a) 5 mm, b) 8 mm, c) 10 mm. 40
Figure 4.14 Conductivity and viscosity changes of the solution according to GO addition ratio 42
Figure 4.15 SEM micrographs and distribution of nanofiber diameters depending on GO ratio [6 kX] 44
Figure 4.16 Effect of GO addition ratio on nanofiber diameters..... 45
Figure 4.17 Effect of GO ratio on nanofiber diameter [nm] 46
Figure 4.18 SEM micrographs and alignments of nanofiber according to different GO ratio [40 kX] 47
Figure 4.19 Alignments of nanofiber bundle according to different GO ratios 48
Figure 4.20 FTIR spectrum of PAN and PAN/GO 50
Figure 4.21 XRD analysis results for 100 plane of PAN and PAN/GO..... 51
Figure 4.22 Raman spectrum of PAN and PAN/GO..... 51
Figure 4.23 TGA analysis of PAN and PAN/GO nanofiber bundles..... 52
Figure 4.24 DSC graph of PAN and PAN/GO nanofiber bundles 54
Figure 4.25 The tensile strength of nanofiber bundle according to GO ratio..... 56
Figure 4.26 The Young's modulus of nanofiber bundle according to GO ratio 57

LIST OF ABBREVIATIONS

AC	Alternative Current
DC	Direct Current
DMF	Dimethylformamide
DSC	Differential Scanning Calorimetry
FE-SEM	Field Emission Scanning Electron Microscopes
FTIR	Fourier Transform Infrared
GO	Graphene Oxide
H_2SO_4	Sulfuric Acid
H_3PO_4	Phosphoric Acid
$KMnO_4$	Potassium Permanganate
kV	Kilo Volts
kX	Magnification, 1000
Mw	Average Molecular Weight
PAN	Polyacrylonitrile
RAMAN	Raman Spectroscopy
RH	Relative Humidity
TCD	Tip to Collector Distance
TGA	Thermogravimetric Analysis
TUBITAK	The Scientific and Technological Research Council of Türkiye
XRD	X-Ray Diffraction

CHAPTER 1
INTRODUCTION

1.1 Introduction

Nanofibers have the potential for many advanced uses thanks to their small pores, high surface area, and superior physical and mechanical properties [1], [2], [3]. Many methods are used for the production of nanofibers, including template synthesis, phase separation, self-assembly, electrospinning, meltblown and bicomponent [4]. Among these methods, the electrospinning method has become a common practice in recent years due to nanofiber quality, efficiency, morphology and wide usage area [5].

In order to increase the current utilization areas of nanofibers, many studies have been carried out to improve the properties of nanofibers by adding different additions. Thus, the produced nanofibers are used for increasing battery capacity [6], [7] improving thermal and tensile strength [7], [8], [9], [10] and air filtration [11], improving the dyeability and hydrophilic properties of fibers [12], [13] in electrochemical sensors [14], heat protective or flame retardant it can be used in material production [15].

Recently, studies on the alignment of nanofibers produced by electrospinning method have accelerated significantly popular. One of the methods is the parallel electrode method [16]. With this method, nanofibers can be directed by manipulating the electric field without any mechanical movement. Studies have shown that the structure and layout of parallel electrodes are effective in aligning nanofibers [17], [18], [19].

However, the general approach in electrospinning studies is to produce nanofibers as a nonwoven surface in a random order. Nonwoven surfaces cannot be used in weaving and knitting areas. For this reason, researchers have carried out improvement studies on the electrospinning mechanism and produced nanofibers in the form of threads to have a wider usage area. It is thought that especially the continuous parallel production

of nanofibers will improve many functional properties, especially mechanical properties.

1.2 Objective of Thesis

Among various production methods of nanofibers, electrospinning is considered the most effective method in terms of simple installation, nanofiber quality and diversity of usage areas. In recent years, many studies have been carried out to improve the morphological, mechanical and thermal properties of nanofibers by adding different additions to them.

Graphene oxide (GO) was synthesized by the modified Hummers method within the scope of the thesis and was added to the polyacrylonitrile (PAN) polymer at different contribution rates (1-5 wt.%). The effect of graphene oxide on the morphological, mechanical and thermal properties of polyacrylonitrile nanofiber bundles were investigated. Thus, the usage areas of the produced nanofibers were expanded. No research has been found in the literature on the continuous parallel production of PAN/GO nanofiber bundles.

The main goal of this thesis is to produce nanofiber bundles with a uniquely designed needleless electrospinning method using parallel electrodes. At the same time, nanofiber bundles were produced in a continuously parallel aligned form with parallel electrodes that will be placed sequentially within the conveyor belt. It is aimed to fulfill the following conditions during the production phase of PAN/GO nanofiber bundles.

- ✓ Obtaining structures in accordance with literature results by applying SEM, FTIR, XRD, TGA and Raman spectroscopy tests to the synthesized GO.
- ✓ Enhancing the parallel alignment of PAN nanofibers with the help of parallel electrodes
- ✓ Homogeneous, beadless and uniform production of PAN/GO nanofibers
- ✓ Increasing the alignment, tensile strength and thermal resistance of nanofiber bundles with GO addition
- ✓ Continuous parallel production of nanofiber bundles

If this thesis is successful, continuous parallel nanofiber bundles were produced with the help of conveyors and was contributed to mass production.

1.3 Nanofibers and Nanotechnology

Nanotechnology has facilitated the precise control of material structures at the nano scale. Nanofibers constitute a subset within the nanotechnology. Although the definition of nanofibers varies according to references, they are generally characterized as fibers with a diameter less than 1 μm [20].

Nanofibers have become increasingly important in recent years due to their special properties such as high specific surface area, permeability, flexibility and biomimetic potential. These special characteristics of nanofibers applicable to a numerous of fields, including energy production [21], energy storage [22], catalysis [23], protective clothing [24], sensors [25], filtration [26] and drug release [27]. The diverse applications of nanofibers highlight their versatility as a material within the domain of nanotechnology, and its potential to offer innovative solutions across various sectors.

1.4 Nanofiber Production by Electrospinning

1.4.1 Electrospinning

Various methods have been used to prepare nanofibers, including template synthesis [28], hydrothermal methods [29], phase separation [30], centrifugation [31], bicomponent spinning [32], drawing [33], solution blowing [34], chemical vapor deposition [35] and electrospinning [36], [37], [38]. Among these methodologies, electrospinning emerges as a notably effective technique to produce polymer-based nanofibers. The distinctive properties of the electrospinning method include its uncomplicated setup, cost-effectiveness, efficacy in nanofiber production, adaptability for straightforward modifications, and potential for industrial-scale application. These properties give electrospinning a distinct advantage compared to alternative techniques [39].

The electrospinning method, discovered by Formals in 1934, is a process that involves producing nanofibers from a solution or molten liquid using high voltage. In the electrospinning method, the fundamental components include a syringe pump to feed the solution, a power source for applying high voltage, and a plate for collecting the nanofibers. The essential elements of the electrospinning system are illustrated in **Figure 1.1**.

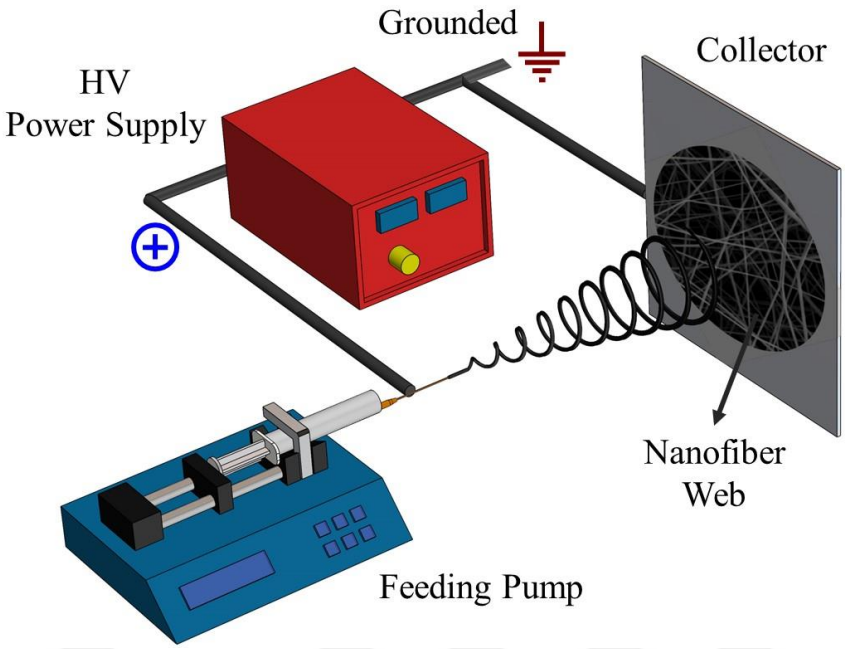

Figure 1.1 Basic electrospinning set-up

In the electrospinning method, a polymer solution is fed through a syringe with a needle via a feeding pump. High voltage is applied to the needle at the tip of the syringe by a power source. Consequently, the solution droplet at the needle tip becomes electrically charged. As the applied voltage increases, the solution droplet converts into a cone shape, and when it overcomes surface tension, a thin jet forms at the Taylor cone's apex. The jet progresses towards the grounded collector, elongating and thinning due to mutual repulsion of like electrical charges. During the progression, the polymer jet initially follows a straight path and later the jet a spiral trajectory called as whipping motion. Meanwhile, the solvent within the polymer solution evaporates, depositing nanofibers randomly onto the collector surface.

The electrospinning setups can be classified into needle and needleless systems about the feeding component. Needle-based electrospinning system confronts challenges such as needle clogging and decreased production rates. In response to these challenges, needleless electrospinning setups have been developed innovatively employed a rotating disk instead of a needle for the fabrication of nanofibers [40]. Furthermore, feeding components such as cylinders [41], [42], [43], [44], [45], [46], [47], [48], [49], cones [50], discs [47], [51], spirals [52], wires [53], [54] and pyramids [55], [56] have been utilized in pertinent investigations. Needleless

electrospinning systems provide a significant advantage in nanofiber productivity compared to needle systems [44], [47], [50], [57].

1.4.2 Important Parameters in Electrospinning

Many factors affect both nanofiber characteristics and the electrospinning process. These factors can be grouped into three main categories; solution parameters, process parameters, and ambient parameters [58], [59]. These parameters are given in **Table 1.1**.

Table 1.1 Parameters affecting the electrospinning process

Solution Parameters	Process Parameters	Ambient Parameters
Molecular weight	Applied voltage	Relative humidity
Concentration	Feed rate	Temperature
Viscosity	Tip to collector distance	Atmosphere type
Surface Tension	Collector type	Pressure
Conductivity	Diameter of pipette orifice	

1.4.2.1 Solution Parameters

One of the factors influencing solution viscosity is the molecular weight of the polymer. When comparing solutions prepared from polymers with high and low molecular weights of the same polymer, it has been observed that the solution with a higher molecular weight polymer exhibits greater solution viscosity [59].

Another factor influencing the viscosity of the solution is the polymer concentration. Similar to molecular weight, an increase in concentration leads to an enhancement in polymer chain complexity, thereby ensuring the continuity of the jet during the electrospinning process [59]. Optimal concentration needs to be determined due to bead formation at low concentrations and detrimental effects at high concentrations.

The electrospinning process, a minimum polymer chain complexity and, consequently, minimum viscosity are required. Excessively high viscosity impedes the smooth pumping of the solution. Additionally, very high viscosity may lead to premature drying of the solution at the tip of the nozzle before the onset of electrospinning [59], [60].

The increase in viscosity is associated with an increase in fiber diameters. This is likely due to the increased resistance to stretching of the solution jet caused by the charges in the jet [59]. Another effect of high viscosity is a smaller collection area. Increased viscosity can prevent the whipping instability of the jet. In this case, the path followed by the jet decreases, resulting in fibers spreading over a smaller area. The reduction in the path followed by the jet leads to less elongation of the solution and the formation of larger diameter fibers [59], [60].

In the electrospinning method, the surface tension of the electrically charged polymer solution must first be overcome. Additionally, surface tension is a parameter that can lead to bead formation even after the formation of the jet. To produce beadless nanofibers, it may be necessary to reduce surface tension. Surface tension causes the free solvent molecules to come together. Naturally, an increase in viscosity will reduce the number of free solvent molecules, thus preventing this agglomeration [59].

The solution undergoes stretching due to the repulsion of charges on its surface in the electrospinning process. If the conductivity of the solution is increased, a greater amount of charge can be conveyed in the electrospinning jet. Solution conductivity can be augmented through the addition of ions, particularly by incorporating salts, resulting in elevated conductivity values for polymer solutions. The higher the conductivity value, the lower the critical voltage level required for application [61].

Although electrical conductivity is beneficial for the electrospinning process, it becomes difficult, and even impossible, beyond a certain limit. In the electrospinning process, it becomes challenging to maintain charges in the droplet at the tip when the solution's conductivity is very high [60], [62].

1.4.2.2 Process Parameters

The application of voltage influences the elongation and acceleration of the jet through the created electric field. With higher applied voltage, the solution will stretch more due to the increased coulomb forces within the jet. This not only leads to a decrease in fiber diameter but also results in obtaining drier fibers by causing faster evaporation of the solvent.

As the voltage increases, the electrostatic repulsive forces on the jet also increase, resulting in reduction in the fiber diameter and, generally, a decrease in bead formation

[59]. However, at very high voltages, an increase in jet instability can occur due to the retraction of the Taylor cone into the needle, leading to an increase in bead formation [58]. Up to a certain value, an increase in voltage reduces bead formation, and the bead shapes transform from spherical to flat. However, with further voltage increase, the beads tend to return to a more spherical form. Thus, there should be an upper limit to the applied voltage [60].

Feed rate is a crucial parameter directly influencing the transfer rate and material spraying speed. It determines the quantity of the polymer solution supplied in the electrospinning method. As the flow rate increases, nanofiber diameters become thicker, and bead formation and size increase. However, there is a limit to the increase in fiber diameter associated with high feed rates [59], [60].

The morphology and structure of electrospun fibers are primarily influenced by the between tip the collector distance (TCD), which is related to the deposition time and the instability range or whipping. When the distance between the collector and the needle tip is reduced, the flying time is reduced but the charge density (CD) is higher. As there may not be enough time for the solvent to evaporate, a shorter flight time can lead to bead formation. On the other hand, a higher CD can accelerate the jet. Therefore, TCD should be optimally defined to produce uniform and smooth electrospun nanofibers [59].

The inner diameter of the needle has a significant impact on the flow of the electrospinning method. A decrease in the needle diameter has been observed to result in a reduction in fiber diameter and bead formation. However, a needle with an excessively small inner diameter does not allow solution droplets to exit from the tip of the needle and can lead to clogging issues [59]. Additionally, it introduces the problem of blockage [60].

The shape of the collector, like the collector material, has an impact on the electrospinning process and the structure of the resulting nanofibers. Various designs of both moving and stationary collectors have been employed in studies. The most used collector is aluminum plates. Additionally, metal grids, rotating drums, rotating disks, conveyor belts, triangular frames, parallel rings, and a liquid bath are used to collect nanofibers produced by electrospinning (**Figure 1.2**) [60].

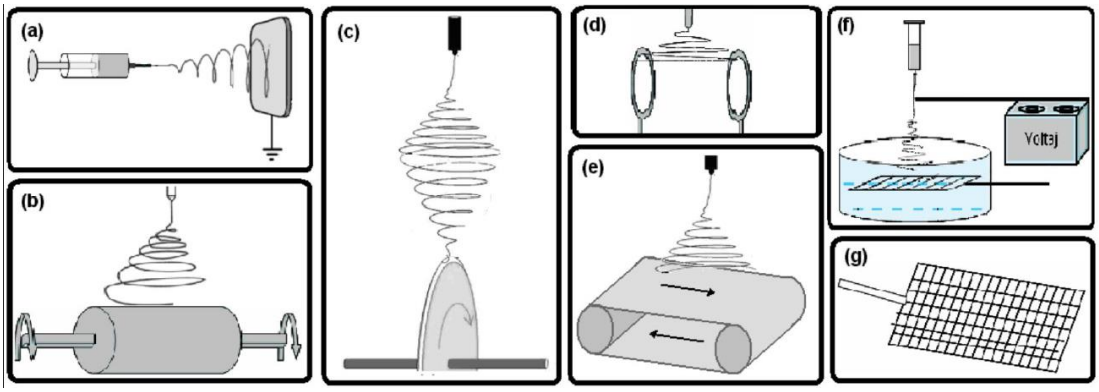

Figure 1.2 Some collector types used in electrospinning: a) stationary plate, b) rotating drum, c) rotating disk, d) parallel rings, e) conveyor belt, f) liquid bath, g) metal grid [62]

1.4.2.3 Ambient Parameters

The high humidity of the environment particularly affects the morphology of fibers obtained through electrospinning, especially when using a volatile solvent in the prepared solutions. Additionally, relative humidity determines the evaporation rate of the solvent. In very low relative humidity, the solvent can evaporate very quickly, even while the solution is still at the tip, resulting in solidification at the tip. This can lead to clogging and consequently hinder electrospinning [59]. In studies examining the relationship between the relative humidity (RH) of the environment and the fiber diameters, an increase in obtained fiber diameters with respect to RH increase, has been observed. In other words, an increase in RH reduces the electric field force required for the thinning of the jet [60].

The temperature of the solution causes a decrease in viscosity and an increase in the evaporation rate. Lower viscosity enables better dissolution of the polymer, resulting in more uniform nanofibers. Additionally, as viscosity decreases, the solution can create more tension, allowing the production of finer fibers [63], [64].

A steady state electrospinning cannot be achieved when the ambient air pressure decreases, as the droplet will easily flow outward. Bubbles can be observed in the droplet at very low pressures, and on the other hand, there may be an electrical arc due to insufficient air [59], [60].

1.5 Nanofiber Alignment in Electrospinning

The collector design plays a crucial role in determining and directing the alignment of nanofiber collection patterns [50], [65]. Consequently, numerous collector types have been investigated to produce uniaxially aligned nanofibers. In various studies, collector types such as cylinder [66], grid [67], parallel electrode [66], [16], plate [68], a bath [69], [59], a disc [70], [71], a needle [72], a membrane [73], a funnel [74], conveyor belt [75] among others have been utilized. These collector types are shown schematically in **Figure 1.3.**

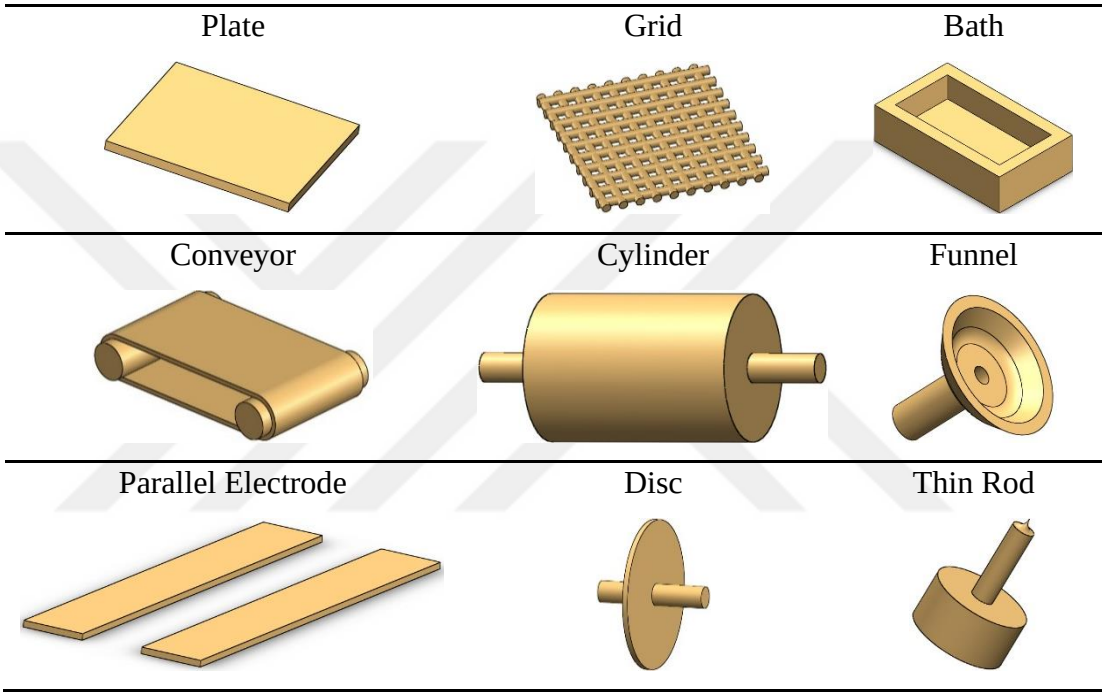

Figure 1.3 Collector types utilized in electrospinning [76]

The conveyor belt from these collectors is crucial for continuous nanofiber production. The conveyor allows the collection of nanofibers in a specific area and facilitates continuous nanofiber production. In a similar manner, a drum collector is crucial for aligned nanofiber production. The production of nanofibers with a drum collector for uniaxial alignment is the oldest and simplest method. In this type of collector, nanofibers are collected on a rotating drum that is unidirectionally aligned due to high-speed rotation. Additionally, there are other collectors such as rotating disks [77], rotating funnels [71], [78], dynamic liquid baths [69], [79] and so forth. The rotation speed of the cylinder is a critical parameter. It affects the alignment and density of the collected nanofibers.

Aligned electrospun nanofibers are also obtained with parallel electrode collectors. The primary advantage of parallel electrodes utilized in aligning nanofibers is their independence from any moving parts. In this method, electrostatic forces on the gap between electrodes lead to the unidirectional alignment and deposition of nanofibers [19], [80], [81]. In the parallel electrode technique, the gap distance between electrodes and characteristics of the plates (width and thickness) are crucial, particularly in terms of aligning nanofibers [17], [18], [19].

1.6 Graphene Oxide

Graphite, graphene, and graphene oxide are all forms of carbon with distinct structures and properties. The comparison table of these three materials is given in **Table 1.2**.

Table 1.2 Graphite, graphene and graphene oxide comparison

	Graphite	**Graphene**	**Graphene Oxide**
Chemical Modal	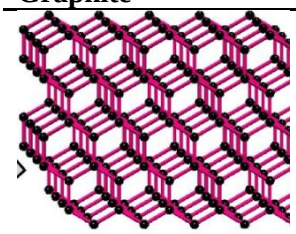	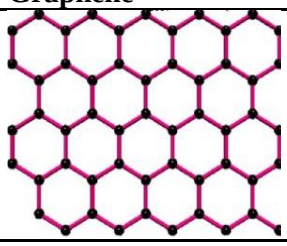	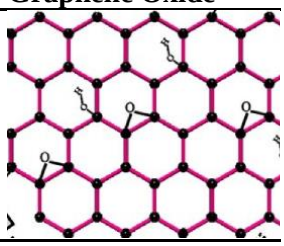
Molecular Structure	Graphite is made up of a hexagonal lattice structure of carbon atoms, with each layer being known as graphene.	The structure of graphene, a two-dimensional material, is formed by a single layer of carbon atoms arranged in a hexagonal lattice.	Graphene oxide is a derivative of graphene that contains oxygen-containing functional groups, obtained through a modification process
Properties	- Conductive - Good mechanical strength	-Highly conductive -Exceptional mechanical strength	- Insulating -Mechanical properties can very depending on the degree of oxidation
Application	- Lubricants - Pencils - Electrodes	- Electronics - Sensors - Composites - Energy storage	- Biosensor - UV protection -Antibacterial activity

1.6.1 Graphene Oxide Synthesis

The chemical synthesis of GO is based on the oxidation of graphite and can be classified according to the oxidant used (**Table 1.3**).

Table 1.3 GO synthesis methods with different oxidants

	Methods	Oxidant	Reaction Temp. Time	(°C)	Specifications
$KClO_3$ Based	Brodie [82]	$KClO_3$, HNO_3	3-4 day	60	Oldest methods, long process, efficient, toxic gas release, explosive reaction
	Staudenmaier [83]	$KClO_3$, HNO_3, H_2SO_4	4 day	25	
	Hofmann [84]	$KClO_3$, HNO_3, H_2SO_4	6-7 day	10-35	
$KMnO_4$ Based	Hummers [85]	$KMnO_4$, H_2SO_4, $NaNO_3$	<2 hour	20-98	Short process, better oxidation, high-quality GO, high metal pollution, toxic gas release, explosive reaction
	Fu [86]	$KMnO_4$, H_2SO_4, $NaNO_3$	<2 hour	35	
	Eigler [87]	$KMnO_4$, H_2SO_4, $NaNO_3$	16 hour	10	
	López-Díaz [88]	$KMnO_4$, H_2SO_4, $NaNO_3$	<2 hour	35	
	Nekahi [89]	$KMnO_4$, H_2SO_4, $NaNO_3$	24 hour	25	
	Drewniak [90]	$KMnO_4$, H_2SO_4, $NaNO_3$	2 hour	5-50	
	Su [91]	$KMnO_4$, H_2SO_4	4 hour	25	Short process, large size GO, efficient
	Sun [92]	$KMnO_4$, H_2SO_4	<2 hour	90	
	Chen [93]	$KMnO_4$, H_2SO_4	<1 hour	20-95	
	Marcano [94]	$KMnO_4$, H_2SO_4, H_3PO_4	12 hour	50	Short process, high quality GO, double component acid, less toxic gas
	Ranjan [95]	$KMnO_4$, H_2SO_4, H_3PO_4	>24 hour	35-95	
	Santamaría-J. [96]	$KMnO_4$, H_2SO_4, H_3PO_4	12 hour	35-50	
	Panwar [97]	$KMnO_4$, H_2SO_4, H_3PO_4, HNO_4	3 hour	50	Short process, high quality GO
	Yu [98]	$KMnO_4$, H_2SO_4, K_2FeO_4, H_3BO_3	5 hour	5-95	Less pollution
Others	Shen [99]	$C_{14}H_{10}O_4$	10 minute	110	Very short process, acid-free
	Chandra [100]	$K_2Cr_2O_7$, H_2SO_4, $NaNO_3$	72 hour	10-98	Long process, safe process
	Peng [101]	K_2FeO_4, H_2SO_4	1 hour	25	Short process, less pollution
	Rosillo-L. [102]	HNO_3	20 hour	25	Nano size GO
	Dimiev [103]	$(NH_4)_2S_2O_8$, H_2SO_4	3-4 hour	25	Less oxidation, high efficiency

Initially, potassium chlorate ($KClO_3$) was employed by Brodie [82]. This method was later modified and improved [83], [84]. These methods are known as $KClO_3$ based GO synthesis methods. Subsequently, potassium permanganate ($KMnO_4$) was used as the oxidant by Hummers [85], and researchers have further developed Hummers method [86], [98] These methods are known as $KMnO_4$ based methods or modified Hummers methods. Both methods have disadvantages, such as the release of toxic gases, the occurrence of explosive reactions, and the formation of polluting metal ions [94].

Although modified methods have been attempted to eliminate these disadvantages, these problems have not been completely resolved [99]. In the literature, different types of oxidants have been used to address these disadvantages [99], [103]. However, the efficiency and oxidation quality of these methods remain debated topics.

The oxidation of graphite was first proposed by Hummers and Offeman in 1958, utilizing potassium permanganate ($KMnO_4$) as the oxidant [85]. In this method, potassium permanganate ($KMnO_4$) is employed as the oxidant. Hummers and Offeman suggested that GO could be obtained by processing it with sulfuric acid (H_2SO_4), sodium nitrate ($NaNO_3$), and potassium permanganate ($KMnO_4$). While this method has advantages such as a short processing time, improved oxidation, and the production of higher-quality GO, it has drawbacks like high metal contamination (Mn_2^+), toxic gas emission (NO_X), and a risk of explosion when the temperature is uncontrolled (Mn_2O_7). Despite addressing some issues with the change of oxidant to, $KClO_3$ problems such as excessive metal contamination and the risk of explosion during the reaction persist [102].

Researchers have contributed to the synthesis of higher-quality GO and the reduction of processing time by modifying the synthesis procedure [86], [90]. Some studies based on $KClO_3$ have excluded the significant role of $NaNO_3$ in the sufficient oxidation of graphite and thus eliminated its use [91], [92]. These studies have emphasized the potential to obtain larger sized GO and reduce the formation of toxic gases. In various research efforts, the oxidation process has been enhanced by excluding $NaNO_3$, increasing the amount of $KMnO_4$, and adding H_3PO_4 [94], [96]. This oxidation technique has increased the oxidation efficiency, resulting in the production of a greater quantity of GO with reduced formation of toxic gases. Two and three-component oxidants have been employed to enhance the oxidation efficiency of GO [97]. The $KMnO_4$ based methods initiated by Hummers are referred to as the modified Hummers method. In addition to $KClO_3$ and $KMnO_4$ based methods, researchers have pursued methods for large scale GO production that are devoid of toxic gases and contaminating heavy metals, and free from explosion risks, emphasizing ultra-fast and cost-effective approaches. Therefore, various types of oxidizing agents have been employed in the production of GO. In this context, researchers have used potent oxidants such as benzoyl peroxide ($C_{14}H_{10}O_4$) [99], potassium dichromate ($K_2Cr_2O_7$)

[100], potassium ferrate (K_2FeO_4) [101], nitric acid (HNO_3) [102], and ammonium persulfate [$(NH_4)_2S_2O_8$] [103]. These methods offer advantages such as large-scale production, short processing times, safe synthesis, lower contamination with heavy metals, higher quality, and high efficiency [99], [100], [101], [103].

1.6.2 Application Areas of Graphene Oxide

GO can impart excellent properties to materials by forming bonds with richly oxygen-containing functional groups. Additionally, the oxygen containing groups expand the interlayer spacing of GO. Thus, GO can introduce new characteristics to the material by entering the spaces between molecules or groups [104]. GO finds applications in textile applications such as UV protection [105], supercapacitors [106], humidity sensors [107], biosensors [108], conductivity [109], electromagnetic shielding [110], antibacterial activity [111], strength and elongation [112], gas permeability [113], and conferring hydrophobic properties [114]. One of its most significant applications is its use as a precursor material for the large-scale preparation of reduced graphene oxide (RGO) or graphene [115].

CHAPTER 2
LITERATURE SURVEY

2.1 Polyacrylonitrile/Graphene Oxide Studies

A literature review has been conducted on producing PAN/GO nanofibers. Summaries of these studies are provided below.

Tiyek et al. [8] conducted a study investigating PAN nanofibers' production parameters and structural characteristics with GO additions. They observed that the prepared GO-modified nanofibers improved thermal resistance and tensile strength. The optimum tensile strength was reported at a 3 wt.% GO addition ratio, showing a 48.8 wt.% increase compared to neat PAN nanofibers.

Zhu et al. [6] found that GO addition increased the rate capacity and stability of lithium-sulfur batteries in PAN nanofibers. They particularly emphasized the self-discharge property of PAN/GO nanofibers. PAN/GO samples with a 3 wt.% addition ratio reported an improvement in the capacity and stability of the batteries.

Abdel-Mottaleb et al. [11] indicated in their study that GO in PAN/GO solution reduces friction in the resulting nanofibers. Consequently, it was observed that it delays sliding between the flow and filter surfaces. Based on mechanical tests of PAN/GO nanofibers, it was determined that the tensile strength increased by 64.6 wt.%, and Young's modulus increased by 71.4 % Thus, GO modified PAN nanofibers were found to be advantageous for mechanical enhancement.

Zhang et al. [116] prepared PAN/GO nanofibers for air filtration using the electrospinning method. It improved the air filtration properties of GO nanofibers. The optimal air filtration performance was reported to be at a 0.05 wt.% GO addition. Moreover, the highest strength was achieved with 0.05 wt.% GO addition. The authors

emphasized that PAN/GO nanofibers have a broad application potential in the air filtration industry, contributing to cleaner air and a healthier living environment.

Hou et al. [9] investigated the hydrophilic and mechanical properties of PAN hybrid nanofibers with GO additions. According to the obtained data, nanofibers with GO additions ranging from 0.1 to 0.4 wt.% exhibited a 50 % increase in hydrophilic properties and a 3-4 times improvement in strength. Additionally, as the amount of GO increased, the nanofiber diameter also increased. The authors recommended the usability of PAN/GO nanofibers for water purification applications. Hou et al. [10] discussed improving PAN nanofibers' structural and mechanical properties with GO additions. They particularly emphasized that GO significantly increased the nanofiber strength while reducing the water contact angle. According to their strength results, they reported that the optimal GO addition was 4 wt.%.

Li et al. [12] investigated the antibacterial activity properties of PAN nanofibers with GO additions. They noted an increase in hydrophilic properties and surface roughness with the addition of GO to PAN nanofibers. Additionally, nanofibers with 0.3 wt.% GO addition showed an antibacterial rate of 98.5 wt.%.

Ghaderi et al. [14] investigated the electrochemical sensor activation property of PAN nanofibers with GO additions in their study. They emphasized the significance of GO-incorporated nanofibers synthesized through various methods for sensors and highlighted their potential to contribute to future research in this field.

Zhang et al. [12] created porous PAN/GO nanofibers to efficiently adsorb chromium (VI) ions. The GO nano-layers, with their hydrophilic oxygen-containing groups, improved the interfacial compatibility between chromium (VI) aqueous solutions and porous PAN/GO nanofibers.

Gergin et al. [15] conducted studies to investigate the oxidation durations of PAN/GO nanofibers at different time intervals (1 and 3 h) and temperatures (25, 250, 280, and 300 °C). They mentioned that the addition of GO to PAN polymer accelerated the final structure's oxidation and development. The authors suggested that PAN/GO nanofibers could find applications in industries requiring heat-resistant and flame-retardant properties, such as protective applications against heat for industrial gaskets and packaging, as well as flame-retardant textiles.

Jang et al. [13] conducted a study in which they performed the electrospinning process of PAN/GO nanofibers using Cetyl Trimethyl Ammonium Chloride (CTAC) as a surfactant. They successfully incorporated GO into the PAN polymer up to 30 wt.% using CTAC, facilitating a nonstop electrospinning process. They noted an increase in water absorbency of the nanofibers due to CTAC, indicating an improvement in the dyeability of PAN/GO nanofibers. The authors reported that with an increase in pore size and thickness of the nanofibers, there could be a significant enhancement in the hydrophilic property, which is crucial for water treatment applications. Additionally, they suggested that GO modified nanofibers could offer advantages in the removal of heavy metal ions and toxic organic compounds under various conditions.

Ashrafi et al. [117] investigated the adsorption of uranium ions from aqueous environments using PAN/GO nanofibers. They examined adsorption capacities by incorporating different amounts of GO into PAN polymer (0.2, 0.4, 0.6 wt.%). The highest adsorption capacity was determined to be 345.084 mg/g at a 0.2 wt.% GO addition ratio.

Zhang et al. [118] investigated the strength of PAN nanofibers with GO additions. The addition of 0.5 wt.% GO to the PAN polymer resulted in the highest strength. According to their findings, the strength increased by 2.45 times. However, as the concentration of GO increased, they observed a restriction in the movement of molecular chains due to excessive interaction. They suggested that further studies on mechanical stretching should be conducted to enhance mobility by increasing the heat treatment temperature.

Almafie et al. [7] investigated the impact of adding different amounts of GO (0.04, 0.14, and 0.24) to PAN polymer on the morphological, mechanical, and dielectric properties of nanofibers. The nanofibers produced with the lowest GO content exhibited a Young's modulus of 2.16 MPa, while those with the highest GO content measured 23.50 MPa. Additionally, the relative permeability increased from 32.2 to 86.4 with the increasing amount of GO. As a result, it was reported that the study could serve as an example for the preparation of PAN/GO composite materials with superior properties for use in energy storage applications.

2.2 Parallel Electrode Studies

A literature review was conducted on the gap distance between electrodes, electrode width, and electrode thickness for the alignment of nanofibers. Into parallel electrode studies summaries of these studies are provided below.

Liu and Dzenis et al. [119] investigated the impact of gap distance and residual charges on nanofiber alignment using the traditional parallel electrode method. The parameters included a PEO solution concentration of 4.5 wt.% by weight, a TCD of 40 cm, applied voltage of 12 kV, and electrode gap distances of 3-18 cm. They conducted their studies, observing that an increase in the electrode gap distance led to enhanced alignment. The optimum gap distance was determined to be 18 cm.

Yan et al. [120] investigated the production of directed electrospun nanofibers using dielectric materials. Their studies were conducted with PVA polymer under the conditions of a 10 cm TCD, 5 cm gap distance, and 15 kV. Firstly, they used an epoxy resin collector with an approximate gap distance of 4 cm. Secondly, they replaced the epoxy resin collector with ferrite, setting the electrode gap distance to approximately 6 cm. While the nanofibers in the first study were produced randomly, in the second study, they successfully achieved the production of aligned nanofibers.

Vasudha Chaurey et al. [121] studied the impact of gap distance on nanofiber alignment. They conducted their studies with 15 wt.% PLAGA, a 5 cm TCD, 10 kV voltage, and gap distances ranging from 0.2 mm to 20 cm. As a result, they demonstrated that an increase in the gap distance led to an enhancement in the alignment of nanofibers.

Pokorny et al. [122] investigated the impact of gap distance on nanofiber alignment. The parameters included 16 wt.% PVA polymers, a TCD of 16 cm, voltage ranging from 20 to 25 kV, and gap distances of 1-45 mm. They observed that as the gap distance increased, nanofiber alignment initially increased and then decreased. They determined that the best results were achieved with a 10 mm gap distance.

Wei Liang et al. [47] evaluated the influence of gap distance on nanofiber alignment. They conducted their studies with a 16 wt.% PVA concentration, gap distances of 4-6 cm, TCD of 6-10 cm, and applied voltages of 12-18 kV. According to the researchers, a larger gap between electrodes resulted in less aligned nanofibers. They highlighted

the order of importance as applied voltage, spinning distance, and electrode gap distance. They specified the optimum values as 12 kV of voltage, 6 cm of TCD, and 5 cm of gap distance.

Yusril Yusuf et al. [123] investigated the impact of gap distance and solution concentration on the diameter and alignment of nanofibers. They conducted their studies with PVA polymer at concentrations of 11-19 wt.%, a voltage of 15 kV, TCD of 9 cm, and gap distances of 5-20 mm. They noted that increasing the gap distance decreased the alignment of nanofibers, and the nanofiber diameter would initially decrease and then increase again. However, they mentioned that as the concentration increased, the average diameter of nanofibers also increased, while the concentration did not affect the alignment. They stated that the best alignment occurred for a 10 mm gap distance with a 15 wt.% PVA concentration.

Rouhollah Jalili et al. [19] investigated the effect of gap distance and charge density on the alignment of nanofibers. The process parameters included 15 wt.% PAN polymer, gap distances of 2-5 cm, applied voltages of 10-13 kV and a TCD of 15-20 cm. They found that as the gap distance increased, the alignment of nanofibers initially increased and then decreased. They stated that the optimal result was achieved with a 3 cm of gap distance. Additionally, they observed that an increase in applied voltage initially led to an increase in nanofiber alignment, followed by a decrease.

Xiaomei Cai et al. [124] researched producing highly aligned and very long nanofibers using the electrospinning method. They carried out their studies with a 12 wt.% PVDF polymer concentration and gap distances of 1-60 cm. As a result, they concluded that well-aligned fibers with lengths exceeding half a meter could be produced, and they identified the optimal gap distance as 50 cm.

Christopher Fryer et al. [125] studied the impact of gap distance on the modulus, alignment, and diameter of nanofibers using the conventional parallel plate method. They conducted their studies with an 8 wt.% POE polymer concentration, 20 cm TCD, 18 kV voltage, and gap distances of 4-10 cm. They found that increasing the gap distance improved the alignment of nanofibers, and they specified the optimal value as a 10 cm gap distance. Additionally, they discovered that electrostatic alignment

produced smaller diameter fibers compared to non-aligned fibers, and aligned nanofibers had, on average, a finer diameter than non-aligned nanofibers.

İçoğlu et al. [16] investigated the effects of gap distance and plate width, CD and TCD on the alignment of PVA nanofibers under three main categories. Initially, they examined gap distance at intervals of 1-5 cm and plate widths of 1.5-30 mm. In the second study, CD parameters were investigated at 1-3 cm, and in the third study, TCD parameters were examined at 9-21. Generally, as the gap distance increased, the average diameter decreased. The optimal alignment formations occured at 1 kV/cm CD. The alignment of nanofibers decreases while the average diameter increased with an increase in CD. As TCD increases, the alignment of nanofibers decreased, but the average nanofiber diameter did not seem to have a significant impact.

He et al. [126] investigated the impact of electrode height and inter-electrode gap distance on the alignment of nanofibers in their study. They set the working parameters as voltage at 15 kV, distance at 6 cm, and electrode at 0.5-7.5 cm. According to the experimental results, they stated that relatively better nanofiber alignment would be achieved when the electrode plates' height was 5.5 cm. In the inter-electrode gap distance study, the parameters were set as height at 5.5 cm, voltage at 15 kV, and inter-electrode gap distances at 2-12 cm. The study's results showed that the highest nanofiber alignment was observed at a 6 cm gap distance.

Yıldırım et al. [76] investigated the effects of plate width, gap distance, and plate thickness on the alignment of PAN nanofibers. The parameters in the study were given as plate widths of 5-15 mm, gap distances of 20-40 mm, and plate thicknesses of 1 and 1.5 mm, respectively. Additionally, an auxiliary electrode was employed to enhance nanofiber alignment. However, the obtained results revealed that the nanofibers exhibited alignment along the x and y axes.

Researchers also examined the impact of the gap distance on the average diameter of nanofibers [19], [121], [123], [127], [128]. Ishii et al. [127] and İçoğlu et al. [128] discovered that the typical nanofiber diameter decreased as the gap distance increased. Whereas, Yusuf et al. [123] noted that the gap distance initially decreased, followed by an increase in nanofiber diameter.

In the literature provided above, the addition of GO to PAN polymer has been observed to induce various changes in the mechanical, physical, and thermal properties of nanofibers. Furthermore, variations in the results have been identified depending on the quantity of GO utilized. Only needle-based electrospinning has been employed in all PAN/GO studies. Moreover, there is only one study on PAN/GO with parallel electrodes [7]. This thesis possesses original significance by aiming to achieve the continuous (using a conveyor belt) and parallel aligned (using parallel plates) production of PAN/GO nanofiber bundles for mass production (using the needleless electrospinning method). Firstly, the effects of plate thickness, gap distance, and plate width on the alignment and morphology of electrospun PAN nanofibers were investigated. Secondly, GO synthesis and analysis were performed. Lastly, the nanofibers were electrospun by incorporating GO into PAN solutions at different addition ratios, alignment, morphological, mechanical, structural, and thermal properties of electrospun nanofiber bundles were examined.

CHAPTER 3
MATERIALS AND METHODS

3.1 Materials

3.1.1 Materials for Parallel Electrode Study

The polymer used as a constituent in the preparation of electrospinning solutions, polyacrylonitrile polymer (PAN, Mw = 150,000 g/mol), was procured from Aksa Acrylic Chemical Industry Inc. (Yalova, Turkey), while the solvent used, dimethylformamide (DMF, C_3H_7NO), was sourced from Sigma Aldrich.

3.1.2 Materials for PAN/GO Study

Graphene oxide synthesis materials, including graphite (<20 μm), sulfuric acid (H_2SO_4, wt.% 96.4), hydrogen peroxide (H_2O_2, wt.% 30), sodium nitrate ($NaNO_3$), and potassium permanganate ($KMnO_4$), were obtained from Merck.

3.2 Method

3.2.1 Electrospinning Design and Installation

A needleless electrospinning setup was employed in this study. Helical spinnerets were utilized as the solution-feeding component. The schematic representation of the employed electrospinning apparatus is presented in **Figure 3.1**. To produce a bundle of nanofibers, two helical spinnerets were used. The helical spinnerets were placed in a Teflon bath and rotated at 9 rpm through a DC motor. A high-voltage positive power supply (Spellman, SL70P300W, Hauppauge, United States) was connected to the helical spinnerets. A conveyor belt, made of polyurethane with a thickness of 0.5 mm and moving at a speed of 15 cm/min, was employed as the collector. Aluminum plates were positioned in the middle of the conveyor belt as parallel electrodes (**Figure 3.2**). Subsequently, a negative voltage was applied to the plates through a high-voltage power supply (Spellman, SL40N30W, Hauppauge, United States).

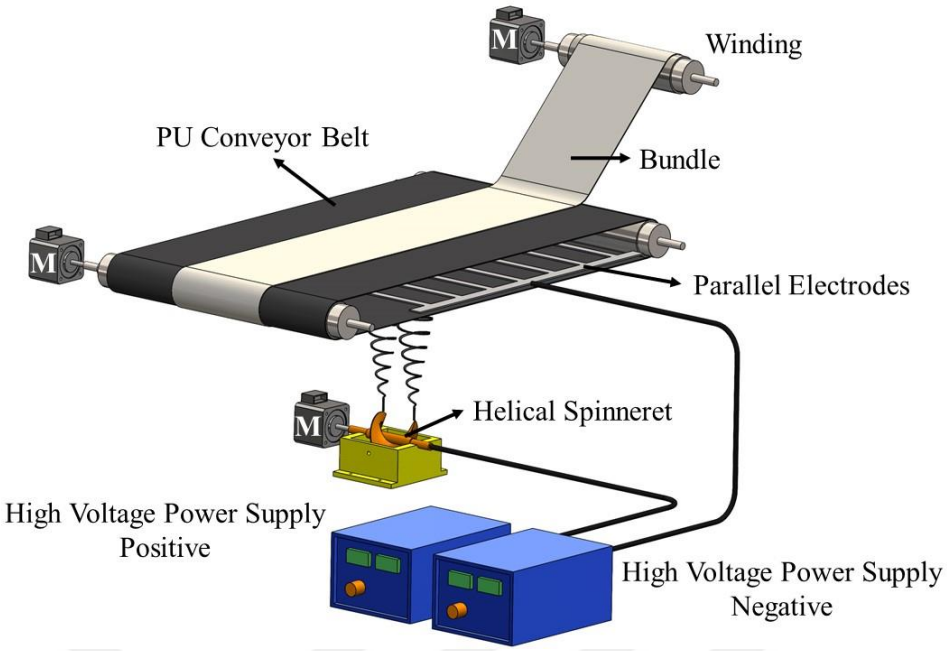

Figure 3.1 Schematic representation of the electrospinning setup to align nanofibers

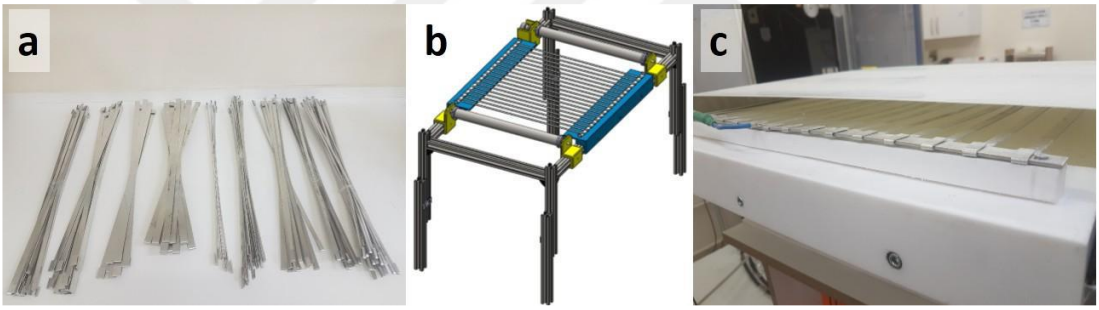

Figure 3.2 a) Aluminum electrodes cut with a laser, b-c) placement of the electrodes into the conveyor belt.

3.2.2 Graphene Oxide Synthesis

The modified Hummers method, a chemical approach, was employed for the synthesis of GO from graphite [129]. This method comprised five stages, and images depicting the synthesis stages are provided in **Figure 3.3**. In the first stage, 5 g of graphite powder, 2.5 g of sodium nitrate ($NaNO_3$), and 115 mL of sulfuric acid (H_2SO_4) were stirred in an ice bath at approximately 5° C for 1 hour (**Figure 3.3**a-b). In the second stage, a strong oxidizing agent, 15 g of potassium permanganate ($KMnO_4$), was slowly added to the mixture, and the solution was stirred for 2 hours, ensuring it did not exceed 35 °C (**Figure 3.3**c-d). In the third stage, 500 mL of deionized water was added to the mixture and stirring continued at 35° C for 1 hour (**Figure 3.3**e-f). In the fourth stage, 10 mL of hydrogen peroxide (H_2O_2) with a concentration of 30 wt.% was added to the

mixture and stirring continued for an additional 2 hours (**Figure 3.3**g-h). After these processes, in the fifth stage, the mixture was filtered with deionized water until the pH of the filtrate reached 7 (**Figure 3.3**i-j). Finally, the dark brown material remaining on the filter paper, appearing as a dense mud (**Figure 3.3**k), was dried in an oven at 50 °C for 24 hours (**Figure 3.3**m) to obtain graphene oxide in powder form (**Figure 3.3**n).

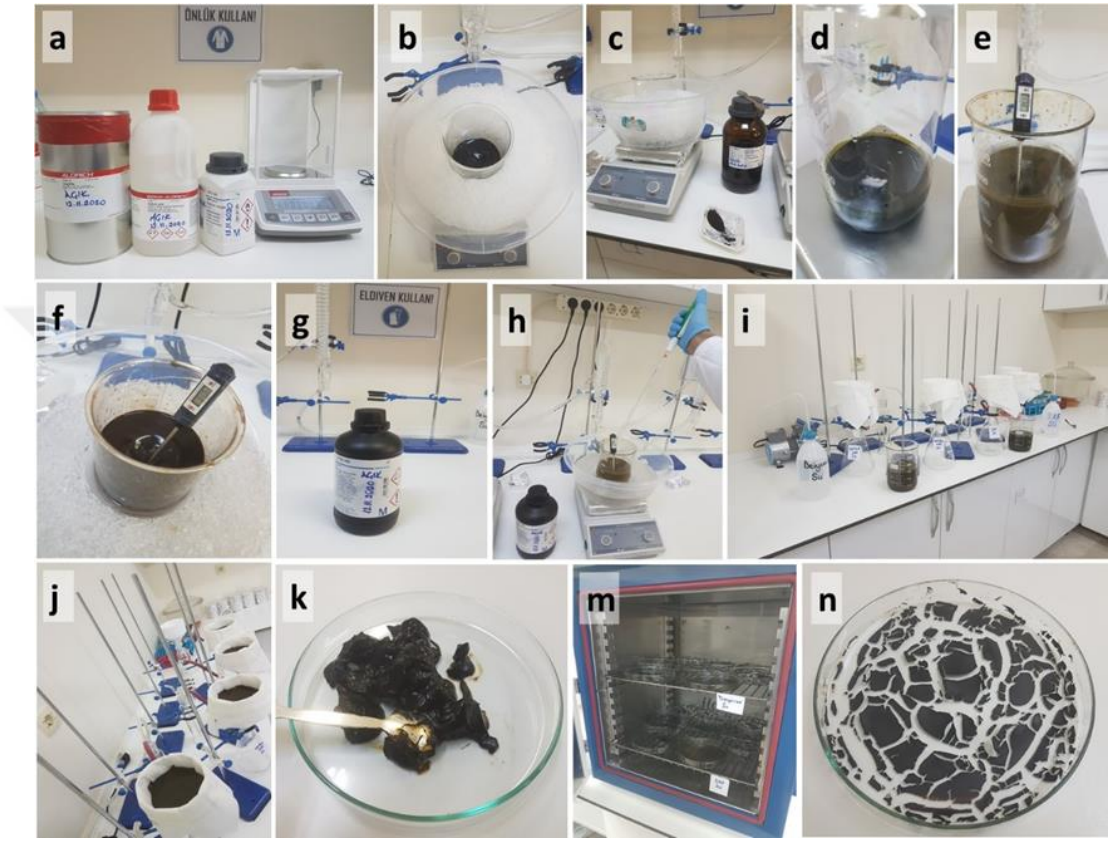

Figure 3.3 Graphene oxide synthesis steps

3.2.3 Nanofiber Fabrication

3.2.3.1 PAN Nanofiber Fabrication

PAN was used as the polymer, and DMF was used as the solvent in electrospinning studies. PAN/DMF solution 12 wt.% was prepared by stirring in a beaker at 80 °C for 4 hours, and the solution was prepared for the electrospinning process.

According to the study parameters, plates were placed inside the conveyor. All plates were centrally aligned on the conveyor belt. The conveyor belt was held stationary, and a black Teflon sheet was placed on it. In the electrospinning method for producing PAN nanofibers, the applied voltage, TCD, ambient temperature and RH were kept constant at 54 kV (+46 kV, -8 kV), 18 cm, 25 ± 1 °C, and 50 ± 5%, respectively. The

independent variables and their value ranges investigated in this study are provided in **Table 3.1**.

Table 3.1 Production process table for PAN polymer

Plate Thickness (mm)	Gap Distance (mm)	Plate Width (mm)
1	20 - 30 - 40	5 – 8 – 10
1.5	20 - 30 - 40	5 – 8 – 10

3.2.3.2 PAN/GO Nanofiber Fabrication

To prepare PAN/GO solutions, PAN polymer dissolved in DMF solvent at a 12 wt.% concentration, stirring for 4 hours at 80 °C. For the PAN/GO nanofiber production, GO at specified ratios was dispersed in DMF in a separate container using an ultrasonic bath at 24 °C for 2 hours. This ultrasonic process helped prevent the clumping and settling of GO in the PAN solution, ensuring a more even distribution.

The resulting GO mixtures were slowly added drop by drop to the PAN solution with a burette and stirred overnight at 80 °C. We repeated this process for each 1-5 wt.% GO addition ratio according to PAN polymer weight. Additionally, a pure PAN solution was used as a reference. The steps for preparing PAN/GO solutions are shown in **Figure 3.4**.

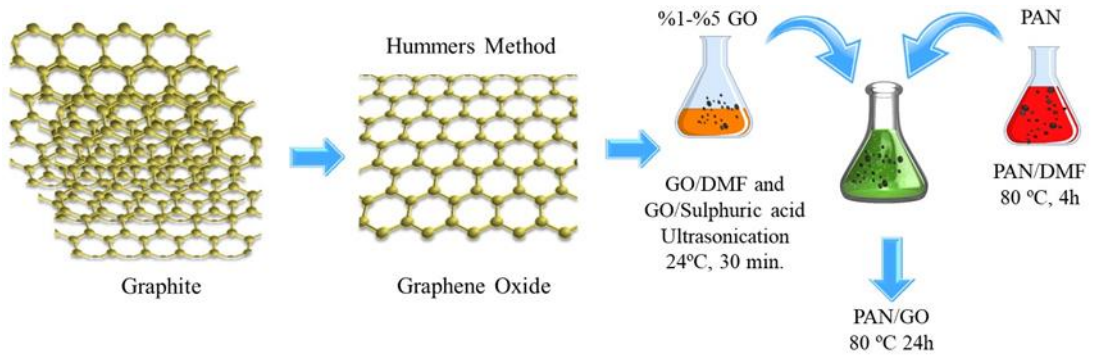

Figure 3.4 The stages of preparing the PAN/GO solution

The parallel electrode study involved placing the selected plates inside the conveyor. All plates were centrally aligned in the conveyor belt. In the electrospinning method for producing PAN/GO nanofibers, the applied voltage, TCD, ambient temperature, and RH were kept constant at 61 kV (+53 kV, -8 kV), 18 cm, 25 ± 2 °C, and 50 ± 5%,

respectively. The parallel electrode study, the independent variable (GO ratio) and the range of values investigated, along with the parallel electrode parameters selected for the study, are presented plate thickness 1.5 mm, gap distance 40 mm, plate width 40 mm. In the production of PAN/GO nanofiber bundles, the high voltage was adjusted according to the highest GO contribution rate of 5 wt.%.

Table 3.2 Production process table for PAN/GO solutions

Sample Code	PAN (wt.%)	GO (wt.%)	Solid Matter Ratio (wt.%)
PAN	12	0	12
PAN/GO1	11.88	0.12	12
PAN/GO2	11.76	0.24	12
PAN/GO3	11.64	0.36	12
PAN/GO4	11.52	0.48	12
PAN/GO5	11.40	0.60	12

3.3 Characterization

3.3.1 GO Characterization

In the parallel electrode study, Scanning Electron Microscopes (SEM) images were captured at magnifications of 5 kX, 30 kX, and 50 kX using the Field Emission Scanning Electron Microscopes (FE-SEM) ZEISS Gemini SEM 300 instrument. Fourier Transform Infrared Spectrometer (FTIR) analysis was conducted with a Diamond ATR Reflectance module on the Shimadzu IRTracer100 device. For Thermogravimetric Analysis (TGA), samples were tested on the Exstar TG/DTA 6300 apparatus with a nitrogen flow rate of 100 ml/min, a heating rate of 5 °C/min, and a temperature range of 0-700 °C. X-ray Diffraction (XRD) analyses were performed on the Philips X'Pert PRO diffractometer device. Raman Spectroscopy analyses were carried out on the RENISHAW in Via instrument with a 785 nm laser source.

3.3.2 Solution Characterization

Viscosity, conductivity, and surface tension analyses of GO added PAN solutions were performed. A Brookfield DV-3 Ultra® rheometer was used to measure the viscosity of the polymer solutions, an Attension Theta® optical tensiometer device was employed for measuring surface tension, and an Orion 4 Star Plus® pH and conductivity meter device was used for conductivity measurements. All measurements were conducted at a solution temperature of 25 ºC ± 1 ºC.

3.3.3 Nanofiber Characterization

3.3.3.1 Morphological Properties

SEM images were again utilized for morphological examination. An image processing program (Image J) was employed to measure the diameters of nanofibers. The average diameter and standard deviation of nanofibers were determined by averaging 30 measurements. SEM images at 2 kX magnification were used for morphology results and 15 kX magnification for nanofiber diameter measurements.

3.3.3.2 Nanofiber Alignment Measurement

The arrangement of consecutive parallel plates inside the conveyor was intended to create a regular and parallel pattern in nanofibers, where they follow each other in an orderly manner.

SEM images were captured at magnifications of 2 kX, 6 kX, 10 kX, and 15 kX using the FE-SEM ZEISS Gemini SEM 300 instrument. Using an image processing program (Image J), the alignment of each nanofiber was determined by measuring the angle distribution in SEM micrographs. The angles of the nanofibers were calculated by measuring their deviation from a reference line drawn horizontally across the top of the image. The nanofibers were produced in the 30 seconds for SEM images. The conveyor was stationary to obtain the SEM micrographs during the production of the nanofibers. Black glassine papers with a 50 g/m^2 density were adhered to the constant conveyor to take SEM images.

The electric field distribution across different parallel electrode arrangements in electrospinning was studied through a three-dimensional finite element analysis using the electrostatics module in COMSOL Multi-physics™ 6.1.

3.3.3.3 Mechanical Properties

Tensile strength and elongation of nanofiber bundles were measured using a Titan brand universal mechanical testing machine according to the EN ISO 2062 standard. The nanofiber bundles were transformed into a linear form by giving them a slight twist. Measurements were taken from 10 different samples, each being 50 cm long, and the averages were calculated. The distance between the jaws was set to 250 mm, the pre-tension to 0.50 cN/tex, and the extension rate to 250 mm/min. The samples were conditioned under standard laboratory conditions before testing.

3.3.3.4 Structural Properties

FTIR analysis was performed using the Diamond ATR Reflectance module on the Shimadzu IRTracer100 device. XRD analyses were carried out using the Philips X Pert PRO diffractometer device. Raman Spectroscopy analyses were conducted on the RENISHAW inVia instrument with a 785 nm laser source.

3.3.3.5 Thermal Properties

Differential Scanning Calorimetry (DSC) analyses were conducted on the Shimadzu DSC-60 apparatus within the temperature range of 25-350 °C, using a heating rate of 10 °C/min and a nitrogen flow rate of 100 mL/min.

TGA was performed on the Exstar TG/DTA 6300 apparatus within the temperature range of 0-800 °C and a nitrogen flow rate of 100 ml/min. For PAN/GO nanofiber samples, the heating rate was set at 10 °C/min, while for GO, it was conducted at a heating rate of 5 °C/min.

3.3.4 Statistical Analysis

Statistical analysis was conducted using JMP statistical software (trial version). To evaluate the effects of parallel electrodes and GO addition on diameter and alignment, statistical variance analysis (ANOVA) and the Tukey-Kramer test were employed. The data analysis was complemented with visual and self-explanatory graphics. Significance was determined at a threshold of $p \leq 0.05$.

CHAPTER 4
RESULT AND DISCUSSION

4.1 Graphene Oxide Study Results

4.1.1 SEM Analysis

Images of the layered GO structure were taken with the SEM device at magnifications of 5 kX, 30 kX, and 50 kX (**Figure 4.1**). It was observed that the layered GO seen in the SEM images were dispersed in single or several layers (**Figure 4.1**a). GO structures approximately 4-5 microns in size were observed (**Figure 4.1**b). These results were consistent with the literature [130], [131]. Whitish areas in the images indicate that the layer was thinner.

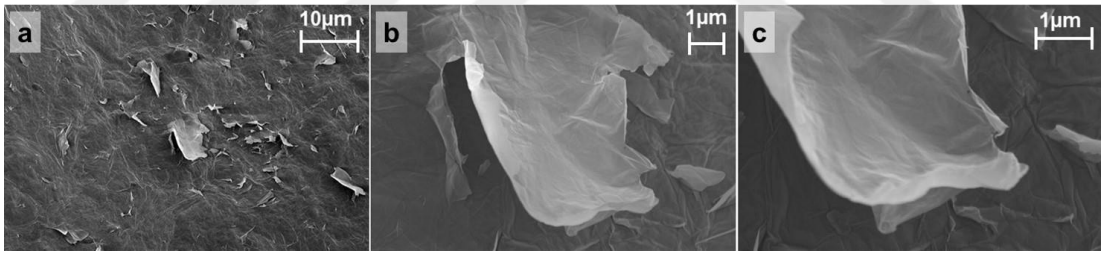

Figure 4.1 SEM images; a) GO [5 kX], b) GO [30 kX], c) GO [50 kX]

4.1.2 FTIR Analysis

Functional groups and bond structures in GO were examined by FTIR spectroscopy. FTIR spectrum of graphite and GO are given in **Figure 4.2**.

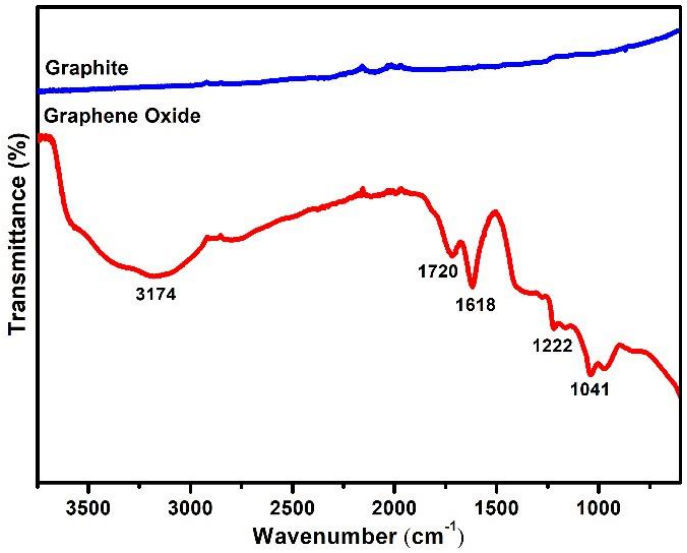

Figure 4.2 FTIR spectrum of graphite and GO

Functional bond structures were not observed in the spectrum of graphite. However, different bond structures were formed in GO obtained from graphite. In the FTIR spectrum of GO, alkoxyl bond (C-O) at 1041 cm^{-1}, epoxy bond (C-O) at 1222 cm^{-1}, aromatic bond (C=C) at 1618 cm^{-1}, carbonyl bond (C=O) at 1720 cm^{-1}, and hydroxyl bond (-OH) at 3174 cm^{-1} were evident. The presence of these bond structures in the graphene oxide spectrum, which were not present in graphite, indicated the successful occurrence of oxidation. These results were consistent with the existing literature [65], [129], [132], [133].

4.1.3 XRD Analysis

Crystalline properties of GO layers and interlayer changes were examined by XRD. The analysis results for the 002 plane are given in **Table 4.1** and the XRD graph of graphite and GO is given in **Figure 4.3**. It was similar to the literature that the 26.44° peak in the graphite structure was not seen in GO after oxidation, and instead the 10.51° peak was formed [130].

Table 4.1 XRD analysis results for the 002 plane of graphite and GO

	Peak Position (2θ)	Peak Height (cts)	D- Spacing (Å)
Graphite	26.4375°	3123	0.337
GO	10.5125°	468	0.841

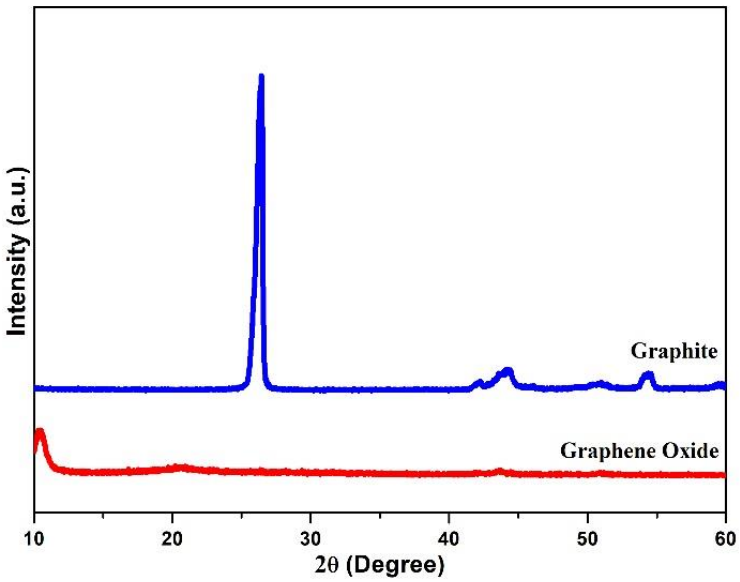

Figure 4.3 XRD spectrum of graphite and GO

The d-spacing of between planes, which was 0.337 nm in graphite, was measured as 0.841 nm in GO. These results prove that graphite was a carbon-based material that was highly oriented by its transformation into GO [129], [130].

4.1.4 Raman Spectroscopy Analysis

The crystal structures of graphite and GO were examined by Raman spectroscopy. Raman spectrum of graphite and GO are shown in **Figure 4.4**.

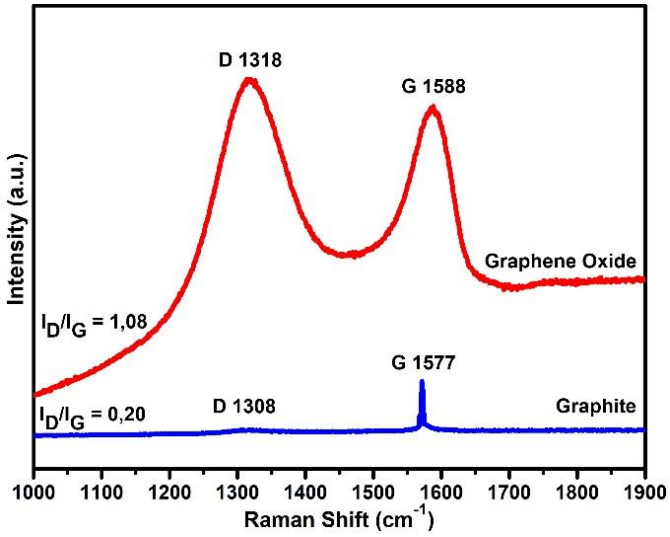

Figure 4.4 Raman spectrum of graphite and GO

In the spectrum, regular structures in carbon are expressed with the G (sp^2) band, and irregular and amorphous structures are expressed with the D (sp^3) band. [65], [131], [132].

In the Raman spectrum of GO, the D peak was detected as 1318 cm^{-1} and the G peak was detected as 1588 cm^{-1}. The I_D/I_G ratio of the GO structure was determined as 1.08. As can be seen from the spectra and I_D/I_G ratios, regular structures in GO outnumber irregular structures. Therefore, it has been determined that regular structures were formed. These results of GO were found to be compatible with the literature [129], [130].

4.2 Parallel Electrode Study Results

4.2.1 Solution Properties

Viscosity, surface tension and conductivity of PAN/DMF solution (12 wt.%) were approximately 820 cP, 37.8 mN/m and 77.8 μS/cm at 25˚C, respectively.

4.2.2 Morphology Analysis

SEM images were examined for plate thicknesses of 1 and 1.5 mm. SEM images for electrodes with a plate thickness of 1 mm are given in **Figure 4.5**.

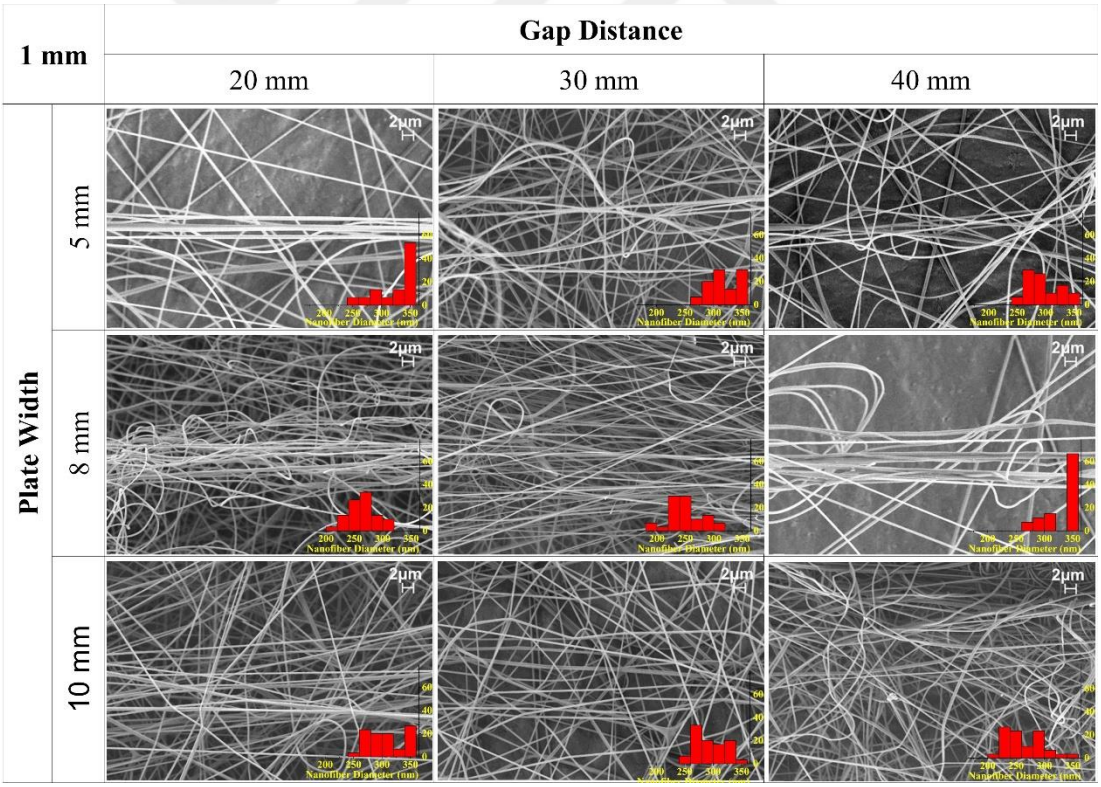

Figure 4.5 SEM images for electrodes with plate thickness of 1 mm [6 kX]

SEM images showed that the nanofibers produced with 1 mm thick electrodes were beadless and uniform. Nanofibers have different alingments depending on the gap distance and plate width. It has been observed that nanofiber diameter distributions

vary according to plate width and gap distance. The widest diameter distribution was seen in the sample with plate width 10 mm and gap distance 40 mm, and the lowest diameter distribution was seen in the sample with plate width 8 mm and gap distance 30 mm. SEM images for electrodes with a plate thickness of 1.5 mm are given in **Figure 4.6**.

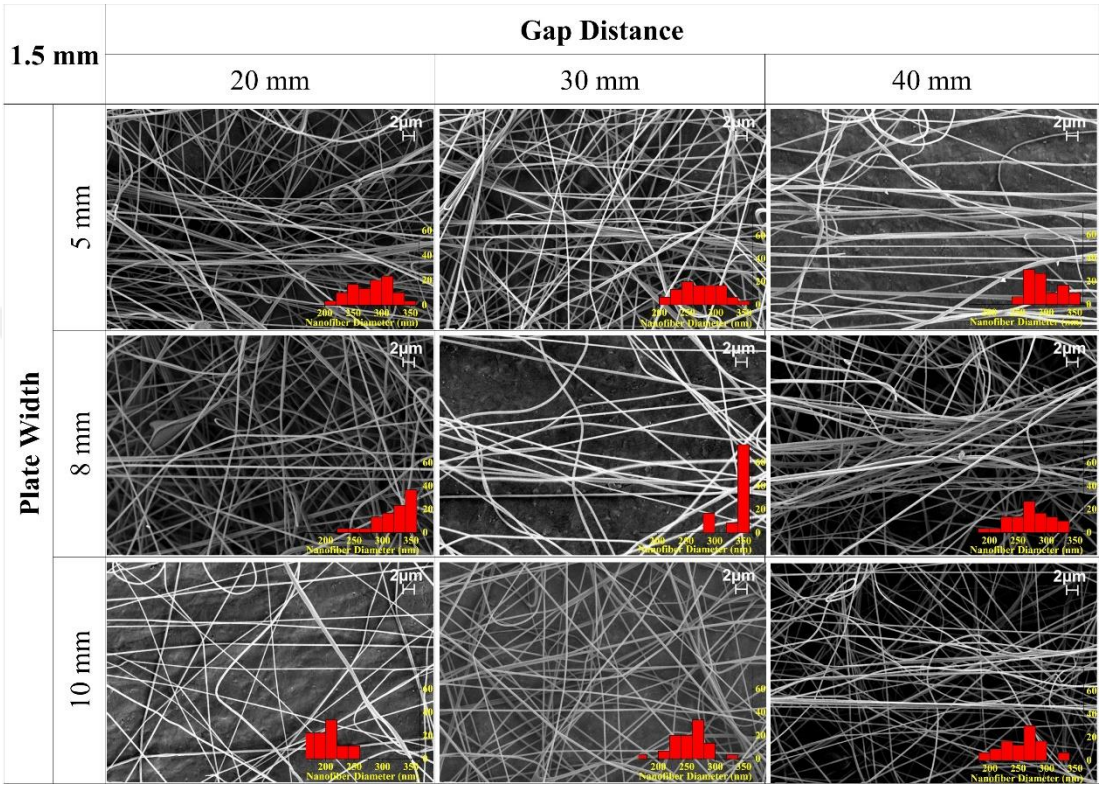

Figure 4.6 SEM images for electrodes with plate thickness of 1.5 mm [6 kX]

SEM images showed that the nanofibers produced by 1.5 mm thick plates were beadless and uniform. The widest diameter distribution was seen in all samples with plate width 5 mm, and the lowest diameter distribution was seen in the sample with plate width 8 mm and gap distance 30 mm. In general, it has been determined that nanofiber distributions occur in a wider area than the 1 mm plate width.

The average diameters of the nanofibers are given in **Table 4.2**. The average nanofiber diameters in all samples ranged from 203 to 380 nm. It has been observed that plate width and gap distance have an effect on nanofiber diameters. However, no significant relationship could be established for these changes.

Table 4.2 The average nanofiber diameters by plate width, gap distance 5and plate thickness

Plate Width (mm)	Gap Distance (mm)	1 mm Thickness (nm)	1.5 mm Thickness (nm)
5	20	338 ± 46	285 ± 38
	30	326 ± 37	272 ± 39
	40	298 ± 29	277 ± 53
8	20	265 ± 25	325 ± 36
	30	250 ± 32	380 ± 59
	40	364 ± 60	274 ± 36
10	20	309 ± 34	203 ± 27
	30	295 ± 28	256 ± 31
	40	267 ± 36	228 ± 27

Effect of combined plate width, gap distance and plate thickness on nanofiber diameter was given in **Table 4.3** and **Figure 4.7**.

Table 4.3 Effect of plate width, gap distance and plate thickness on nanofiber diameter [nm]

Property	Level	Number			Mean	SD	LL	UL	Prob>F
Plate Witdh (mm)	5	149	A		297.8	44.5	289.5	306.1	**0.0001**
	8	159	A		300.6	61.3	292.6	308.6	
	10	120		B	274.6	43.8	265.4	283.8	
Gap Distance (mm)	20	135	A		300.6	42.9	291.8	293	**0.0193**
	30	132	A	B	294.6	52.9	285.4	285	
	40	161		B	283.7	57.9	275.7	274	
Plate Thickness (mm)	1	252	A		298.3	50.1	291.9	304.8	**0.0044**
	1.5	176		B	283.7	54.4	276.1	291.4	

Note: *Sub-levels of a variable are classified by alphabetical capital letters (e.g. A, B, C). The sub-levels not connected by the same alphabetical capital letter are significantly different from each other at significance level of 0.05. n:number of observations, SD: standard deviation, LL: lower limit, UL: upper limit. Limits are based on a confidence level of 95%.*

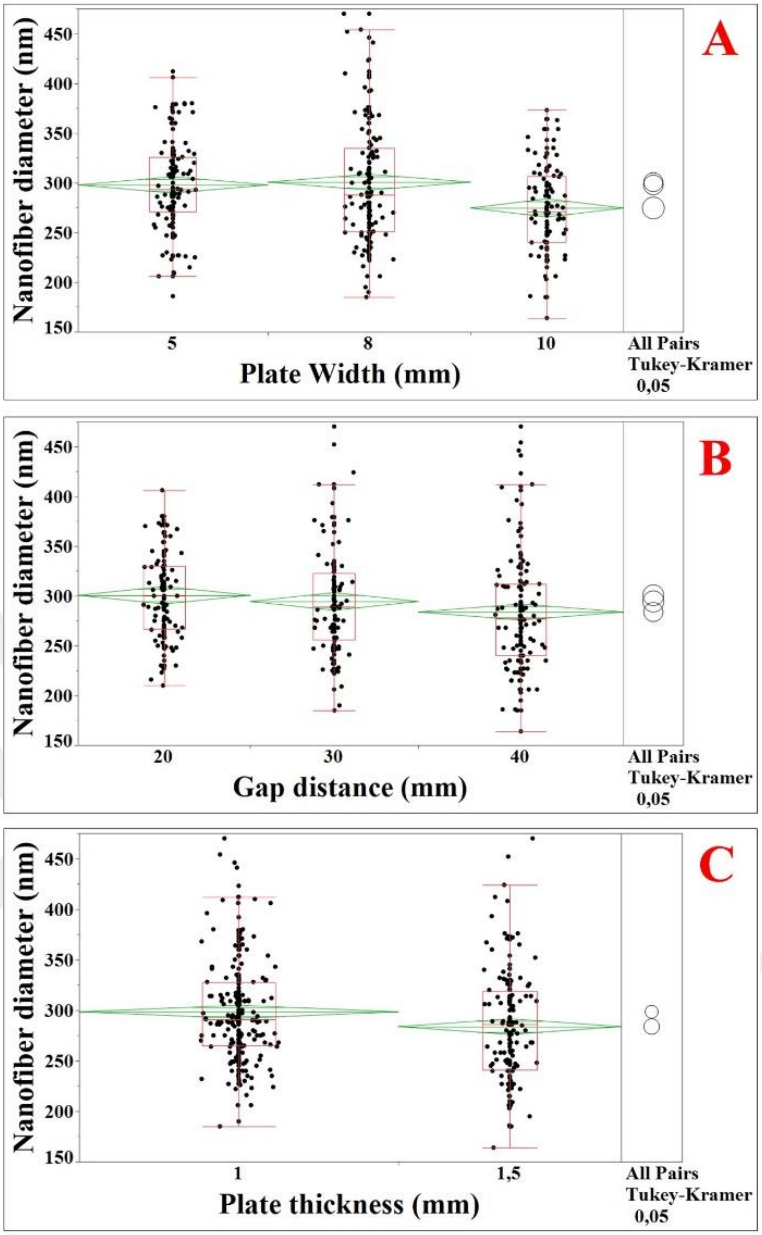

Figure 4.7 Effect of plate width (a), gap distance (b) and plate thickness (c) on nanofiber diameter

Notes: *The distance between top and bottom ends of green diamond represents the 95% confidence interval. Comparison circles (given on the right column) for means those are significantly different either do not intersect, or intersect slightly. The height of red box (known as interquartile range) is a quantitative indication of variation.*

Plate width affected average nanofiber diameters, significantly ($p<0.0001$). While there was no significant difference between 5 mm and 8 mm of plate width values, 10 mm of plate width caused to decrease in nanofiber diameter, significantly. Gap distance showed significant effect on nanofiber diameter ($p=0.0193$). 40 mm of gap distance caused to decrease in nanofiber diameter according to 20 mm of gap distance.

Plate thickness showed significant effect on nanofiber diameter (p=0.0044). When plate thickness increased, average nanofiber diameter decreased significantly.

4.2.3 Nanofiber Alignment

Graphical representation is presented, illustrating a surface-arrow plot delineating the electric field strength and vectors within the x-y plane **Figure 4.8**. This depiction elucidates the variations in electric field characteristics as influenced by both plate width and gap distance.

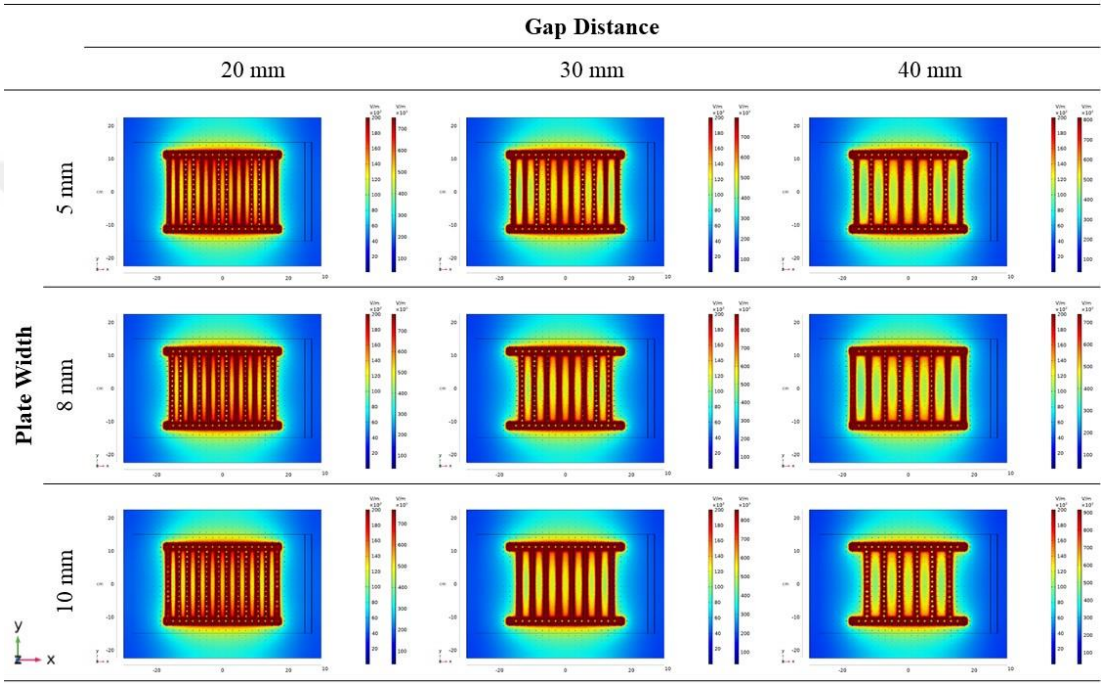

Figure 4.8 A two-dimensional surface-arrow plot illustrates the electric field strength and vectors within the x-y plane, contingent upon variations in both plate width and gap distance.

When examining parallel electrodes, a discernible pattern in the electric field intensity emerges, with heightened levels evident along and in proximity to the electrode edges, visually represented by reddish areas. Conversely, within the inter-electrode space, a contrasting lower intensity electric field is observed, marked by yellowish regions. Notably, distinct electric fields manifest around each adjacent electrode pair, a phenomenon attributed to the whipping instability of the nanofiber jet, as it traces a spiral trajectory and exhibits attraction towards regions characterized by higher electric field intensity [134].

The electrostatic forces generated at the interface of adjacent electrodes induce the elongation and alignment of nanofibers in a parallel orientation between the electrodes. Noteworthy is the observation that the gap distance between electrodes exerts a more substantial influence on the distribution of the electric field compared to the width of the electrode plates. Specifically, an increase in electrode width corresponds to an expanded surface area, resulting in increased electric field intensity on the electrode surface. Conversely, minimal alterations in electric field intensity are detected in the inter-electrode gap. An increase in gap distance, however, is associated with a decrease in electric field intensity within this region. **Figure 4.9** provides graphical representations illustrating the variation of electric potential concerning plate width (W) and gap distance (G).

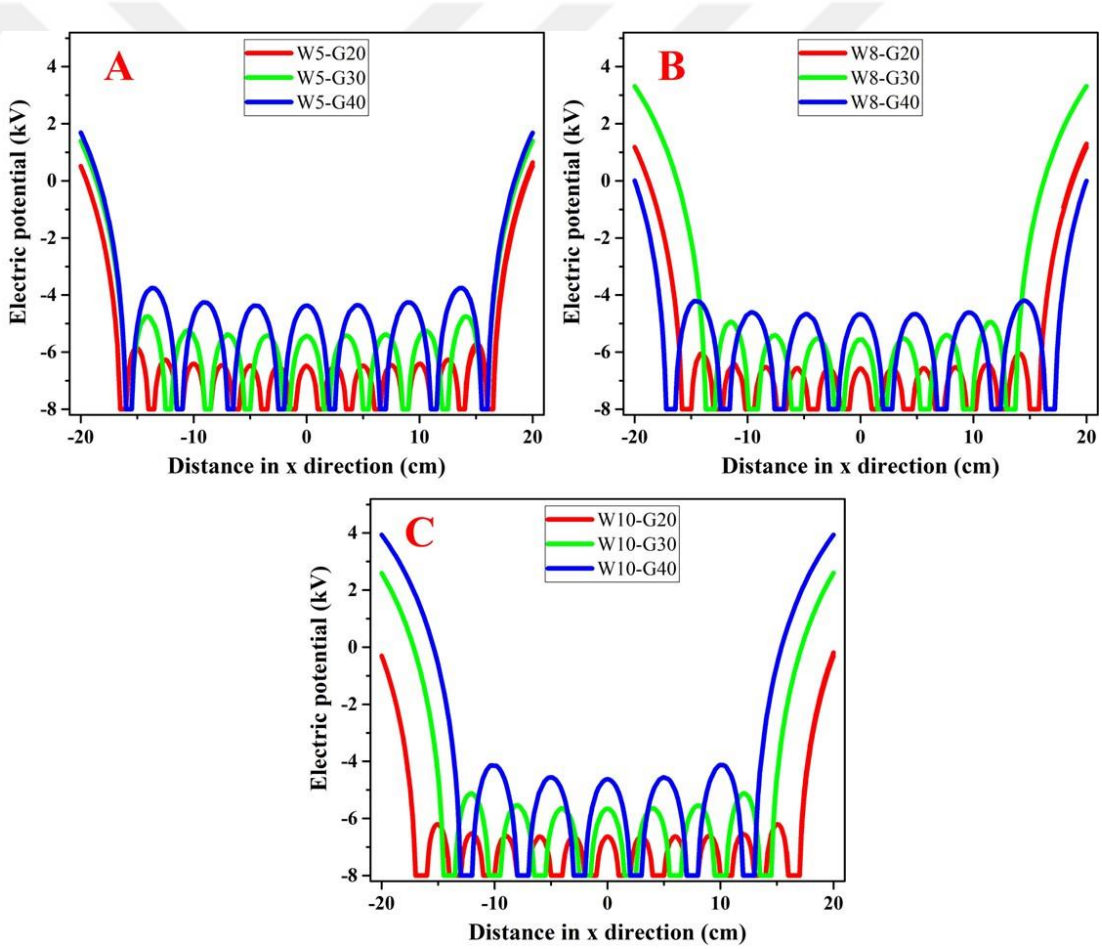

Figure 4.9 The electric potential exhibits distinct alterations with varying plate widths: a) 5 mm, b) 8 mm, c) 10 mm

The examination revealed that the potential difference between the electrodes and gaps exhibited a decreasing trend with an increase in electrode width, while conversely increasing with an increase in gap distance, as pictured in **Figure 4.9**. These findings

demonstrated alignment with the trends evident in the electric field distribution graphs (**Figure 4.8**). A heightened electric potential difference was envisaged to cause more strong electrostatic attraction forces acting upon the nanofibers, thereby resulting in a more pronounced alignment of the nanofiber structure.

The stationary state of the conveyor system contributed to a progressive increase in the thickness of the accumulating nanofiber layer, at the same time giving rise to the deposition of residual charge. This accrued residual charge exerted electrostatic repulsion forces upon incoming charged nanofibers, adversely affecting their alignment, as elucidated by Liu et al. [119]. Notably, the dynamic motion of the conveyor, coupled with the continuous removal of produced nanofibers, forestalled the cumulative buildup of residual charge over time, thereby averting any adverse effects on alignment.

SEM images of nanofibers produced using 1 and 1.5 mm thick plates were examined. SEM images of nanofibers produced using 1 mm thick plates are given in **Figure 4.10**.

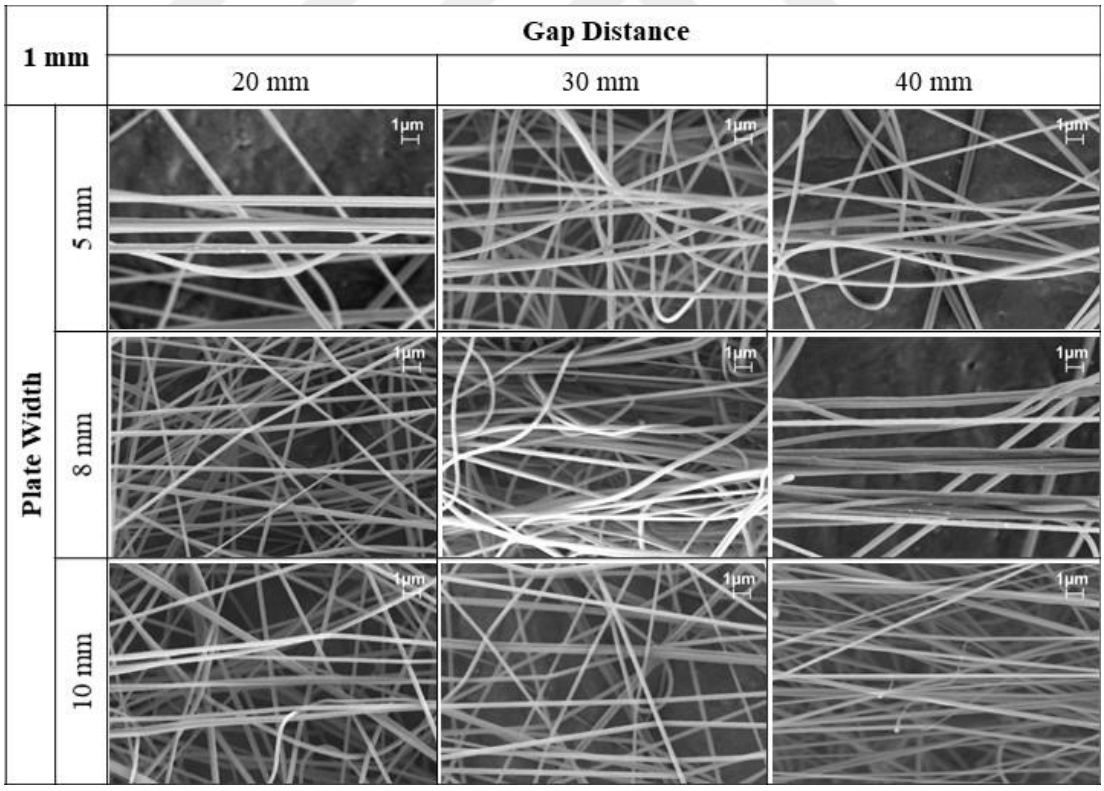

Figure 4.10 SEM images of PAN nanofibers produced with 1 mm electrode thickness [15 kX]

Nanofibers have different alignments depending on the gap distance and plate width. In general, alignment was observed in all samples. The alignment of nanofibers according to plate width and gap distance is given in **Figure 4.11**.

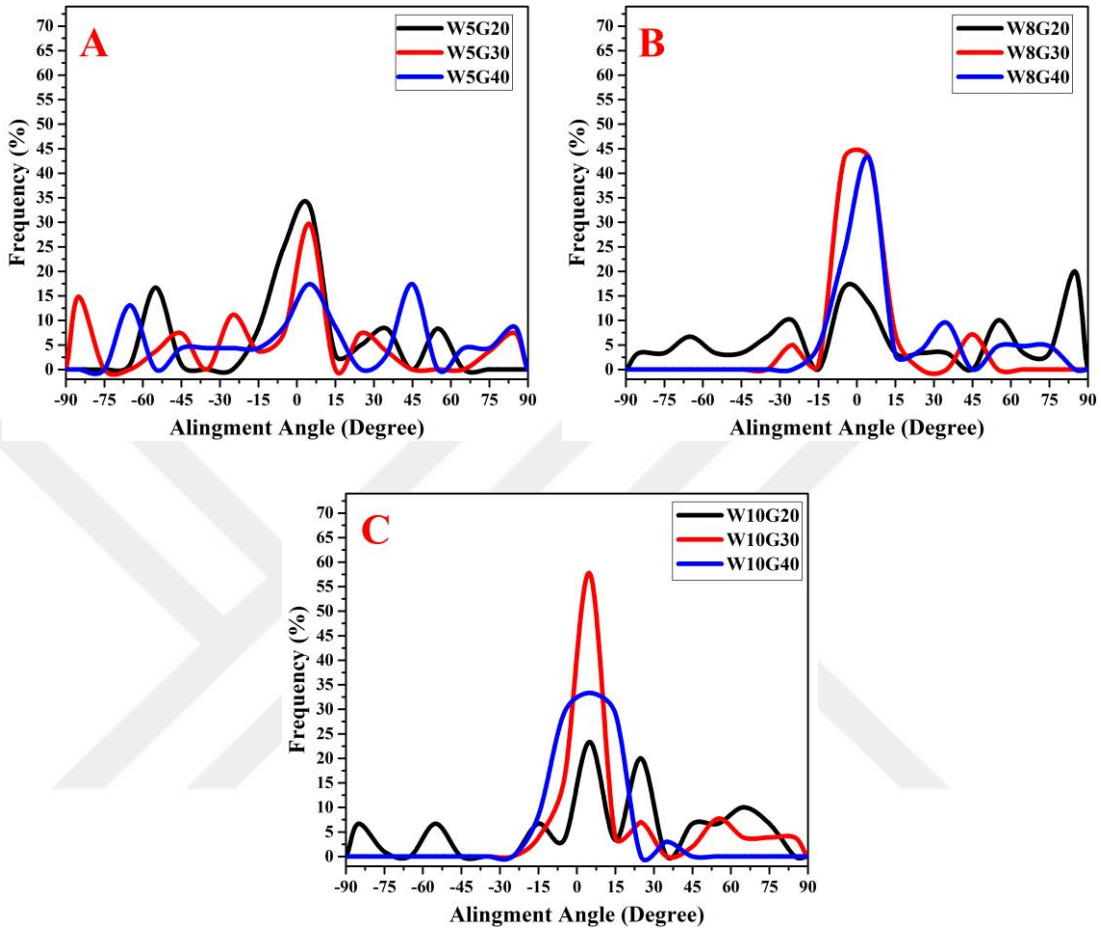

Figure 4.11 Alignment of nanofibers depending on the gap distance for different widths of 1 mm thick electrodes (W): a) 5 mm, b) 8 mm, c) 10 mm

The alignment angle of the nanofibers varies depending on the angle of collection. In the graphics, W represents the plate width and G represents the gap distance. Plate width and gap distance were effective in the alignment of nanofibers. In general, the nanofibers were concentrated at 0° alignment angle for all plate widths and gap distances at 1 mm electrode thickness. In other aspects the deposition was lower. As the plate width increased, the nanofibers concentrated at 0° alignment angle. The highest alignment was obtained at 10 mm plate width and 30 and 40 mm gap distance. The standard deviation of alignments of nanofibers according to gap distance for 1 mm electrode angles according to plate width and gap distance for 1 mm plate thickness is given in **Table 4.4**.

Table 4.4 Deviation [°] from 0° according to electrode widths and gap distance for 1 mm electrode thickness

1 mm Thickness		Gap Distance (mm)		
		20	**30**	**40**
Plate Width (mm)	**5**	30.7	48.1	45.8
	8	48.8	14.8	34.4
	10	46.4	32.1	9.6

The standard deviation of the alignment angles is an indicator of the level of alingment of the nanofibers. When calculating the standard deviation value, the deviation of the angles from 0 degrees was taken into account. As the standard deviation decreases, the angle decreases and alignment increases. The standard deviation of the alignment angles generally decreased as the plate width increased and the gap distance increased. As the standard deviation of the angles decreased, nanofiber alignment increased. The highest value in the standard deviations of the alignment angles of the nanofibers was obtained for 10 mm plate width and 40 mm gap distance, and the lowest value was obtained for 8 mm plate width and 20 mm gap distance.

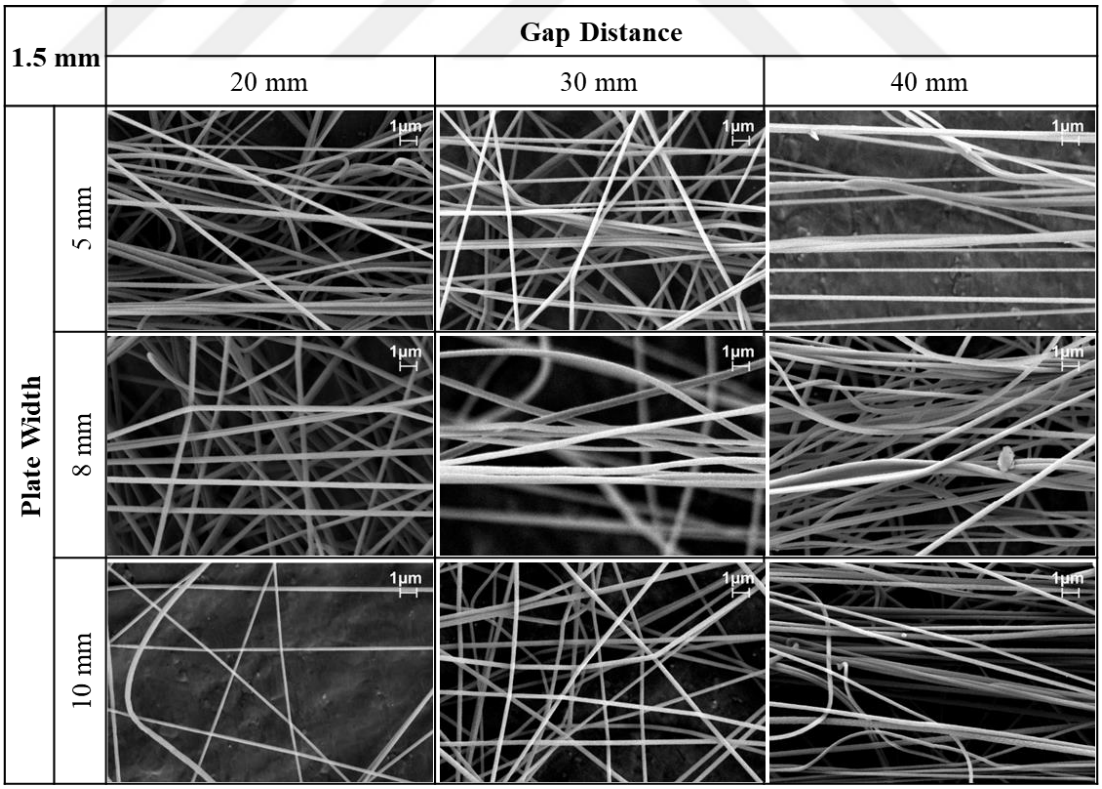

Figure 4.12 SEM images of PAN nanofibers produced with 1.5 mm electrode thickness [15 kX]

Nanofibers showed intense alignment according to gap distance and plate width for 1 mm as well as 1.5 mm thickness (**Figure 4.12**). Generally, alignment was observed in all samples. The alignment angle of the nanofibers depending on the plate width and gap distance is given in **Figure 4.13** for a plate thickness of 1.5 mm.

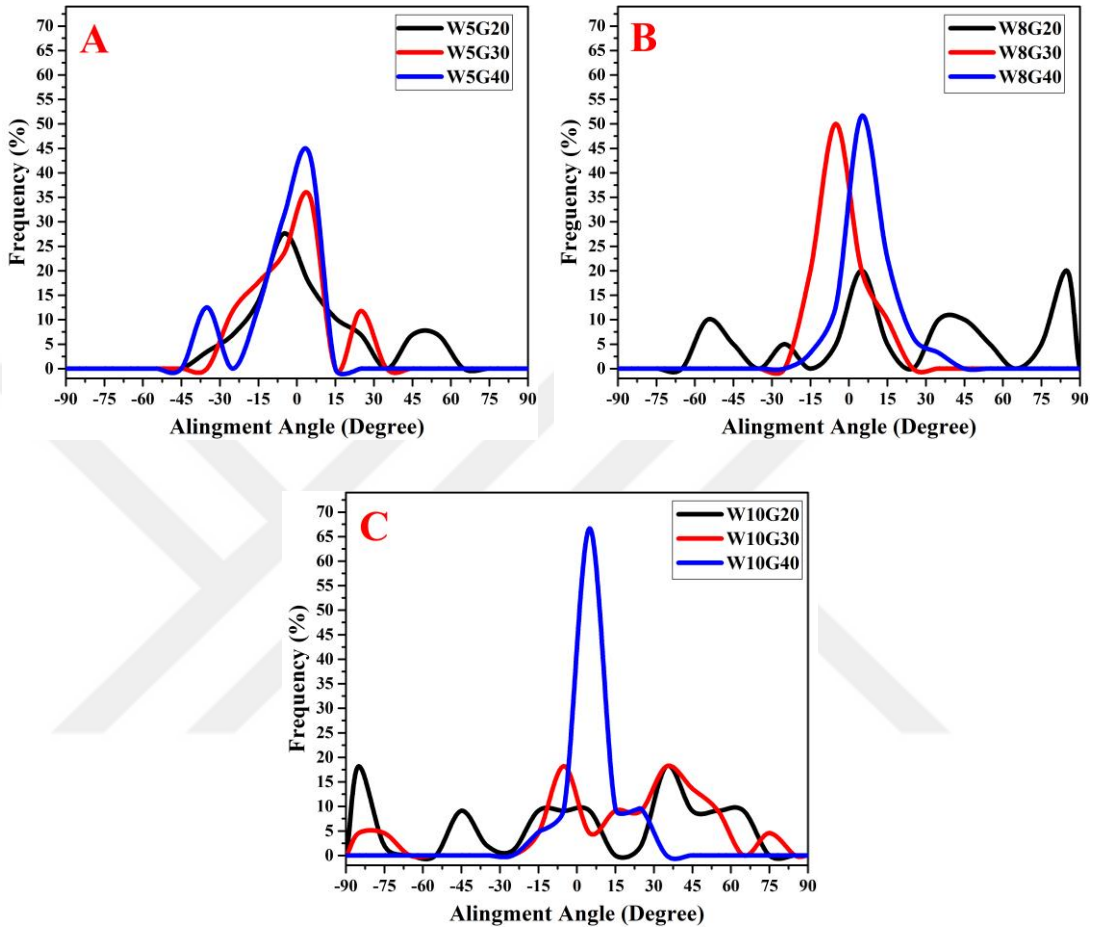

Figure 4.13 Alignment of nanofibers depending on the gap distance for different widths of 1.5 mm thick electrodes (W): a) 5 mm, b) 8 mm, c) 10 mm

Nanofibers are generally concentrated at 0° alignment angle for all plate widths and gap distances at 1.5 mm plate thickness. Compared to a plate width of 1 mm, nanofiber alignment is higher at a plate width of 1.5 mm. Nanofiber alignment As in the 1 mm plate width, in the 1.5 mm plate width, as the plate width increased, the nanofibers concentrated at 0° alignment angle. The gap distance or plate width affected the alignment angle of the nanofibers. The gap distance led to different alignment results at different plate widths. The maximum alignment was observed at a gap distance of 40 mm in all samples. The highest nanofiber alignment was obtained with a plate width of 10 mm and a gap distance of 40 mm. The standard deviation of alignment angles

according to plate width and gap distance for 1.5 mm plate thickness is given in **Table 4.5**.

Table 4.5 Deviation [°] from 0° according to electrode widths and gap distance for 1.5 mm electrode thickness

1.5 mm Thickness		Gap Distance (mm)		
		20	**30**	**40**
Plate Width (mm)	**5**	23.6	15.3	12.1
	8	53.0	9.3	12.8
	10	54.6	44.1	8.5

In general, the standard deviation of the alignment angles of nanofibers at 1.5 mm electrode thickness was lower than that of 1 mm. Similarly, the alignment of nanofibers was higher with a plate thickness of 1.5 mm. With these findings, as in 1 mm, the increase in plate width and gap distance led to a decrease in the standard deviation. With this decrease, there was an increase in the alignment of the nanofibers. The best nanofiber alignment was achieved with a plate width of 10 mm and a gap distance of 40 mm. Standard deviation results are compatible with alignment angle graphs.

Additionally, Yıldırım et al. [76] investigated the effect of the same parameters on nanofiber alignment used auxiliary electrode in his study. When the results were compared, it was determined that the standard deviation results obtained without using auxiliary electrode were lower and therefore the nanofiber alignment were higher [76]. With these results, not using auxiliary electode positively affects nanofiber alignment.

4.3 PAN/GO Study Results

4.3.1 Solutions Properties

Surface tension, conductivity and viscosity changes of PAN solutions according to different GO addition ratios are given in **Table 4.6**, respectively.

Table 4.6 GO addition PAN/DMF electrospinning solution properties

GO Ratio (wt.%)	Surface Tension (mN/m)	Conductivity (µS/cm)	Viscosity (cP)
0	37.8	77.8	820
1	38.1	98.6	683
2	37.8	118.5	667
3	38.3	147.3	583
4	38.4	167.1	580
5	34.4	193.2	626

Generally, no significant change was observed in the surface tension in the solution with the amount of GO added. It was observed that the surface tension decreased when the GO addition amount was used at the highest value (5 wt.%). The conductivity and viscosity changes of the solution according to the contribution ratio of GO are given in **Figure 4.14**.

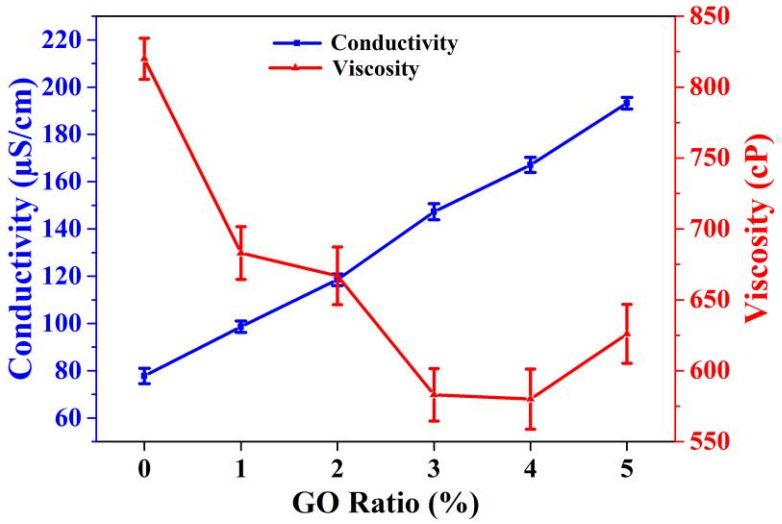

Figure 4.14 Conductivity and viscosity changes of the solution according to GO addition ratio

As the amount of GO increases, the conductivity increases linearly. The highest conductivity was measured as 193.2 µS/cm at 5 wt.% GO addition ratio, and the lowest conductivity was measured as 77.8 µS/cm in the pure PAN sample. The fact that GO is conductive had a similar effect on the solution and increased the conductivity of the solution.

As the amount of GO increased, viscosity decreased up to 4 wt.% addition ratio. When the GO addition amount was 5 wt.%, the viscosity increased as the intermolecular interaction increased. Agglomeration of GO due to higher concentration could cause this situation. The highest viscosity was measured as 820 cP for pure PAN solution, and the lowest was 580 cP for 4 wt.% addition ratio.

4.3.2 Morphology Analysis

SEM images were examined separately for different GO addition ratios. SEM micrographs and nanofiber diameter distributions of PAN nanofibers according to different GO addition ratios are given in **Figure 4.15**.

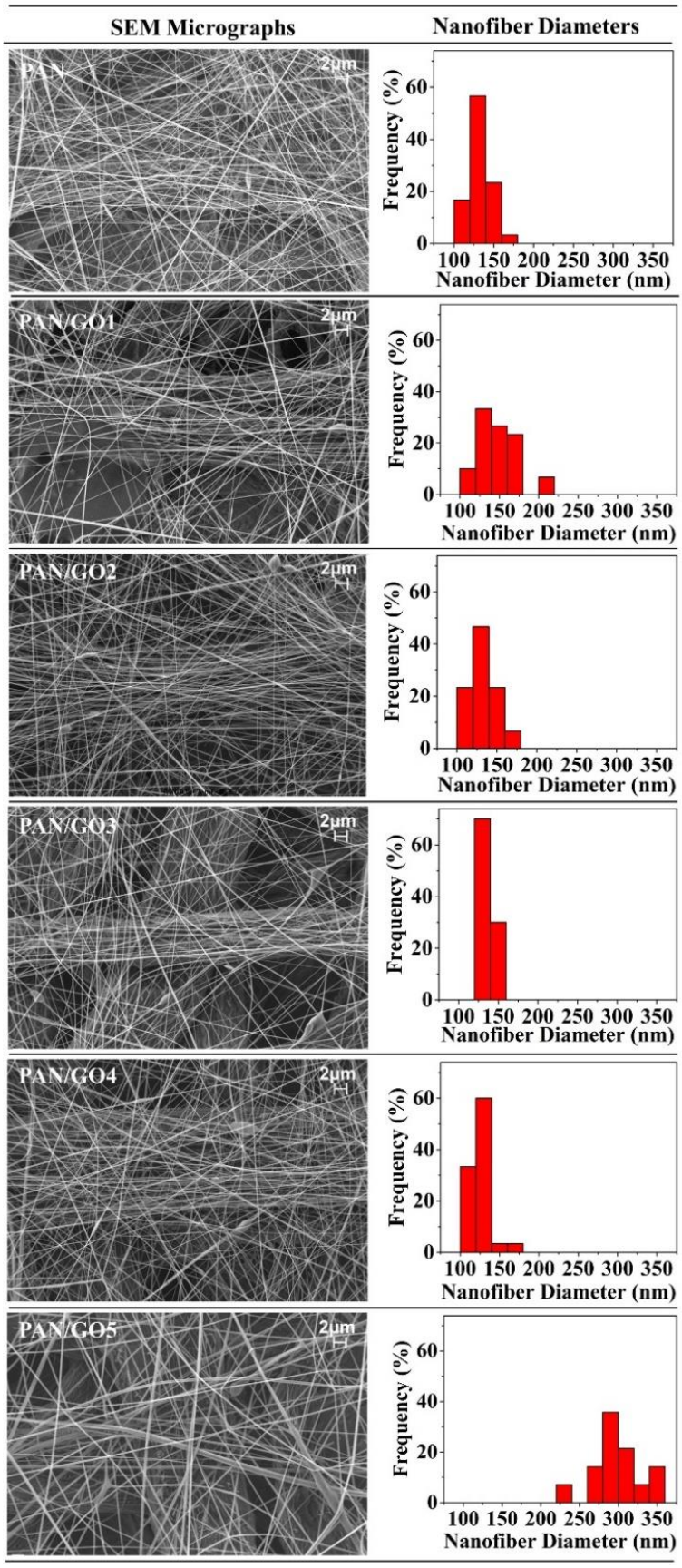

Figure 4.15 SEM micrographs and distribution of nanofiber diameters depending on GO ratio [6 kX]

When the SEM micrographs of the samples were examined, it was seen that the nanofibers were produced uniformly. A small amount of bead formation was seen in the SEM images at all addition ratios. It is thought that the bead formation seen in nanofibers is caused by GO particles insoluble in PAN/DMF solution. When GO is added to the PAN solution, the diameter variation decreases. In particular, the diameter variation of the nanofibers decreased in the PAN/GO 3 wt.% and PAN/GO 4 wt.% samples compared to the raw PAN sample. The effect of GO addition on nanofiber diameters is given in detail in **Figure 4.16.**

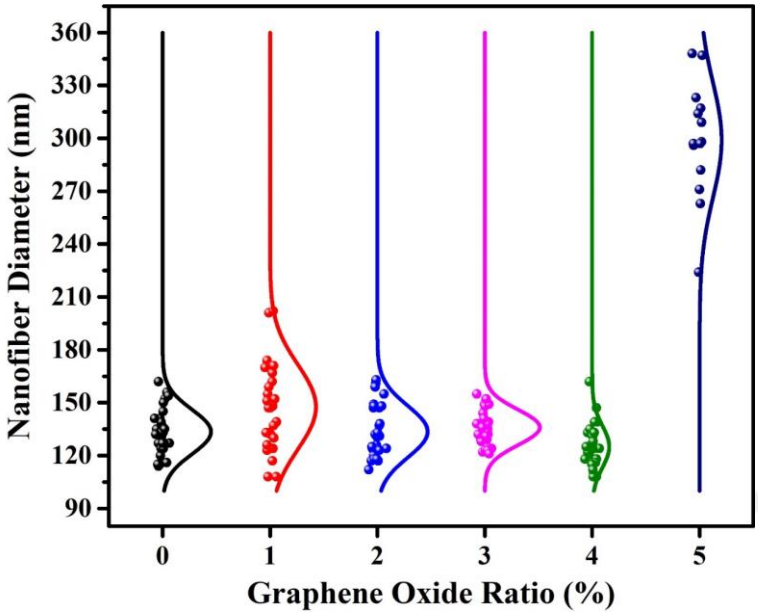

Figure 4.16 Effect of GO addition ratio on nanofiber diameters

When all samples were examined, the average nanofiber diameter values were between 125-150 nm up to 4 wt.% contribution rate and showed a significant increase at 5 wt.% contribution rates. The enhancement of solution conductivity is directly correlated with the increase attributed to GO. As the solution's conductivity rises, there is a concurrent increase in the surface charge of the jet. This heightened surface charge intensifies the elongational forces acting upon the jet, thereby imparting increased strength. Consequently, this phenomenon yields nanofibers that exhibit a defect-free morphology, characterized by uniformity and a reduced diameter distribution [135].

There was a dramatical increase in nanofiber diameter for 5 wt.% of GO addition. This could be related to agglomeration of GO and high conductivity. PAN polymer coated GO agglomeration result in thicker nanofiber. Also, high conductivity could cause

short flight time that limits elongation and stretching of polymer jet. Hence thicker nanofibers were seen for 5 wt.% of GO addition.

Combined effect of GO ratio on nanofiber diameter was given in **Figure 4.17** and **Table 4.7**. GO ratio showed significant effect on nanofiber diameter ($p<0.0001$). While there was no significant difference between 2, 3, 4 wt.% of GO ratios and reference, 5 wt.% of GO ratio caused to increase in nanofiber diameter, significantly.

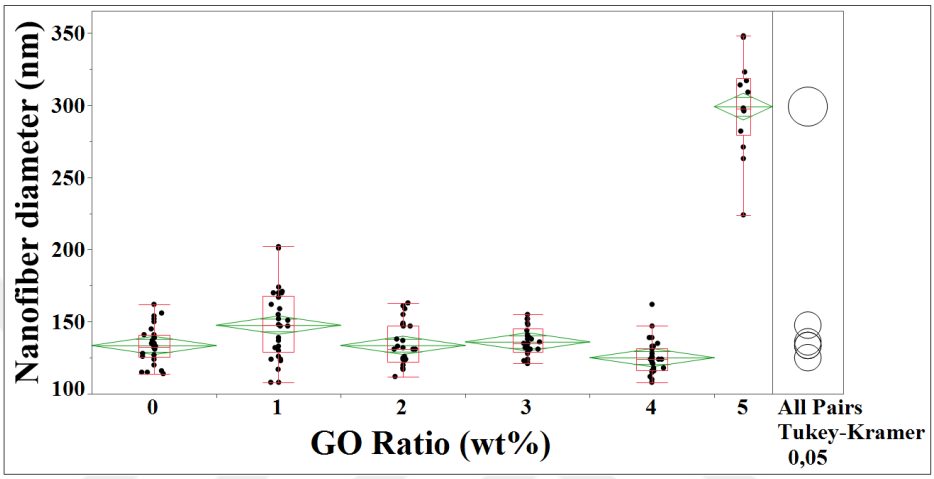

Figure 4.17 Effect of GO ratio on nanofiber diameter [nm]

Table 4.7 Effect of GO ratio on nanofiber diameter [nm]

Property	Level	Number				Mean	SD	LL	UL	Prob>F
GO Ratio (wt.%)	0	30	A			133.5	12.6	127.8	139.8	0.0001
	1	30		B		147.6	24.1	141.2	153.9	
	2	30	A			133.6	14.6	127.2	139.9	
	3	30	A	B		136.1	10.3	129.7	142.3	
	4	30	A			125.1	11.7	118.7	131.3	
	5	14			C	299.1	32.7	289.7	308.2	

4.3.3 Alignment Measurement

SEM images were examined separately for different GO addition ratios. The effect of GO amount on nanofiber alignment is given in detail in **Figure 4.18**.

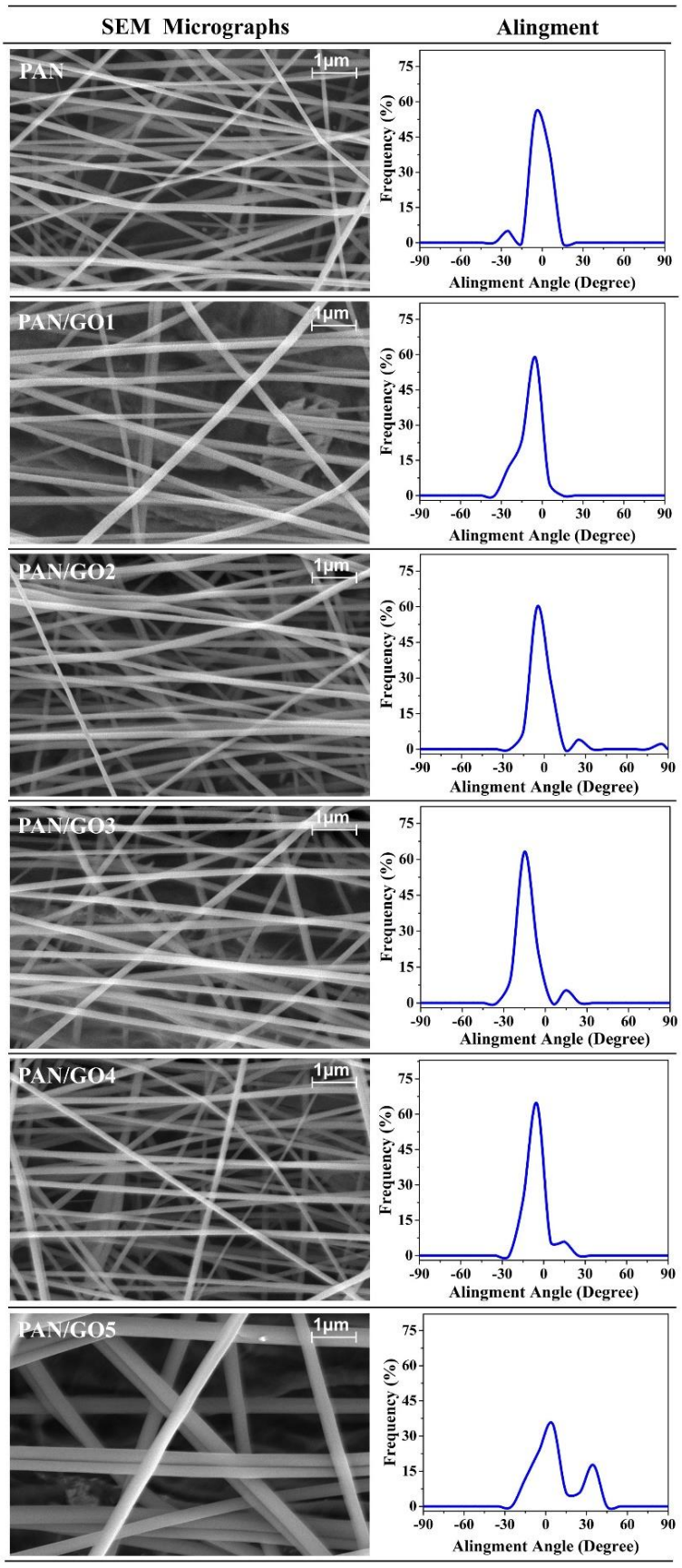

Figure 4.18 SEM micrographs and alignments of nanofiber according to different GO ratio [40 kX]

Nanofibers have different alignments depending on the amount of GO. When all samples were examined, a significant increase in the alignment of the nanofiber bundles was observed as the amount of GO increased. Generally, nanofibers are concentrated at 0° alignment angle. The graph showing the alignment of all samples is given in **Figure 4.19**.

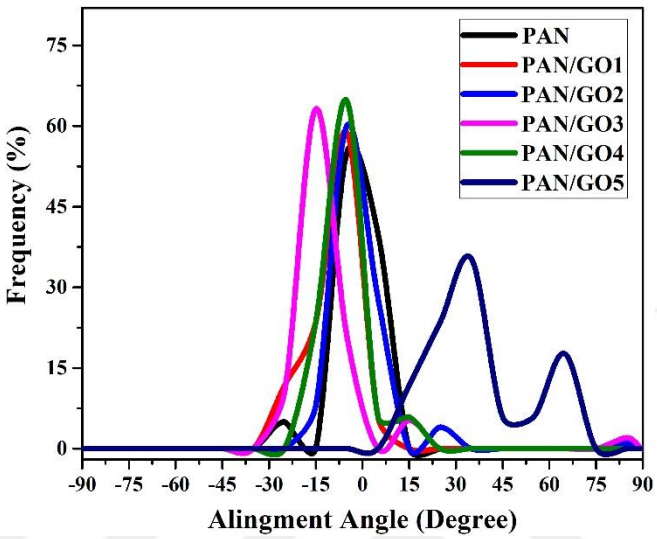

Figure 4.19 Alignments of nanofiber bundle according to different GO ratios

The lowest alignment was seen in the 5 wt.% GO sample, and the highest alignment was seen in the 4 wt.% GO addition rates. It can be said that GO addition has a significant effect on the alignment of nanofibers. While the contribution of GO increases the solution conductivity, it also increases the conductivity of the nanofibers [136]. There is a negatively charged electrostatic force of attraction on parallel plates. There is a positively charged electrostatic attraction force on the nanofibers. When nanofibers are collected between the plates, the positive residual charges on the nanofibers are attracted by the negative electrostatic charges on them between the plates. These electrostatic forces ensure the parallel alignment of the nanofibers between the plates. The conductivity of nanofibers facilitates the movement of electrostatic charges. By increasing the nanofiber conductivity, GO addition facilitates the movement of electrostatic charges. In this way, the parallel alignment of the nanofibers increases. However, although the electrical conductivity of the solution increased at 5 wt.% GO ratios, it was observed that the alignment deteriorated dramatically. It can be said that the main reason for this situation is the increase in viscosity (**Table 4.6**).

As the GO ratio increased, viscosity decreased up to 4 wt.%, while a significant increase was observed for 5 wt.%. Since increasing viscosity increased the force in the opposite direction to the stretching of the nanofibers, it negatively affected the parallel alignment of the nanofibers between the plates. The standard deviation of the alignment angles of the nanofibers according to the amount of GO is given in **Table 4.8**.

Table 4.8 Deviation from 0° result according to different GO ratios

GO Ratio (wt.%)	**0**	**1**	**2**	**3**	**4**	**5**
Standard Deviation (°)	11.5	11	10.5	10	9.7	25

As the GO addition ratio increased, the standard deviation of the nanofiber alignment angles decreased. As the standard deviation decreased, the parallel alignment of the nanofibers increased. However, the standard deviation of alignment angles is higher in all other samples, including the raw PAN sample, at 5 wt.% GO addition rate. As mentioned before, it was caused by the viscosity being higher than the critical value at 5 wt.% GO addition rate. These results are consistent with the distribution of parallel alignment angles. The lowest standard deviation was seen in the 4 wt.% GO addition ratio, while the highest deviation was seen in the 5 wt.% GO sample. In line with the findings, it was determined that GO addition significantly improved nanofiber alignment.

4.3.4 Structural Analysis

FTIR, XRD and Raman spectroscopy analyzes of the produced PAN/GO nanofiber bundle were performed. The selected as reference GO was compared with the PAN and PAN/GO sample. For the PAN/GO sample was selected 3 wt.% GO addition rate. The results of the analyzes are given below.

4.3.4.1 FTIR Analysis

FTIR spectrum of nanofiber bundles are given **Figure 4.20**.

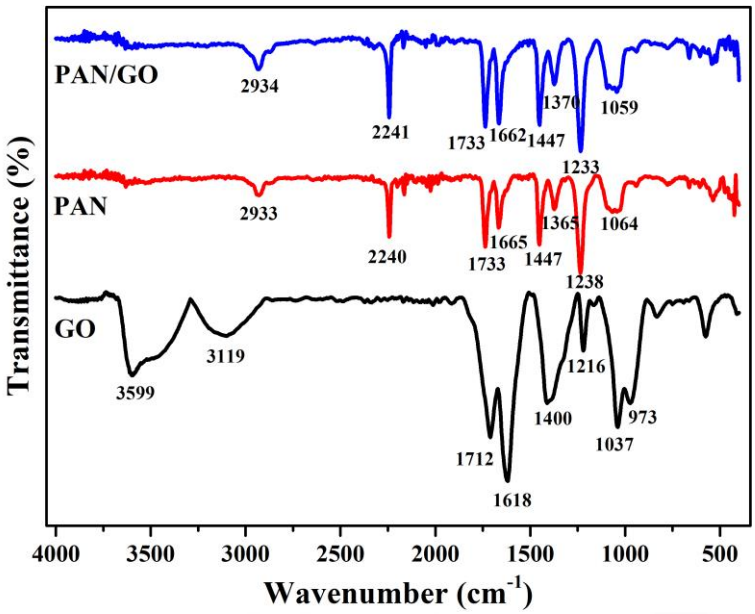

Figure 4.20 FTIR spectrum of PAN and PAN/GO

PAN/GO nanofiber bundles are observed at wave numbers of 2934 cm^{-1}, 2241 cm^{-1}, 1733 cm^{-1}, 1662 cm^{-1}, 1447 cm^{-1}, 1370 cm^{-1}, 1233 cm^{-1} and 1059 cm^{-1}. The peaks confirm the presence of PAN. In the FTIR analysis of PAN and PAN/GO nanofiber bundles, the peaks corresponding to PAN were seen similarly in PAN/GO. Since the peaks in PAN also contain the characteristic peaks of GO, no evidence can be provided regarding the formation of chemical bonds in the PAN/GO nanofiber bundle. However, there were differences in the intensity and peak widths of the FTIR peaks of PAN and PAN/GO nanofiber bundles. The change occurring in these peaks can be interpreted as the inclusion of the bond structures of GO into the chemical structure together with PAN. This result is also supported by previously reported studies [137].

4.3.4.2 XRD Analysis

XRD analysis of nanofiber bundles are given **Figure 4.21**.

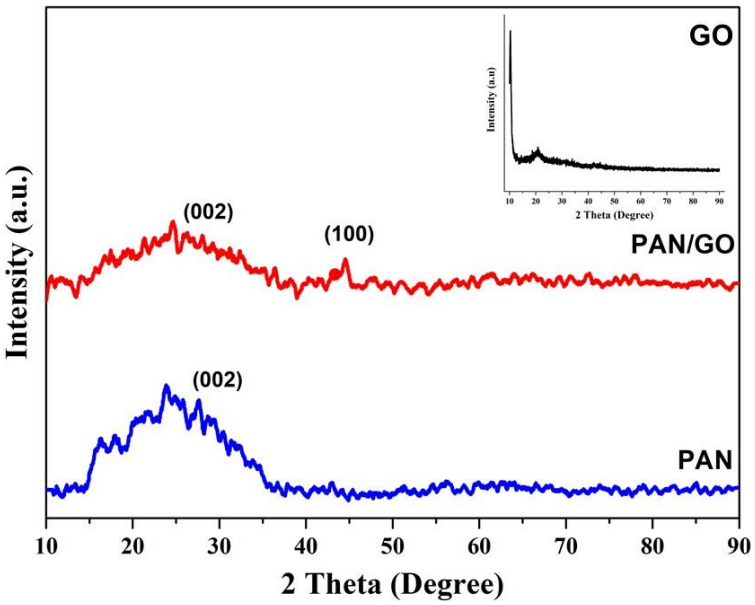

Figure 4.21 XRD analysis results for 100 plane of PAN and PAN/GO

The structures of PAN and PAN/GO nanofiber bundles were examined by XRD. Two typical diffractions were seen in XRD. The first one was seen at 2θ = 25.5° in 002 diffraction and the other was seen at 2θ = 44° in 100 diffractions. The diffraction of PAN/GO nanofiber bundles at 2θ = 44° is more obvious than PAN nanofiber bundles. These results are consistent with the literature [138].

4.3.4.3 Raman Spectroscopy Analysis

Raman spectrum nanofiber bundles are given in **Figure 4.22**.

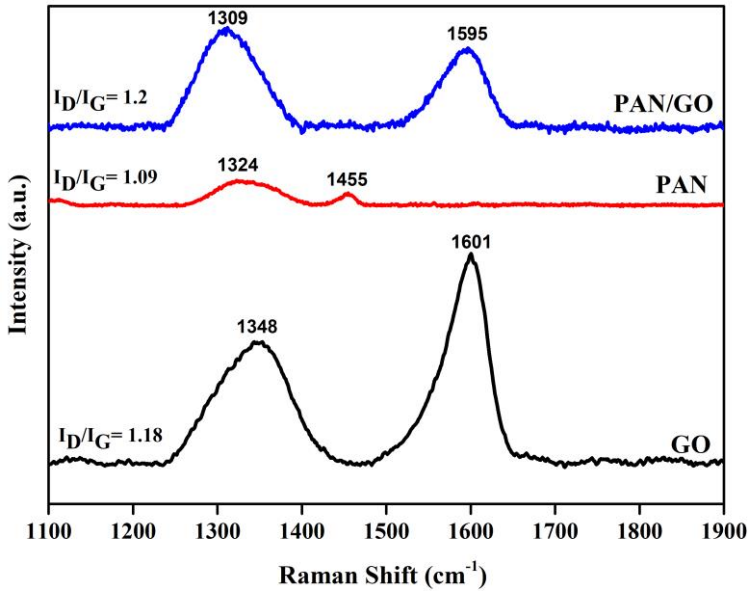

Figure 4.22 Raman spectrum of PAN and PAN/GO

PAN/GO, PAN and GO nanofiber bundles have two characteristic peaks known as D (disordered) and G (ordered) bands. The GO, I_D/I_G ratio was calculated as 1.18 with peaks at 1348 cm^{-1} and 1601 cm^{-1}. For PAN nanofiber bundles, the I_D/I_G ratio was calculated as 1.09 with peaks at 1324 cm^{-1} and 1455 cm^{-1}. In PAN/GO nanofiber bundles, the I_D/I_G ratio was calculated as 1.2 at the peaks of 1309 cm^{-1} and 1595 cm^{-1}. As a result, the I_D/I_G ratios show that the structures meet the description of the carbonic material, however, the closeness of the PAN and PAN/GO ratios shows that there is a uniform distribution of GO particles [139]. These results are also in agreement with the XRD results.

4.3.5 Thermal Analysis

TGA and DSC analyzes were performed to examine the thermal properties of PAN nanofiber bundles produced with different GO addition ratios. The results of the analyses are given below.

4.3.5.1 TGA Analysis

TGA curves of nanofiber bundles with different GO addition ratios are given in **Figure 4.23**.

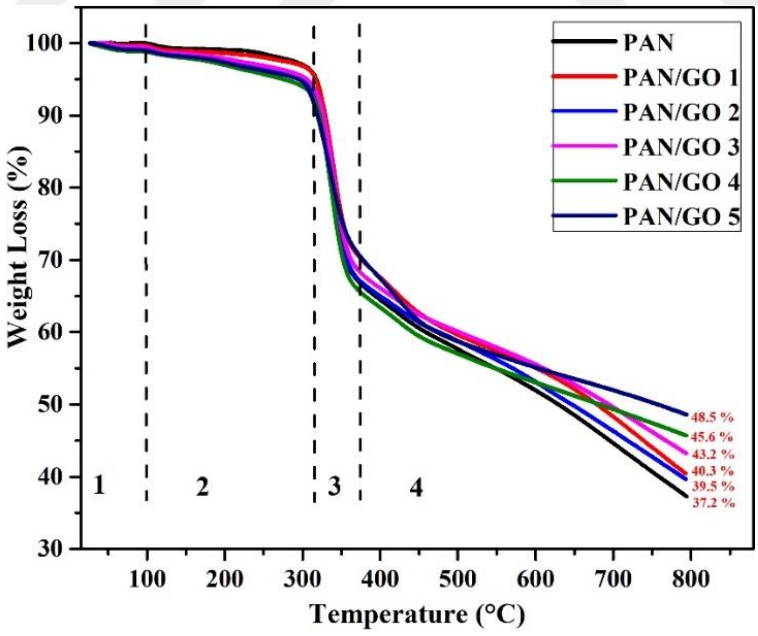

Figure 4.23 TGA analysis of PAN and PAN/GO nanofiber bundles

A four-stage degradation was observed in the TGA analysis of nanofiber bundles with different GO addition ratios. By calculation these data, the residue amounts were obtained shown in **Figure 4.23** and the weight losses were given in **Table 4.9**. In the

degradation curve of nanofibers, water molecules in the structure disappeared in the section up to 98 °C, and in the section up to 305 °C, functional groups containing oxygen in the structure left the structure in the form of CO and CO_2 gases. Finally, above 360 °C, the remaining unstable carbon atoms in the structure decomposed. In the last two stages, two significant thermal decompositions were observed in the temperature ranges 305-360 °C and 360-800 °C. When the TGA curves of the nanofiber surfaces were examined, the weight loss generally decreased as the amount of GO addition added to the PAN nanofiber bundles, which was the reference sample, increased. Particularly, the addition of 4 wt.% and 5 wt.% GO to PAN nanofibers significantly increased the thermal durability of the nanofiber surface.

Table 4.9 TGA analysis results of PAN and PAN/GO nanofiber bundles

Region	**Temperature (°C)**	**Weight loss according to GO ratio (wt%)**					
		0	**1**	**2**	**3**	**4**	**5**
1	30- 98	0	0.4	0.5	0	1.2	1
2	98- 305	3.3	3.1	5.4	4.6	4.5	5
3	305- 360	27.8	24.1	25.2	24.5	26.4	21.3
4	360- 800	31.7	32.1	29.4	27.7	22.3	24.2
Total Weight Loss (%)		**62.8**	**59.7**	**60.5**	**56.8**	**54.4**	**51.5**

Weight losses observed at all stages are given in detail in **Table 4.9**. The highest weight loss was seen in the 3rd and 4th stages. The highest weight loss was seen in the pure PAN sample, and the lowest weight loss was seen at 5 wt. % GO addition. It has been observed that adding GO to the structure of PAN nanofibers increases the thermal stability of the nanofibers.

4.3.5.2 DSC Analysis

The DSC graph of nanofiber bundles with different GO addition ratios is given in **Figure 4.24.**

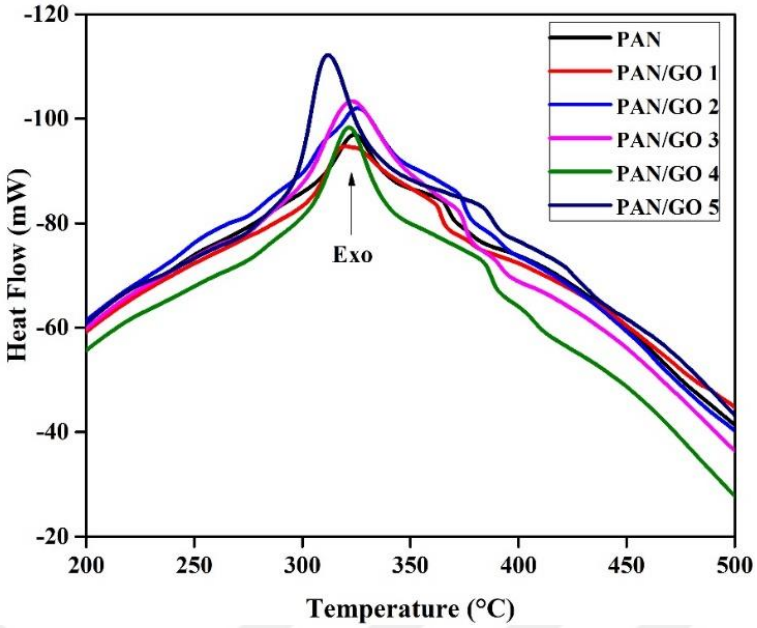

Figure 4.24 DSC graph of PAN and PAN/GO nanofiber bundles

The data obtained from the DSC graph of nanofiber bundles with different GO addition ratios are given in **Table 4.10** .

Table 4.10 DSC data of PAN and PAN/GO nanofiber bundles

GO Ratio (wt.%)	Heat Flow (m/W)	Temperature (°C)
0	96.8	323
1	94.4	321
2	101.8	325
3	103.2	322
4	98.2	321
5	111.2	311

In the DSC graph of nanofiber bundles with different GO addition ratios, the exothermic reaction band of the PAN bundle was measured as 323 °C. There was no relationship between the amount of GO addition and the degradation temperatures, and all temperature values were found to be close to each other.

In addition, the highest heat flux was detected in the samples 3 wt. % GO and 5 wt. % GO addition ratios. In addition, after 385 °C, the heat flow required for the degradation of PAN/GO nanofiber bundles continued to decrease. The formation of cross-links between -CN groups in the PAN polymer with GO addition makes the ring closing

reactions slightly difficult. This situation made the PAN nanofiber bundles thermally more stable with the addition of GO, and the results are compatible with the literature [8].

4.3.6 Mechanical Analysis

The count and productivity for different GO addition ratios nanofibers according to GO ratio results are given in **Table 4.11**.

Table 4.11 Productivity and count nanofiber bundle according to GO ratio

GO Ratio (wt.%)	Productivity (g/h)	Count (tex)
0	0.61 ± 0.20	149 ± 0.3
1	0.53 ± 0.02	130 ± 0.3
2	0.46 ± 0.13	114 ± 0.3
3	0.88 ± 0.21	215 ± 0.4
4	0.49 ± 0.70	114 ± 0.3
5	0.90 ± 0.10	220 ± 0.2

Depending on the amount of GO addition, the productivity (g/h) and count (tex) results of the nanofiber bundles also differed. The highest production amount was measured as 0.90 ± 0.1, 5 wt.% GO addition sample and the lowest production amount was 0.46 ± 0.13, 2 wt.% GO sample. These results are thought to be due to changes in environmental conditions in the production of PAN/GO nanofiber bundles. The highest linear density of nanofiber bundles was measured as 220 ± 0.2 tex (5 wt.% GO). The tensile strength, elongation and Young's modulus, results are given in **Table 4.12**.

Table 4.12 Elongation, tensile strength and Young's modulus nanofiber bundle according to different ratio of GO

GO Ratio (wt.%)	Tensile Strength (cN/tex)	Elongation (%)	Young's Modulus (cN/tex)
0	1.9 ± 0.3	22.5 ± 5.5	21.3 ± 9.1
1	2.0 ± 0.3	30.5 ± 6.6	21.6 ± 8.2
2	2.1 ± 0.3	25.5 ± 4.9	25.9 ± 6.6
3	2.3 ± 0.4	32.9 ± 7.5	45.6 ± 6.0
4	1.6 ± 0.2	28.2 ± 5.6	29.8 ± 3.1
5	1.7 ± 0.2	27.0 ± 6.9	26.6 ± 6.0

Depending on the different GO addition amounts, the tensile strength (cN/tex), Young's modulus (cN/tex), and % elongation results of the nanofiber bundles also varied. According to the tensile strength results, the highest value was measured as 2.3 ± 0.4 cN/tex in the 3 wt.% GO addition sample, and the lowest value was 1.6 ± 0.2 cN/tex in the 4 wt.% GO addition sample. According to Young's modulus results, the highest value was measured as 45.6 ± 6 cN/tex in the 4 wt.% GO addition sample, and the lowest value was 21.3 ± 9.1 cN/tex in the PAN sample.

According to the % elongation results, the highest value was measured as 32.9 ± 7.5 cN/tex in the 3 wt.% GO addition sample, and the lowest value was 28.2 ± 5.6 cN/tex in the 4 wt.% GO addition sample.

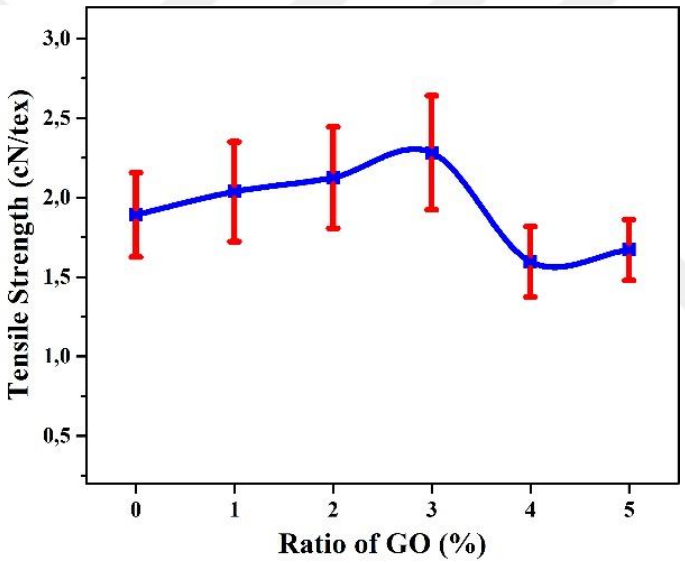

Figure 4.25 The tensile strength of nanofiber bundle according to GO ratio

Tensile strength results of PAN and PAN/GO nanofiber bundles are given in **Figure 4.25**. The tensile strength of the nanofiber bundles increased up to 3 wt.% GO amount and then decreased. Similar results were seen in previous studies [8].

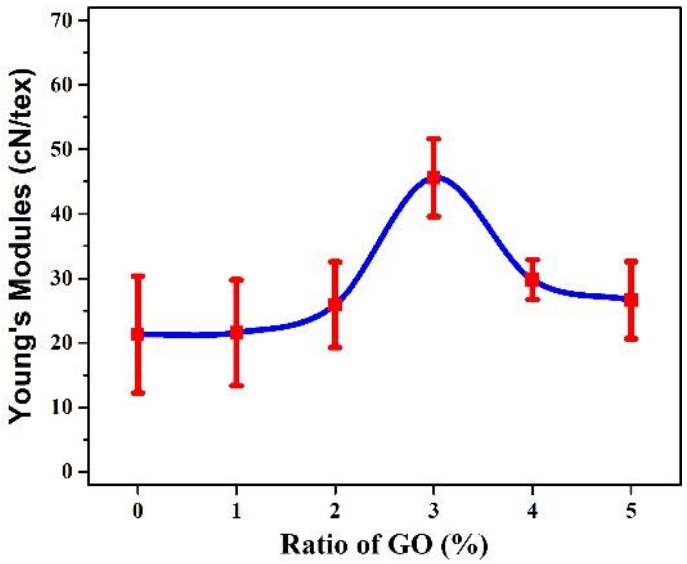

Figure 4.26 The Young's modulus of nanofiber bundle according to GO ratio

Young's modulus results of PAN and PAN/GO nanofiber bundles are given in **Figure 4.26**. The elasticity modulus of PAN nanofiber bundles was lower than PAN/GO nanofiber bundles. It can be said that GO addition causes an increase in the elasticity modulus up to a certain amount. Therefore, it can be said that PAN nanofiber bundles have lower stiffness than PAN/GO nanofiber bundles. With the addition of GO, the strength that nanofibers can withstand without permanent shape change has also increased. This force was highest at 3 wt.% GO contribution rates. This ratio greatly improved the elasticity of PAN nanofibers.

When all mechanical analysis findings are evaluated, it shows that GO addition improves the properties of PAN nanofibers such as breaking strength, % elongation and Young's modulus. However, 3 wt.% GO contribution rate was seen as the critical value for mechanical properties. Using more additions than this value negatively affects the properties of nanofibers.

CHAPTER 5
CONCLUSIONS AND RECOMMENDATIONS

In this thesis, GO was synthesized from graphite by the modified Hummers method. The synthesized GO was added to the PAN solution at different ratios. Firstly, PAN nanofibers were produced using different parallel electrodes according to 1 and 1.5 mm thickness, 5, 8 and 10 mm electrode width and 20, 30, 40 mm gap distance. Then, PAN/GO nanofibers were produced at different GO addition ratios with selected parallel electrode parameters. The morphological structure and alignment angles of PAN and PAN/GO nanofibers were determined according to the GO ratio. The mechanical, structural and thermal properties of the produced PAN/GO nanofiber bundles were analysed. Additionally, the results were analysed statistically.

SEM, FTIR, XRD and Raman spectroscopy analyses of GO were performed. According to SEM results, structures approximately 4-5 microns in size were observed. According to FTIR results, alkoxyl, epoxy, aromatic, carbonyl, and hydroxyl bonds were formed in GO. According to the XRD results, the characteristic peak of GO was observed. According to Raman spectroscopy results, it was determined that the amount of ordered structure increased in GO. According to all analysis results for GO, it was determined that the produced GO was compatible with the literature.

According to SEM results, it was observed that the produced PAN and PAN/GO nanofibers were beadless and had a uniform structure. In general, nanofiber diameter distributions occurred in a wider area in 1.5 mm thick plates than in 1 mm plates. While the widest diameter distribution was seen in the sample with a plate width of 10 mm and a gap distance of 40 mm, the lowest diameter distribution was seen in the sample with a plate width of 8 mm and a gap distance of 30 mm. It has been observed that plate width and gap distance influence nanofiber diameters. Statistically, it has been

observed that plate width, gap distance and plate thickness have a significant effect on the nanofiber diameter.

According to the COMSOL results, it was seen that the electric field intensity was higher at the edges and surroundings of the electrodes, and the electric field intensity was lower in the gap between the electrodes. Similarly, the potential difference of the electric field on the electrodes and in the gaps decreased as the electrode width increased but increased as the gap distance increased.

The plate thickness, plate width and gap distance had an impact on the alignment of the nanofibers. The alignment of the nanofibers increased as the plate width and gap distance increased for 1 and 1.5 mm plate thickness. Both angle measurements and standard deviation results of the angles supported this finding. Nanofiber alignment at 1 mm of thickness is higher than at 1.5 mm. The highest alignment was produced at 10 mm plate width and 40 mm gap distance, while the lowest alignment was produced at 8 mm plate width and 20 mm gap distance.

The amount of GO added to the PAN solution did not affect the surface tension in the solution. As the GO addition ratio increased, the solution conductivity increased. The surface tension of the solution increased as the GO addition ratio increased and decreased by 5 wt.%.

From the SEM images, it was seen that the PAN/GO nanofibers were homogeneous and uniform and there was a small amount of bead formation. While there was no significant change in nanofiber diameter between 0-4 wt.% GO addition, 5 wt.% of GO addition.

In PAN/GO nanofibers, the alignment of nanofibers increased as the amount of GO increased up to 4 wt.% addition ratios. The highest alignment was seen at 4 wt.% GO contribution rates, while the lowest alignment was seen at 5 wt.% GO contribution rates. These findings were supported by the standard deviation results of the alignment angles.

According to the FTIR results of PAN/GO nanofibers, characteristic PAN and GO chemical bonds were observed. According to the XRD results of PAN/GO nanofibers, a characteristic peak of GO was observed, unlike the PAN results. According to Raman

spectroscopy results, PAN/GO nanofibers were found to be suitable for carbonic material structure.

According to the TGA results of PAN/GO nanofibers, a four-stage degradation occurred. It was observed that as the amount of GO addition added to the PAN nanofiber bundles increased, the weight loss generally decreased. According to DSC results, GO addition increased the heat flow required for the degradation of PAN nanofibers. According to TGA and DSC results, the thermal strength and stability of PAN increased with the addition of GO.

Nanofiber productivity and tex values differed depending on the GO addition ratio in PAN/GO nanofibers. The highest nanofiber productivity and tex values were seen in the PAN/GO 5 % sample.

According to the breaking strength and Young's modulus results, GO contribution increased up to 3 wt.% and decreased after this value. According to the breaking strength, % elongation and Young's modulus results, 3 wt.% GO addition rate was seen as the critical value according to the performance criteria of nanofiber bundles.

It may offer a more in-depth evaluation of how PAN/GO nanofibers can perform in specific applications. For example, one might focus on the potential for use of these nanofibers in biomedical, electronics or materials science fields.

REFERENCES

[1] C. Meng, Y. Xiao, P. Wang, L. Zhang, … Y. L.-A., and undefined 2011, "Quantum-dot-doped polymer nanofibers for optical sensing," *Wiley Online LibraryC Meng, Y Xiao, P Wang, L Zhang, Y Liu, L TongAdvanced Materials, 2011•Wiley Online Library*, vol. 23, no. 33, pp. 3770–3774, Sep. 2011, doi: 10.1002/adma.201101392.

[2] Z. Huang, Y. Zhang, … M. K.-C. science and, and undefined 2003, "A review on polymer nanofibers by electrospinning and their applications in nanocomposites," *Elsevier*, Accessed: Jan. 22, 2024. [Online]. Available: https://www.sciencedirect.com/science/article/pii/S0266353803001787

[3] G. Rutledge, S. F.-A. drug delivery reviews, and undefined 2007, "Formation of fibers by electrospinning," *Elsevier*, Accessed: Jan. 22, 2024. [Online]. Available: https://www.sciencedirect.com/science/article/pii/S0169409X07001846

[4] Y. Kiyak, E. C.-/Tasit T. E. Dergisi, and undefined 2014, "Nanofiber Production Methods.," *search.ebscohost.comYE Kiyak, E CakmakElectronic Journal of Vehicle Technologies/Tasit Teknolojileri, 2014•search.ebscohost.com*, Accessed: Jan. 22, 2024. [Online]. Available: https://search.ebscohost.com/login.aspx?direct=true&profile=ehost&scope=site&authtype=crawler&jrnl=1309405X&AN=116501684&h=KbeEfVtm6yHeA3Ttba68PMXTG83VFbkDiPaG2Yc7e37NmaEbguZrUkY4NC4Go9DubQqj%2FvlrpbpTRPqRaWLa8Q%3D%3D&crl=c

[5] H. İçoğlu, B. Yıldırım, A. Kılıç, M. Türkoğlu, … A. K.-M. T., and undefined 2023, "Controlled fiber deposition via modeling the auxiliary electrodes of the needleless electrospinning to produce continuous nanofiber bundles," *Elsevier*, Accessed: Jan. 22, 2024. [Online]. Available: https://www.sciencedirect.com/science/article/pii/S2352492822018074

[6] J. Zhu *et al.*, “Highly porous polyacrylonitrile/graphene oxide membrane separator exhibiting excellent anti-self-discharge feature for high-performance lithium–sulfur,” *Elsevier*, Accessed: Jan. 22, 2024. [Online]. Available: https://www.sciencedirect.com/science/article/pii/S0008622316301002

[7] M. R. Almafie, L. Marlina, R. Riyanto, J. Jauhari, Z. Nawawi, and I. Sriyanti, “Dielectric Properties and Flexibility of Polyacrylonitrile/Graphene Oxide Composite Nanofibers,” *ACS Omega*, vol. 7, no. 37, pp. 33087–33096, Sep. 2022, doi: 10.1021/ACSOMEGA.2C03144.

[8] İ. Tiyek *et al.*, “Nanolif yapili poli (akrilonitril-vinil asetat)/grafen oksit yapilarin karakterizasyonu,” *dergipark.org.trİ TİYEK, M YAZICI, MH ALMA, U DÖNMEZ, B YILDIRIM, T SALAN, U Serhan, Ş KARATAŞTekstil ve Mühendis, 2016•dergipark.org.tr*, vol. 23, no. 102, pp. 82–92, 2016, doi: 10.7216/1300759920162310201.

[9] J. Hou, J. Yun, H. B.- Membranes, and undefined 2019, “Fabrication and characterization of modified graphene oxide/PAN hybrid nanofiber membrane,” *mdpi.comJ Hou, J Yun, H ByunMembranes, 2019•mdpi.com*, 2019, doi: 10.3390/membranes9090122.

[10] J. Hou, J. Yun, S. Kim, H. B.-A. Sciences, and undefined 2019, “Highly controlled integration of graphene oxide into PAN nanofiber membranes,” *mdpi.comJ Hou, J Yun, S Kim, H ByunApplied Sciences, 2019•mdpi.com*, doi: 10.3390/app9050962.

[11] M. M. Abdel-Mottaleb, A. Mohamed, S. A. Karim, T. A. Osman, and A. Khattab, “Preparation, characterization, and mechanical properties of polyacrylonitrile (PAN)/graphene oxide (GO) nanofibers,” *Taylor & FrancisMM Abdel-Mottaleb, A Mohamed, SA Karim, TA Osman, A KhattabMechanics of Advanced Materials and Structures, 2020•Taylor & Francis*, vol. 27, no. 4, pp. 346–351, Feb. 2018, doi: 10.1080/15376494.2018.1473535.

[12] J. H. Li, H. Zhang, W. Zhang, and W. Liu, “Nanofiber membrane of graphene oxide/polyacrylonitrile with highly efficient antibacterial activity,” *J Biomater*

Sci Polym Ed, vol. 30, no. 17, pp. 1620–1635, Nov. 2019, doi: 10.1080/09205063.2019.1652793.

[13] W. Jang *et al.*, "Mixed dye removal efficiency of electrospun polyacrylonitrile–graphene oxide composite membranes," *mdpi.comW Jang, J Yun, Y Seo, H Byun, J Hou, JH KimPolymers, 2020•mdpi.com*, doi: 10.3390/polym12092009.

[14] G. Ghaderi, … H. T.-M. R., and undefined 2019, "Electrospun graphene oxide incorporated PAN nanofibers, before and after activation," *iopscience.iop.orgG Ghaderi, H Tavanai, M BazarganipourMaterials Research Express, 2019•iopscience.iop.org*, vol. 6, p. 105047, 2019, doi: 10.1088/2053-1591/ab3993.

[15] I. Gergin, M. Micusik, … E. I.-… of N. and, and undefined 2020, "Thermally treated graphene oxide/polyacrylonitrile based electrospun carbon nanofiber precursor," *ingentaconnect.comI Gergin, M Micusik, E Ismar, M Omastova, A Sezai SaracJournal of Nanoscience and Nanotechnology, 2020•ingentaconnect.com*, Accessed: Jan. 22, 2024. [Online]. Available: https://www.ingentaconnect.com/contentone/asp/jnn/2020/00000020/00000006/art00015

[16] H. İbrahim İçoğlu *et al.*, "Production of aligned electrospun polyvinyl alcohol nanofibers via parallel electrode method," *Taylor & FrancisHİ İçoğlu, Ş Ceylan, B Yıldırım, M Topalbekiroğlu, A KılıçThe Journal of The Textile Institute, 2021•Taylor & Francis*, vol. 112, no. 6, pp. 936–945, 2020, doi: 10.1080/00405000.2020.1789274.

[17] I. Alghoraibi, S. A.-H. of nanofibers, and undefined 2018, "Different methods for nanofiber design and fabrication," *researchgate.netI Alghoraibi, S AlomariHandbook of nanofibers, 2018•researchgate.net*, pp. 1–46, 2018, doi: 10.1007/978-3-319-42789-8_11-2.

[18] Y. Gou, C. Liu, T. Lei, F. Y.-2014 I. C. on, and undefined 2014, "Nanofiber alignment during electrospinning: effects of collector structures and governing parameters," *ieeexplore.ieee.orgY Gou, C Liu, T Lei, F Yang2014 International Conference on Manipulation, Manufacturing and, 2014•ieeexplore.ieee.org*,

Accessed: Jan. 17, 2024. [Online]. Available: https://ieeexplore.ieee.org/abstract/document/7057341/

[19] R. Jalili, M. Morshed, S. Abdolkarim, and H. Ravandi, "Fundamental parameters affecting electrospinning of PAN nanofibers as uniaxially aligned fibers," *Wiley Online LibraryR Jalili, M Morshed, SAH RavandiJournal of applied polymer science, 2006•Wiley Online Library*, vol. 101, no. 6, pp. 4350–4357, Sep. 2006, doi: 10.1002/app.24290.

[20] E. Zdraveva, J. Fang, B. Mijovic, T. L.-S. and properties of high, and undefined 2017, "Electrospun nanofibers," *Elsevier*, Accessed: Jan. 26, 2024. [Online]. Available: https://www.sciencedirect.com/science/article/pii/B9780081005507000115

[21] C. Boshard *et al.*, "An electrospun poly (vinylidene fluoride) nanofibrous membrane and its battery applications," *Wiley Online LibrarySW Choi, SM Jo, WS Lee, YR KimAdvanced Materials, 2003•Wiley Online Library*, vol. 96, no. 23, p. 155, Dec. 1997, doi: 10.1002/adma.200304617.

[22] J. Li, H. Xie, Y. Li, J. W.-J. of N. and, and undefined 2013, "Fabrication of graphene/polyaniline composite for high-performance supercapacitor electrode," *ingentaconnect.comJ Li, H Xie, Y Li, J WangJournal of Nanoscience and Nanotechnology, 2013•ingentaconnect.com*, Accessed: Jan. 17, 2024. [Online]. Available: https://www.ingentaconnect.com/contentone/asp/jnn/2013/00000013/00000002/art00083

[23] P. Serp, M. Corrias, P. K.-A. C. A. General, and undefined 2003, "Carbon nanotubes and nanofibers in catalysis," *Elsevier*, Accessed: Jan. 17, 2024. [Online]. Available: https://www.sciencedirect.com/science/article/pii/S0926860X03005490

[24] M. Kosal, "Applying Nanotechnology to Revolutionary Chemical and Biological Countermeasures," *Nanotechnology for Chemical and Biological Defense*, pp. 29–87, 2009, doi: 10.1007/978-1-4419-0062-3_3.

[25] J. Park, S. Choi, … S. J.-J. of N., and undefined 2012, "Synthesis of NiO nanofibers and their gas sensing properties," *ingentaconnect.comJY Park, SW Choi, SH Jung, SS KimJournal of Nanoscience and Nanotechnology, 2012•ingentaconnect.com*, Accessed: Jan. 17, 2024. [Online]. Available: https://www.ingentaconnect.com/contentone/asp/jnn/2012/00000012/00000002/art00077

[26] X. Wang, X. Chen, K. Yoon, D. Fang, B. S. Hsiao, and B. Chu, "High flux filtration medium based on nanofibrous substrate with hydrophilic nanocomposite coating," *Environ Sci Technol*, vol. 39, no. 19, pp. 7684–7691, Oct. 2005, doi: 10.1021/ES050512J.

[27] M. Phiriyawirut, T. P.-J. of N. and, and undefined 2012, "Cellulose acetate electrospun fiber mats for controlled release of silymarin," *ingentaconnect.comM Phiriyawirut, T PhaechamudJournal of Nanoscience and Nanotechnology, 2012•ingentaconnect.com*, vol. 12, no. 1, pp. 793–799, 2012, doi: 10.1166/jnn.2012.5343.

[28] C. R. Martin, L. S. Van Dyke, Z. Cai, and W. Liang, "Template Synthesis of Organic Microtubules," *J Am Chem Soc*, vol. 112, no. 24, pp. 8976–8977, 1990, doi: 10.1021/JA00180A050.

[29] T. Xiao, E. Strutt, M. Benaissa, … H. C.-N., and undefined 1998, "Synthesis of high active-site density nanofibrous MnO2-base materials with enhanced permeabilities," *Elsevier*, Accessed: Jan. 17, 2024. [Online]. Available: https://www.sciencedirect.com/science/article/pii/S0965977398001378

[30] P. Ma, … R. Z. B. M. R. A. O., and undefined 1999, "Synthetic nano-scale fibrous extracellular matrix," *Wiley Online LibraryPX Ma, R ZhangJournal of Biomedical Materials Research: An Official Journal of, 1999•Wiley Online Library*, 1999, doi: 10.1002/(SICI)1097-4636(199907)46:1<60::AID-JBM7>3.0.CO;2-H.

[31] K. Sarkar, C. Gomez, S. Zambrano, M. R.-M. today, and undefined 2010, "Electrospinning to forcespinning™," *Elsevier*, Accessed: Jan. 17, 2024.

[Online]. Available: https://www.sciencedirect.com/science/article/pii/S1369702110701991

[32] K. Nakata *et al.*, "Poly (ethylene terephthalate) Nanofibers Made by Sea–Island-Type Conjugated Melt Spinning and Laser-Heated Flow Drawing," *Wiley Online LibraryK Nakata, K Fujii, Y Ohkoshi, Y Gotoh, M Nagura, M Numata, M KamiyamaMacromolecular rapid communications, 2007•Wiley Online Library*, vol. 28, no. 6, pp. 792–795, Mar. 2007, doi: 10.1002/marc.200600624.

[33] T. Ondarçuhu, C. J.-E. letters, and undefined 1998, "Drawing a single nanofibre over hundreds of microns," *iopscience.iop.orgT Ondarçuhu, C JoachimEurophysics letters, 1998•iopscience.iop.org*, vol. 42, no. 2, pp. 215–220, 1998, Accessed: Jan. 17, 2024. [Online]. Available: https://iopscience.iop.org/article/10.1209/epl/i1998-00233-9/meta

[34] E. S. Medeiros, G. M. Glenn, A. P. Klamczynski, W. J. Orts, and L. H. C. Mattoso, "Solution blow spinning: A new method to produce micro-and nanofibers from polymer solutions," *Wiley Online LibraryES Medeiros, GM Glenn, AP Klamczynski, WJ Orts, LHC MattosoJournal of applied polymer science, 2009•Wiley Online Library*, vol. 113, no. 4, pp. 2322–2330, Aug. 2009, doi: 10.1002/app.30275.

[35] Y. Chen, Z. Wang, J. Yin, D. J.-C. physics letters, and undefined 1997, "Well-aligned graphitic nanofibers synthesized by plasma-assisted chemical vapor deposition," *Elsevier*, Accessed: Jan. 17, 2024. [Online]. Available: https://www.sciencedirect.com/science/article/pii/S0009261497880062

[36] 631 JF Cooley - US Patent 692 and undefined 1902, "Apparatus for electrically dispersing fluids.," *Google Patents*, Accessed: Jan. 17, 2024. [Online]. Available: https://patents.google.com/patent/US692631A/en

[37] 691 WJ Morton - US Patent 705 and undefined 1902, "Method of dispersing fluids.," *Google Patents*, Accessed: Jan. 17, 2024. [Online]. Available: https://patents.google.com/patent/US705691A/en

[38] 975,504 F Anton - US Patent 1 and undefined 1934, “Process and apparatus for preparing artificial threads,” *Google Patents*, Accessed: Jan. 17, 2024. [Online]. Available: https://patents.google.com/patent/US1975504A/en

[39] P. B.-J. of colloid and interface science and undefined 1971, “Electrostatic spinning of acrylic microfibers,” *Elsevier*, Accessed: Jan. 17, 2024. [Online]. Available: https://www.sciencedirect.com/science/article/pii/0021979771902414

[40] W. Simm, C. Gosling, R. Bonart, 143,196 BVON Falkai - US Patent 4, and undefined 1979, “Fibre fleece of electrostatically spun fibres and methods of making same,” *Google Patents*, Accessed: Jan. 17, 2024. [Online]. Available: https://patents.google.com/patent/US4143196A/en

[41] E. Kostakova, L. Meszaros, J. G.-M. Letters, and undefined 2009, “Composite nanofibers produced by modified needleless electrospinning,” *Elsevier*, Accessed: Jan. 17, 2024. [Online]. Available: https://www.sciencedirect.com/science/article/pii/S0167577X09006156

[42] Z. Ahmadi, S. Ravandi, F. Haghighat, F. D.-F. and Polymers, and undefined 2020, “Enhancement of the mechanical properties of PAN nanofiber/carbon nanotube composite mats produced via needleless electrospinning system,” *SpringerZ Ahmadi, SAH Ravandi, F Haghighat, F DabirianFibers and Polymers, 2020•Springer*, vol. 21, no. 6, pp. 1200–1211, Jun. 2020, doi: 10.1007/s12221-020-9726-x.

[43] O. Jirsak, F. Sanetrnik, D. Lukas, … V. K.-U. P., and undefined 2009, “Method of nanofibres production from a polymer solution using electrostatic spinning and a device for carrying out the method,” *Google Patents*, 2009, Accessed: Jan. 17, 2024. [Online]. Available: https://patents.google.com/patent/US7585437B2/en

[44] O. O. Dosunmu, O. O. Dosunmu, G. G. Chase, J. S. Varabhas, W. Kataphinan, and D. H. Reneker, “Polymer nanofibers from multiple jets produced on a porous surface by electrospinning,” *researchgate.netOO Dosunmu, GG Chase, JS Varabhas, W Kataphinan, DH RenekerNanotechnology*,

2006•researchgate.net, 2006, Accessed: Jan. 17, 2024. [Online]. Available: https://www.researchgate.net/profile/Oludotun-Dosunmu/publication/268274141_Polymer_Nanofibers_from_Multiple_Jets_Produced_on_a_Porous_Surface_by_Electrospinning/links/57c6b8b808aec24de0421412/Polymer-Nanofibers-from-Multiple-Jets-Produced-on-a-Porous-Surface-by-Electrospinning.pdf

[45] A. Keirouz, G. Fortunato, M. Zhang, … A. C.-M. engineering &, and undefined 2019, "Nozzle-free electrospinning of Polyvinylpyrrolidone/Poly (glycerol sebacate) fibrous scaffolds for skin tissue engineering applications," *Elsevier*, Accessed: Jan. 17, 2024. [Online]. Available: https://www.sciencedirect.com/science/article/pii/S1350453319301031

[46] V. Kundrat, V. Vykoukal, Z. Moravec, … L. S.-J. of A. and, and undefined 2022, "Preparation of polycrystalline tungsten nanofibers by needleless electrospinning," *Elsevier*, Accessed: Jan. 17, 2024. [Online]. Available: https://www.sciencedirect.com/science/article/pii/S0925838821049525

[47] L. Wei, H. Yu, L. Jia, and X. Qin, "High-throughput nanofiber produced by needleless electrospinning using a metal dish as the spinneret," *Textile Research Journal*, vol. 88, no. 1, pp. 80–88, Jan. 2018, doi: 10.1177/0040517516677232.

[48] S. Petrik, M. M.-M. O. P. L. (OPL), and undefined 2009, "Production nozzle-less electrospinning nanofiber technology," *cambridge.orgS Petrik, M MalyMRS Online Proceedings Library (OPL), 2009•cambridge.org*, Accessed: Jan. 17, 2024. [Online]. Available: https://www.cambridge.org/core/journals/mrs-online-proceedings-library-archive/article/production-nozzleless-electrospinning-nanofiber-technology/D29BD16E3D468218DD801DE4C346F7CE

[49] J. Xiong *et al.*, "Mass production of high-quality nanofibers via constructing pre-Taylor cones with high curvature on needleless electrospinning," *Elsevier*, Accessed: Jan. 17, 2024. [Online]. Available: https://www.sciencedirect.com/science/article/pii/S0264127520307826

[50] B. Lu *et al.*, “Superhigh-throughput needleless electrospinning using a rotary cone as spinneret,” *Small*, vol. 6, no. 15, pp. 1612–1616, Aug. 2010, doi: 10.1002/SMLL.201000454.

[51] W. Liang, Y. Liu, W. Shou, … W. G.-A. S., and undefined 2012, “Production of highly aligned nanofibers via two-electrode electrospinning,” *ingentaconnect.comW Liang, Y Liu, W Shou, W Gao, M Zhang, R WangAdvanced Science Letters, 2012•ingentaconnect.com*, Accessed: Jan. 22, 2024. [Online]. Available: https://www.ingentaconnect.com/contentone/asp/asl/2012/00000010/00000001/art00119

[52] W. Lu *et al.*, “Gelatin nanofibers prepared by spiral-electrospinning and cross-linked by vapor and liquid-phase glutaraldehyde,” *Elsevier*, Accessed: Jan. 17, 2024. [Online]. Available: https://www.sciencedirect.com/science/article/pii/S0167577X14019466

[53] J. Holopainen, T. Penttinen, E. Santala, M. R.- Nanotechnology, and undefined 2014, “Needleless electrospinning with twisted wire spinneret,” *iopscience.iop.orgJ Holopainen, T Penttinen, E Santala, M RitalaNanotechnology, 2014•iopscience.iop.org*, vol. 26, no. 2, Jan. 2015, doi: 10.1088/0957-4484/26/2/025301.

[54] P. Bhattacharjee, † Banani Kundu, † Deboki Naskar, T. K. Maiti, D. Bhattacharya, and S. C. Kundu, “Nanofibrous nonmulberry silk/PVA scaffold for osteoinduction and osseointegration,” *Wiley Online LibraryP Bhattacharjee, B Kundu, D Naskar, TK Maiti, D Bhattacharya, SC KunduBiopolymers, 2015•Wiley Online Library*, vol. 103, no. 5, pp. 271–284, 2014, doi: 10.1002/bip.22594.

[55] G. Jiang, S. Zhang, X. Q.-M. Letters, and undefined 2013, “High throughput of quality nanofibers via one stepped pyramid-shaped spinneret,” *Elsevier*, Accessed: Jan. 17, 2024. [Online]. Available: https://www.sciencedirect.com/science/article/pii/S0167577X13005582

[56] G. Jiang, X. Q.-M. Letters, and undefined 2014, "An improved free surface electrospinning for high throughput manufacturing of core–shell nanofibers," *Elsevier*, Accessed: Jan. 17, 2024. [Online]. Available: https://www.sciencedirect.com/science/article/pii/S0167577X14006429

[57] N. Thoppey, J. Bochinski, L. C.- Nanotechnology, and undefined 2011, "Edge electrospinning for high throughput production of quality nanofibers," *iopscience.iop.orgNM Thoppey, JR Bochinski, LI Clarke, RE GorgaNanotechnology, 2011•iopscience.iop.org*, vol. 22, no. 34, p. 345301, Aug. 2011, doi: 10.1088/0957-4484/22/34/345301.

[58] J. Deitzel, J. Kleinmeyer, D. Harris, N. T.- Polymer, and undefined 2001, "The effect of processing variables on the morphology of electrospun nanofibers and textiles," *Elsevier*, Accessed: Jan. 17, 2024. [Online]. Available: https://www.sciencedirect.com/science/article/pii/S0032386100002500

[59] S. Ramakrishna, "An introduction to electrospinning and nanofibers," 2005, Accessed: Jan. 17, 2024. [Online]. Available: https://books.google.com/books?hl=tr&lr=&id=1MBgDQAAQBAJ&oi=fnd&pg=PR5&dq=Ramakrishna,+S.+(2005).+An+introduction+to+electrospinning+and+nanofibers.+World+Scientific.+&ots=U3bSa58tue&sig=KjRiIxRIIJwgcYgHrBjamk8HWNo

[60] K. Dincer *et al.*, "ELEKTRO-EĞİRME YÖNTEMİYLE NANOFİBER TABAKALI HAVA FİLTRESİ ÜRETİMİ VE KARAKTERİZASYONU," *dergipark.org.trK Dincer, Ö Gürol, A AKDEMİR, M SelbesSelçuk Üniversitesi Mühendislik, Bilim ve Teknoloji Dergisi, 2016•dergipark.org.tr*, 2016, doi: 10.15317/Scitech.2016.57.

[61] W. Son, J. Youk, … T. L.-J. of P., and undefined 2004, "Electrospinning of ultrafine cellulose acetate fibers: studies of a new solvent system and deacetylation of ultrafine cellulose acetate fibers," *Wiley Online LibraryWK Son, JH Youk, TS Lee, WH ParkJournal of Polymer Science Part B: Polymer Physics, 2004•Wiley Online Library*, vol. 42, no. 1, pp. 5–11, Jan. 2004, doi: 10.1002/polb.10668.

[62] "Üstündağ, G.C., Karaca, E., 2009. Polivinil Alkol)/Sod... - Google Akademik." Accessed: Jan. 26, 2024. [Online]. Available: https://scholar.google.com/scholar?hl=tr&as_sdt=0,5&as_ylo=2017&as_yhi=2017&q=%C3%9Cst%C3%BCnda%C4%9F,+G.C.,+Karaca,+E.,+2009.+Polivinil+Alkol)/Sodyum+Aljinat+Kar%C4%B1%C5%9F%C4%B1mlar%C4%B1ndan+Elektro+%C3%87ekim+Y%C3%B6ntemi+ile+Elde+Edilen+Nanolif+Y%C3%BCzeylerin+%C4%B0ncelenmesi.+Uluda%C4%9F+%C3%9Cniversitesi+M%C3%BChendislik+Mimarl%C4%B1k+Fak%C3%BCltesi+Dergisi,+1+(14)+:+159-172.

[63] Y. Wang, C. Wang, … J. W.-J. of applied polymer, and undefined 2007, "High-temperature DSC study of polyacrylonitrile precursors during their conversion to carbon fibers," *Wiley Online LibraryYX Wang, CG Wang, JW Wu, M JingJournal of applied polymer science, 2007•Wiley Online Library*, vol. 106, no. 3, pp. 1787–1792, Nov. 2007, doi: 10.1002/app.26862.

[64] C. Mit-uppatham, M. N.-… C. and Physics, and undefined 2004, "Ultrafine electrospun polyamide-6 fibers: effect of solution conditions on morphology and average fiber diameter," *Wiley Online LibraryC Mit-uppatham, M Nithitanakul, P SupapholMacromolecular Chemistry and Physics, 2004•Wiley Online Library*, vol. 205, no. 17, pp. 2327–2338, Nov. 2004, doi: 10.1002/macp.200400225.

[65] Y. Zhou, Q. Bao, L. A. L. Tang, Y. Zhong, and K. P. Loh, "Hydrothermal dehydration for the 'green' reduction of exfoliated graphene oxide to graphene and demonstration of tunable optical limiting properties," *Chemistry of Materials*, vol. 21, no. 13, pp. 2950–2956, Jul. 2009, doi: 10.1021/CM9006603.

[66] H. Huang *et al.*, "Strong and multi-responsive composite coiled yarn based on electrospun polyamide-6 nanofiber and carbon nanotube," *Elsevier*, Accessed: Jan. 26, 2024. [Online]. Available: https://www.sciencedirect.com/science/article/pii/S2352492821010369?casa_token=k1ZHUNcakPEAAAAA:Fiy5UcroTNe3Gjx4sejs-nsBqaZS5hN2tO_52StdPiuD6ARd1SthoK6H4gLUqdGVNFzzVH8

[67] P. Kumar, “Hizalanmış nano elyaf üretmek için kolletörün elektrospinning üzerindeki etkisi,” 2012, Accessed: Jan. 26, 2024. [Online]. Available: http://ethesis.nitrkl.ac.in/3825/

[68] A. Haghi, “Electrospinning of nanofibers in textiles,” 2011, Accessed: Jan. 26, 2024. [Online]. Available: https://books.google.com/books?hl=tr&lr=&id=TQibToLhbQoC&oi=fnd&pg=PP1&dq=A.+Haghi,+%E2%80%9CElectrospinning+of+nanofibers+in+textiles,%E2%80%9D+2011,+Accessed:+Mar.+29,+2023.+%5BOnline%5D.+Available:+https://books.google.com/books%3Fhl%3Dtr%26lr%3D%26id%3DTQibToLhbQoC%26oi%3Dfnd%26pg%3DPP1%26dq%3DHaghi,%2BA.%2BK.%2B(Ed.).%2B(2011).%2BElectrospinning%2Bof%2Bnanofibers%2Bin%2Btextiles.%2BCRC%2BPress.%26ots%3DLoSQmReOxK%26sig%3D4JxgDictJPg3To7eXXWnKGpUZkw&ots=LpKWoQdJwI&sig=5Q5038_rJ_Rc1S2yttOj1aHG1aM

[69] W. Teo, R. Gopal, R. Ramaseshan, K. F.- Polymer, and undefined 2007, “A dynamic liquid support system for continuous electrospun yarn fabrication,” *Elsevier*, Accessed: Jan. 26, 2024. [Online]. Available: https://www.sciencedirect.com/science/article/pii/S0032386107003977?casa_token=9AjqaGUZNhIAAAAA:bbbomyDruJFHzQa29G3BAWPYuKbnARfKR-E1buNgtsF_Rs-WZV48FXyTwuDfuR2mGnxvyow

[70] S. Chawla, M. Naraghi, A. D.- Nanotechnology, and undefined 2013, “Effect of twist and porosity on the electrical conductivity of carbon nanofiber yarns,” *iopscience.iop.orgS Chawla, M Naraghi, A DavoudiNanotechnology, 2013•iopscience.iop.org*, vol. 24, no. 25, pp. 255708–255717, Jun. 2013, doi: 10.1088/0957-4484/24/25/255708.

[71] A. Theron, E. Zussman, A. Y.- Nanotechnology, and undefined 2001, “Electrostatic field-assisted alignment of electrospun nanofibres,” *iopscience.iop.orgA Theron, E Zussman, AL YarinNanotechnology, 2001•iopscience.iop.org*, vol. 12, p. 384, 2001, Accessed: Jan. 26, 2024. [Online]. Available: https://iopscience.iop.org/article/10.1088/0957-4484/12/3/329/meta?casa_token=s9UC8NvOz9YAAAAA:X9idciqBkYvV8B

rIsTCsi9lYLakLiVpgUDONBXyGjX23nmE2qkchOIQDXl5SACOBPjrFNRnqO58_ijoi-JFf_eBq

[72] C. Bode-Aluko, K. Laatikainen, … O. P.-M. T., and undefined 2019, "Fabrication and characterisation of novel nanofiltration polymeric membrane," *Elsevier*, Accessed: Jan. 26, 2024. [Online]. Available: https://www.sciencedirect.com/science/article/pii/S2352492819304866?casa_token=oPW1DlmS3QEAAAAA:kOSbzC6qTURTwkPzRZjNkkiDQmpeP3wl4kgEX19eIyTvnYib45YLi26vwQix6qh5jcnw-QM

[73] H. Kim, M. Gil, Y. Jung, H. Kim, 354,546 BS Lee - US Patent 7, and undefined 2008, "Process of preparing continuous filament composed of nano fiber," *Google Patents*, 2008, Accessed: Jan. 26, 2024. [Online]. Available: https://patents.google.com/patent/US7354546B2/en

[74] 784 H Kim - US Patent App. 12/554 and undefined 2009, "Method of manufacturing a continuous filament by electrospinning and continuous filament manufactured thereby," *Google Patents*, no. 10, Accessed: Jan. 26, 2024. [Online]. Available: https://patents.google.com/patent/US20090324950A1/en

[75] A. Lotus, "Yarı iletken seramik nanoliflerin sentezi, pn bağlantılarının geliştirilmesi ve elektrospinning ile bant aralığı mühendisliği," 2009, Accessed: Jan. 26, 2024. [Online]. Available: https://search.proquest.com/openview/48f8caac798cd1491e3b66d60595352c/1?pq-origsite=gscholar&cbl=18750

[76] "behzat yıldırım - Google Akademik." Accessed: Jan. 26, 2024. [Online]. Available: https://scholar.google.hu/scholar?hl=tr&as_sdt=0%2C5&q=+behzat+y%C4%B1ld%C4%B1r%C4%B1m&oq=behzat

[77] S. Chawla, M. Naraghi, A. D.- Nanotechnology, and undefined 2013, "Büküm ve gözenekliliğin karbon nanolifli ipliklerin elektriksel iletkenliğine etkisi," *iopscience.iop.orgS Chawla, M Naraghi, A DavoudiNanoteknoloji*,

2013•iopscience.iop.org, vol. 24, no. 25, pp. 255708–255717, Jun. 2013, doi: 10.1088/0957-4484/24/25/255708.

[78] A. M. Afifi, S. Nakano, H. Yamane, and Y. Kimura, "Electrospinning of continuous aligning yarns with a 'funnel'target," *Wiley Online LibraryAM Afifi, S Nakano, H Yamane, Y KimuraMacromolecular Materials and Engineering, 2010•Wiley Online Library*, vol. 295, no. 7, pp. 660–665, Jul. 2010, doi: 10.1002/mame.200900406.

[79] L. Liu, M. Eder, I. Burgert, D. Tasis, … M. P.-A. P., and undefined 2007, "One-step electrospun nanofiber-based composite ropes," *pubs.aip.org*, vol. 90, no. 8, 2014, doi: 10.1063/1.2644379.

[80] D. Li, Y. Wang, and Y. Xia, "Electrospinning of polymeric and ceramic nanofibers as uniaxially aligned arrays," *Nano Lett*, vol. 3, no. 8, pp. 1167–1171, Aug. 2003, doi: 10.1021/NL0344256.

[81] G. K.-J. of P. S. P. B. P. Physics and undefined 2006, "Electrospinning process using field-controllable electrodes," *Wiley Online LibraryGH KimJournal of Polymer Science Part B: Polymer Physics, 2006•Wiley Online Library*, vol. 44, no. 10, pp. 1426–1433, May 2006, doi: 10.1002/polb.20814.

[82] "XIII. On the atomic weight of graphite," *Philos Trans R Soc Lond*, vol. 149, pp. 249–259, Dec. 1859, doi: 10.1098/RSTL.1859.0013.

[83] L. S. deutschen chemischen Gesellschaft and undefined 1898, "Verfahren zur darstellung der graphitsäure," *scholar.archive.org*, Accessed: Jan. 26, 2024. [Online]. Available: https://scholar.archive.org/work/jykncrumqvbbnlumyd4xtp67z4/access/ia_file/crossref-pre-1909-scholarly-works/10.1002%252Fcber.189803101202.zip/10.1002%252Fcber.18980310237.pdf

[84] U. Hofmann, … R. H. G. (A and B. S., and undefined 1939, "Über die Säurenatur und die Methylierung von Graphitoxyd," *Wiley Online LibraryU Hofmann, R HolstBerichte der deutschen chemischen Gesellschaft (A and B*

Series), 1939•Wiley Online Library, vol. 72, no. 4, pp. 754–771, Apr. 1939, doi: 10.1002/cber.19390720417.

[85] W. S. Hummers and R. E. Offeman, "Preparation of Graphitic Oxide," *J Am Chem Soc*, vol. 80, no. 6, p. 1339, Mar. 1958, doi: 10.1021/JA01539A017.

[86] "18. Fu, L., Liu, H. B., Zou, Y. H., Li, B., (2005),... - Google Akademik." Accessed: Jan. 26, 2024. [Online]. Available: https://scholar.google.com/scholar?hl=tr&as_sdt=0%2C5&q=18.%09Fu%2C+L.%2C+Liu%2C+H.+B.%2C+Zou%2C+Y.+H.%2C+Li%2C+B.%2C+%282005%29%2C+Technology+research+on+oxidative+degree+of+graphite+oxide+prepared+by+Hummers+method%2C+Carbon%2C+4%2C+10-14.&btnG=

[87] C. Siegfried Eigler *et al.*, "Wet chemical synthesis of graphene," *Wiley Online Library*, *M Enzelberger-Heim, S Grimm, P Hofmann, W Kroener, A Geworski, C Dotzer, M Röckert…Advanced materials, 2013•Wiley Online Library*, vol. 25, no. 26, pp. 3583–3587, Jul. 2013, doi: 10.1002/adma.201300155.

[88] D. López-Díaz *et al.*, "The role of oxidative debris on graphene oxide films," *Wiley Online LibraryD López-Díaz, M Mercedes Velazquez, S Blanco de La Torre, A Pérez-PisoneroChemPhysChem, 2013•Wiley Online Library*, vol. 14, no. 17, pp. 4002–4009, Dec. 2013, doi: 10.1002/cphc.201300620.

[89] A. Nekahi, P. Marashi, D. H.-A. S. Science, and undefined 2014, "Transparent conductive thin film of ultra large reduced graphene oxide monolayers," *Elsevier*, Accessed: Jan. 26, 2024. [Online]. Available: https://www.sciencedirect.com/science/article/pii/S0169433214000117?casa_token=TASBEmZiyFkAAAAA:uEed0KelKEykJpBisXZxIxndlfylm5pBsiIpuLMKEgHGZxM_dpcfjVtUyebSSYb4zwMZItg

[90] S. Drewniak, T. Pustelny, … R. M.-P. L. of, and undefined 2015, "Investigations of selected physical properties of graphite oxide and thermally exfoliated/reduced graphene oxide in the aspect of their applications in photonic gas," *photonics.plS Drewniak, T Pustelny, R Muzyka, A Stolarczyk, G KoniecznyPhotonics Letters of Poland, 2015•photonics.pl*, Accessed: Jan. 26,

2024. [Online]. Available: http://www.photonics.pl/PLP/index.php/letters/article/view/7-17

[91] C. Y. Su *et al.*, "Electrical and spectroscopic characterizations of ultra-large reduced graphene oxide monolayers," *Chemistry of Materials*, vol. 21, no. 23, pp. 5674–5680, Dec. 2009, doi: 10.1021/CM902182Y.

[92] L. Sun, B. F.-M. Letters, and undefined 2013, "Mass production of graphene oxide from expanded graphite," *Elsevier*, Accessed: Jan. 26, 2024. [Online]. Available: https://www.sciencedirect.com/science/article/pii/S0167577X13010100

[93] J. Chen, Y. Li, L. Huang, C. Li, G. S.- Carbon, and undefined 2015, "High-yield preparation of graphene oxide from small graphite flakes via an improved Hummers method with a simple purification process," *Elsevier*, Accessed: Jan. 26, 2024. [Online]. Available: https://www.sciencedirect.com/science/article/pii/S0008622314009956

[94] D. C. Marcano *et al.*, "Improved synthesis of graphene oxide," *ACS Nano*, vol. 4, no. 8, pp. 4806–4814, Aug. 2010, doi: 10.1021/NN1006368.

[95] D. Jha *et al.*, "ElemNet: Malzemelerin Kimyasını Sadece Elementel Bileşimden Derinlemesine Öğrenme," *nature.comD Jha, L Koğuş, Bir Paul, W Liao, Bir Choudhary, C Wolverton, Bir AgrawalBilimsel raporlar, 2018•nature.com*, doi: 10.1038/s41598-018-35934-y.

[96] G. Santamaría-Juárez, … E. G.-B.-M. R., and undefined 2020, "Safer modified Hummers' method for the synthesis of graphene oxide with high quality and high yield," *iopscience.iop.orgG Santamaría-Juárez, E Gómez-Barojas, E Quiroga-González, E Sánchez-MoraMaterials Research Express, 2020•iopscience.iop.org*, Accessed: Jan. 26, 2024. [Online]. Available: https://iopscience.iop.org/article/10.1088/2053-1591/ab4cbf/meta

[97] V. Panwar, A. Chattree, K. P.-P. E. L. S. and, and undefined 2015, "A new facile route for synthesizing of graphene oxide using mixture of sulfuric–nitric–phosphoric acids as intercalating agent," *Elsevier*, 2015, doi: 10.1016/j.physe.2015.06.006.

[98] L. Bian *et al.*, “Multispectral imaging using a single bucket detector,” *nature.comL Bian, J Suo, G Situ, Z Li, J Fan, F Chen, Q DaiScientific reports, 2016•nature.com*, 2016, doi: 10.1038/srep24752.

[99] J. Shen *et al.*, “Fast and facile preparation of graphene oxide and reduced graphene oxide nanoplatelets,” *Chemistry of Materials*, vol. 21, no. 15, pp. 3514–3520, Aug. 2009, doi: 10.1021/CM901247T.

[100] S. Chandra, S. Sahu, P. P.-M. S. and E. B, and undefined 2010, “A novel synthesis of graphene by dichromate oxidation,” *Elsevier*, Accessed: Jan. 26, 2024. [Online]. Available: https://www.sciencedirect.com/science/article/pii/S0921510710000498

[101] L. Peng *et al.*, “Tek katmanlı grafen oksidin 1 saatlik üretimine demir bazlı yeşil bir yaklaşım,” *nature.comL Peng, Z Xu, Z Liu, Y Wei, H Güneş, Z Li, X Zhao, C GaoDoğa iletişimi, 2015•nature.com*, 2015, doi: 10.1038/ncomms6716.

[102] M. Rosillo-Lopez, C. S.- Carbon, and undefined 2016, “A simple and mild chemical oxidation route to high-purity nano-graphene oxide,” *Elsevier*, Accessed: Jan. 17, 2024. [Online]. Available: https://www.sciencedirect.com/science/article/pii/S0008622316303761

[103] A. M. Dimiev, G. Ceriotti, A. Metzger, N. D. Kim, and J. M. Tour, “Chemical mass production of graphene nanoplatelets in ∼100% yield,” *ACS Nano*, vol. 10, no. 1, pp. 274–279, Jan. 2016, doi: 10.1021/ACSNANO.5B06840.

[104] W. Yu, L. Sisi, Y. Haiyan, L. J.-R. advances, and undefined 2020, “Progress in the functional modification of graphene/graphene oxide: A review,” *pubs.rsc.orgW Yu, L Sisi, Y Haiyan, L JieRSC advances, 2020•pubs.rsc.org*, Accessed: Jan. 26, 2024. [Online]. Available: https://pubs.rsc.org/en/content/articlehtml/2020/ra/d0ra01068e

[105] S. Wang, K. Wang, Q. Ma, C. Q.-M. T. Communications, and undefined 2020, “Fabrication of the multifunctional durable silk fabric with synthesized graphene oxide nanosheets,” *Elsevier*, Accessed: Jan. 26, 2024. [Online]. Available: https://www.sciencedirect.com/science/article/pii/S2352492819305525?casa_t

oken=nl98usffJKkAAAAA:rZHfDiQISW_EnISWy7srbb_EyzpdSwj9dcsgnm2JanYBwNXKgz6VUlb0U8GB7bH3GKjHtXo

[106] D. Gui, C. Liu, F. Chen, J. L.-A. S. Science, and undefined 2014, "Preparation of polyaniline/graphene oxide nanocomposite for the application of supercapacitor," *Elsevier*, Accessed: Jan. 26, 2024. [Online]. Available: https://www.sciencedirect.com/science/article/pii/S0169433214007703?casa_token=VktAsOszblsAAAAA:hp1wiT44FjT2vlTIa6zD0gaD10vTI129dx2nMGBrfGKW7kjrgQzYksHfDa44rBrHsq8C0To

[107] L. Xu *et al.*, "Coolmax/graphene-oxide functionalized textile humidity sensor with ultrafast response for human activities monitoring," *Elsevier*, Accessed: Jan. 17, 2024. [Online]. Available: https://www.sciencedirect.com/science/article/pii/S1385894721002370

[108] D. S. Kinnamon, S. Krishnan, S. Brosler, E. Sun, and S. Prasad, "Screen Printed Graphene Oxide Textile Biosensor for Applications in Inexpensive and Wearable Point-of-Exposure Detection of Influenza for At-Risk Populations," *J Electrochem Soc*, vol. 165, no. 8, pp. B3084–B3090, 2018, doi: 10.1149/2.0131808JES/META.

[109] J. Molina, A. Zille, J. Fernández, A. Souto, J. B.-S. Metals, and undefined 2015, "Conducting fabrics of polyester coated with polypyrrole and doped with graphene oxide," *Elsevier*, Accessed: Jan. 26, 2024. [Online]. Available: https://www.sciencedirect.com/science/article/pii/S0379677915001216?casa_token=byXC2nK2h5IAAAAA:-GcMm-M6v73vxDBagoPUzy2JSbRZ2Kcr-C_p7acnCI3e-CYqQ26F7wlUYQth3XhDZuqEQlI

[110] H. Sim, D. Lee, H. Kim, Y. Jang, G. S.- Carbon, and undefined 2019, "Self-healing graphene oxide-based composite for electromagnetic interference shielding," *Elsevier*, Accessed: Jan. 26, 2024. [Online]. Available: https://www.sciencedirect.com/science/article/pii/S0008622319308838?casa_token=REHoQ6Jk7qIAAAAA:ZQM-lAaxoP9D_E40XyrZtIfDBVPFT-2NTF5bgmrIysbSXmpdPXb4Y_U8RiZO_ah5YJCfOP4

[111] K. Krishnamoorthy, U. Navaneethaiyer, R. Mohan, J. Lee, and S. J. Kim, "Graphene oxide nanostructures modified multifunctional cotton fabrics," *Applied Nanoscience (Switzerland)*, vol. 2, no. 2, pp. 119–126, Jun. 2012, doi: 10.1007/S13204-011-0045-9.

[112] X. Liang, J. Zhao, L. Dong, K. X.-S. reports, and undefined 2013, "Unraveling the origin of exponential law in intra-urban human mobility," *nature.comX Liang, J Zhao, L Dong, K XuScientific reports, 2013•nature.com*, Accessed: Jan. 26, 2024. [Online]. Available: https://www.nature.com/articles/srep02983

[113] Q. Huang, M. Xu, R. Sun, X. W.-I. C. and Products, and undefined 2016, "Large scale preparation of graphene oxide/cellulose paper with improved mechanical performance and gas barrier properties by conventional papermaking," *Elsevier*, Accessed: Jan. 26, 2024. [Online]. Available: https://www.sciencedirect.com/science/article/pii/S0926669016301376?casa_token=PBndyiTOpxsAAAAA:hfayTcdnEp6uwMWmzq_7rJI2BRfT3zjwD6ku0mhF43giILLIoiEcA465UjS-NS1xdgDRmSA

[114] M. Shateri-Khalilabad and M. E. Yazdanshenas, "Preparation of superhydrophobic electroconductive graphene-coated cotton cellulose," *Cellulose*, vol. 20, no. 2, pp. 963–972, Apr. 2013, doi: 10.1007/S10570-013-9873-Y.

[115] Y. Zhu, S. Murali, W. Cai, X. Li, … J. S.-A., and undefined 2010, "Graphene and graphene oxide: synthesis, properties, and applications," *Wiley Online LibraryY Zhu, S Murali, W Cai, X Li, JW Suk, JR Potts, RS RuoffAdvanced materials, 2010•Wiley Online Library*, vol. 22, no. 35, pp. 3906–3924, Sep. 2010, doi: 10.1002/adma.201001068.

[116] C. Zhang, L. Yao, Z. Yang, E. S. W. Kong, X. Zhu, and Y. Zhang, "Graphene Oxide-Modified Polyacrylonitrile Nanofibrous Membranes for Efficient Air Filtration," *ACS Appl Nano Mater*, vol. 2, no. 6, pp. 3916–3924, Jun. 2019, doi: 10.1021/ACSANM.9B00806.

[117] F. Ashrafi, M. F.-F. and Polymers, and undefined 2021, "Preparation of Forcespun Amidoximated Polyacrylonitrile-graphene Oxide Nanofibers and

Evaluation of Their Uranium Uptake from Aqueous Media," *SpringerF Ashrafi, M FirouzzareFibers and Polymers, 2021•Springer*, vol. 22, no. 12, pp. 3289–3297, Dec. 2021, doi: 10.1007/s12221-021-0133-8.

[118] Y. Zhang *et al.*, "Rapid in Situ Polymerization of Polyacrylonitrile/Graphene Oxide Nanocomposites as Precursors for High-Strength Carbon Nanofibers," *ACS Appl Mater Interfaces*, vol. 13, no. 14, pp. 16846–16858, Apr. 2021, doi: 10.1021/ACSAMI.1C02643.

[119] L. Liu, Y. D.- Nanotechnology, and undefined 2008, "Analysis of the effects of the residual charge and gap size on electrospun nanofiber alignment in a gap method," *iopscience.iop.orgL Liu, YA DzenisNanotechnology, 2008•iopscience.iop.org*, 2008, doi: 10.1088/0957-4484/19/35/355307.

[120] H. Yan, L. Liu, Z. Z.-A. P. Letters, and undefined 2009, "Alignment of electrospun nanofibers using dielectric materials," *pubs.aip.org*, Accessed: Jan. 22, 2024. [Online]. Available: https://pubs.aip.org/aip/apl/article/95/14/143114/337886

[121] V. Chaurey, P. C. Chiang, C. Polanco, Y. H. Su, C. F. Chou, and N. S. Swami, "Interplay of electrical forces for alignment of sub-100 nm electrospun nanofibers on insulator gap collectors," *Langmuir*, vol. 26, no. 24, pp. 19022–19026, Dec. 2010, doi: 10.1021/LA102209Q.

[122] M. Pokorny, K. Niedoba, V. V.-A. P. Letters, and undefined 2010, "Transversal electrostatic strength of patterned collector affecting alignment of electrospun nanofibers," *pubs.aip.org*, 2010, doi: 10.1063/1.3430507.

[123] Y. Yusuf *et al.*, "Study of parallel oriented electrospun polyvinyl alcohol (PVA) nanofibers using modified electrospinning method," *AIP Conf Proc*, vol. 1725, Apr. 2016, doi: 10.1063/1.4945558/13723038/020104_1_ONLINE.PDF.

[124] X. Cai, P. Zhu, X. Lu, Y. Liu, T. Lei, and D. Sun, "Electrospinning of very long and highly aligned fibers," *J Mater Sci*, vol. 52, no. 24, pp. 14004–14010, Dec. 2017, doi: 10.1007/S10853-017-1529-0.

[125] C. Fryer, M. Scharnagl, and C. Helms, “Electrostatic alignment of electrospun PEO fibers by the gap method increases individual fiber modulus in comparison to non-aligned fibers of similar diameter,” *AIP Adv*, vol. 8, no. 6, Jun. 2018, doi: 10.1063/1.5027812/12964332/065023_1_ONLINE.PDF.

[126] Y. He *et al.*, “Staggered Nanofiber Scaffolds via Electric-Field-Controlled Assembly for Bone Tissue Regeneration,” *ACS Appl Nano Mater*, vol. 5, no. 5, pp. 6327–6339, May 2022, doi: 10.1021/ACSANM.2C00429.

[127] Y. Ishii, H. Sakai, H. M.-M. Letters, and undefined 2008, “A new electrospinning method to control the number and a diameter of uniaxially aligned polymer fibers,” *Elsevier*, Accessed: Jan. 22, 2024. [Online]. Available: https://www.sciencedirect.com/science/article/pii/S0167577X08002899

[128] H. İ. İçoğlu, Ş. Ceylan, B. Yıldırım, M. Topalbekiroğlu, and A. Kılıç, “Production of aligned electrospun polyvinyl alcohol nanofibers via parallel electrode method,” *Journal of the Textile Institute*, pp. 1–10, 2020, doi: 10.1080/00405000.2020.1789274.

[129] M. Yazici *et al.*, “Modifiye hummers yöntemiyle grafen oksit (GO) sentezi ve karakterizasyonu,” *dergipark.org.trM YAZICI, İ TİYEK, MS ERSOY, MH ALMA, U DÖNMEZ, B YILDIRIM, T SALAN, Ş KARATAŞGazi University Journal of Science Part C: Design and Technology, 2016•dergipark.org.tr*, vol. 4, no. 2, pp. 41–48, 2016, Accessed: Jan. 22, 2024. [Online]. Available: https://dergipark.org.tr/en/pub/gujsc/issue/24939/263249

[130] V. Loryuenyong, … K. T.-A. in M., and undefined 2013, “Preparation and characterization of reduced graphene oxide sheets via water-based exfoliation and reduction methods,” *hindawi.comV Loryuenyong, K Totepvimarn, P Eimburanapravat, W Boonchompoo, A BuasriAdvances in Materials Science and Engineering, 2013•hindawi.com*, Accessed: Jan. 22, 2024. [Online]. Available: https://www.hindawi.com/journals/AMSE/2013/923403/

[131] L. Shahriary, A. A.-Int. J. Renew. E. Environ. Eng, and undefined 2014, “Graphene oxide synthesized by using modified hummers approach,” *researchgate.netL Shahriary, AA AthawaleInt. J. Renew. Energy Environ. Eng*,

2014•researchgate.net, vol. 02, no. 01, 2014, Accessed: Jan. 22, 2024. [Online]. Available: https://www.researchgate.net/profile/Jeffrey_Yang7/post/How_to_wash_graphene_oxide_solution_after_synthesis/attachment/59d626866cda7b8083a233fb/AS:500084322168832@1496240801304/download/modified_hummer_used_for_ftir_uv_and_ram.pdf

[132] S. Ryu, A. S.-C. E. Journal, and undefined 2014, "Influence of long-chain alkylamine-modified graphene oxide on the crystallization, mechanical and electrical properties of isotactic polypropylene," *Elsevier*, Accessed: Jan. 22, 2024. [Online]. Available: https://www.sciencedirect.com/science/article/pii/S1385894714001260

[133] J. Song, X. Wang, C. C.-J. of Nanomaterials, and undefined 2014, "Preparation and characterization of graphene oxide," *hindawi.comJ Song, X Wang, CT ChangJournal of Nanomaterials, 2014•hindawi.com*, Accessed: Jan. 22, 2024. [Online]. Available: https://www.hindawi.com/journals/jnm/2014/276143/abs/

[134] A. Gupta, P. Ayithapu, and R. Singhal, "Study of the electric field distribution of various electrospinning geometries and its effect on the resultant nanofibers using finite element simulation," *Chem Eng Sci*, vol. 235, May 2021, doi: 10.1016/j.ces.2021.116463.

[135] K. Nasouri, A. M. Shoushtari, and M. R. M. Mojtahedi, "Effects of polymer/solvent systems on electrospun polyvinylpyrrolidone nanofiber morphology and diameter," *Polymer Science - Series A*, vol. 57, no. 6, pp. 747–755, Nov. 2015, doi: 10.1134/S0965545X15060164.

[136] "Bakar, N. F. A., Hussain, M. H., İsmail, I., Othman,... - Google Akademik." Accessed: Jan. 26, 2024. [Online]. Available: https://scholar.google.co.nz/scholar?hl=tr&as_sdt=0%2C5&q=Bakar%2C+N.+F.+A.%2C+Hussain%2C+M.+H.%2C+%C4%B0smail%2C+I.%2C+Othman%2C+N.%2C+Tan%2C+H.+L.%2C+Zain%2C+Z.+M.%2C+...+%26+Radacsi%2C+N.+%282021%29.+Geli%C5%9Fmi%C5%9F+iletkenlik+i%C3%A7in+elektrospun+polieterimid-

grafen+oksit+nanofiber+elektrotlar.+Lif+Bilimi+ve+Teknolojisi+Dergisi%2C+77%284%29%2C+136-145.&btnG=

[137] M. Tripathy, G. H.-A. A. P. Materials, and undefined 2019, "Maghemite and graphene oxide embedded polyacrylonitrile electrospun nanofiber matrix for remediation of arsenate ions," *ACS Publications*, vol. 2, no. 2, pp. 604–617, Feb. 2020, doi: 10.1021/acsapm.9b00982.

[138] F. Liu, H. Wang, L. Xue, L. Fan, and Z. Zhu, "Effect of microstructure on the mechanical properties of PAN-based carbon fibers during high-temperature graphitization," *J Mater Sci*, vol. 43, no. 12, pp. 4316–4322, Jun. 2008, doi: 10.1007/S10853-008-2633-Y.

[139] K. Krishnaveni, R. Subadevi, and M. Sivakumar, "Graphene oxide-crowned poly(acrylonitrile)/sulfur as a lithium–sulfur battery cathode: performance and characterization," *SN Appl Sci*, vol. 2, no. 4, Apr. 2020, doi: 10.1007/S42452-020-2576-8.

CURRICULUM VITAE

PROFILE

Name Surname **:** Melike TÜRKOĞLU

EDUCATION

Degree	University	Department	Year
M.Sc.	Gaziantep University	Materials Science and Engineering	2024
B.Sc.	Gaziantep University	Metallurgical and Materials Engineering	2021

PROJECTS

Supporting Project Number	Title of Project	Position	Project Duration
GAÜN - BAP MF.YLT.22.21	Synthesis of Graphene Oxide with Different Methods and Production of Graphene Oxide Additive Polyvinyl Alcohol Nanofibers	Researcher	2022 2023
TÜBİTAK ARDEB-1001 119M342	Design, Development and Manufacturing a Machine for Production of Continuous Twisted Nanofiber Yarns in Industrial Scale with an Innovative Approach	M.Sc. Scholarship	2020 2023
TÜBİTAK BİDEB 2210-C Priority Areas	Production and characterization of graphene oxide polyacrylonitrile nanofibers by needleless electrospinning method	M.Sc. Scholarship	2022 2023

PUBLICATIONS

İçoğlu, H. İ., Yıldırım, B., Kılıç, A., **Türkoğlu, M.,** Köş, A. M., & Topalbekiroğlu, M. (2023). Controlled fiber deposition via modeling the auxiliary electrodes of the needleless electrospinning to produce continuous nanofiber bundles. Materials Today Communications, 34, 104966.

Yıldırım, B., **Türkoğlu, M.**, İçoğlu, H. İ., Topalbekiroğlu, M. Grafen Oksit Sentez Yöntemlerinin İncelenmesi ve Seçilen Bir Yöntem ile Grafen Oksit Sentezi. *UÇTEK*, 29 Eylül 2022, Türkiye, Adana.

Türkoğlu, M., Yıldırım, B., Köş, A. M., Kılıç, A., İçoğlu, H. İ., Topalbekiroğlu, M. Elektro Çekimde Endüstriyel Üretime Uygun Konveyör Bantlı Toplayıcı ile Nanolif Şerit Üretimi. *UÇTEK*, 29 Eylül 2022, Türkiye, Adana.